Theses and Dissertations   1. Thesis and Dissertation Collection, all items

1990

The effects of forebody strakes on asymmetric vortices on a vertically launched missile

Yuan, Chih-Chung

Monterey, California. Naval Postgraduate School

http://hdl.handle.net/10945/37570

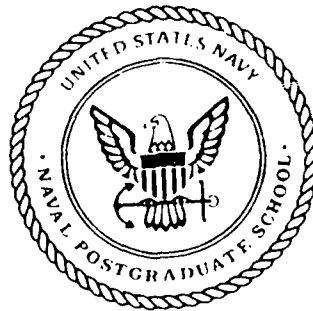# NAVAL POSTGRADUATE SCHOOL
Monterey, California

AD-A239 948

THESIS

THE EFFECTS OF FOREBODY STRAKES ON
ASYMMETRIC VORTICES ON A VERTICALLY
LAUNCHED MISSILE

by

Yuan, Chih-Chung

September 1990

Thesis Advisor: Richard M. Howard

91 8 26 020   91-08878

REPORT DOCUMENTATION PAGE

1a Report Security Classification Unclassified	1b Restrictive Markings
2a Security Classification Authority	3 Distribution Availability of Report
2b Declassification/Downgrading Schedule	Approved for public release; distribution is unlimited.

4 Performing Organization Report Number(s)	5 Monitoring Organization Report Number(s)

6a Name of Performing Organization Naval Postgraduate School	6b Office Symbol (If Applicable) AA/HO	7a Name of Monitoring Organization Naval Postgraduate School

6c Address (city, state, and ZIP code) Monterey, CA 93943-5000	7b Address (city, state, and ZIP code) Monterey, CA 93943-5000

8a Name of Funding/Sponsoring Organization	8b Office Symbol (If Applicable)	9 Procurement Instrument Identification Number

8c Address (city, state, and ZIP code)	10 Source of Funding Numbers

Program Element Number	Project No	Task No	Work Unit Accession No

11 Title (Include Security Classification) THE EFFECTS OF FOREBODY STRAKES ON ASYMMETRIC VORTICES ON A VERTICALLY LAUNCHED MISSILE

12 Personal Author(s) Yuan, Chih-Chung

13a Type of Report Master's Thesis	13b Time Covered From To	14 Date of Report (year, month,day) September 1990	15 Page Count 174

16 Supplementary Notation The views expressed in this thesis are those of the author and do not reflect the official policy or position of the Department of Defense or the U.S. Government.

17 Cosati Codes			18 Subject Terms (continue on reverse if necessary and identify by block number)
Field	Group	Subgroup	Vortex, Vertical Launch, Surface to Air Missile, High Angle of Attack, Turbulence, Strakes, Forebody, Ogive

19 Abstract (continue on reverse if necessary and identify by block number)

Wind tunnel tests were conducted on a vertically launched surface-to-air missile model to investigate the effects of forebody strakes on the side forces and yawing moments induced by nose-generated asymmetric vortices at high angles of attack. The effects of body configuration and a turbulent flowfield on the induced side forces and yawing moments were also examined. Test angles of attack ranged from 0° to 90° at a Reynolds number of 1.15×10^5 based on the model diameter, and at a Mach number of 0.11. Three forebody configurations, two body configurations and two flowfield conditions were investigated. The flowfield with a turbulence length scale on the order of the vortex scale was found to have no significant influence on the induced side forces and yawing moments. The change of body configuration had no strong effects on the side forces and yawing moments either. The "4 STRAKES" forebody demonstrated dramatic results in the yawing moment alleviation; the ranges of angle of attack in the induced side forces and yawing moments were also decreased by this modification. The "8 STRAKES" forebody gave no significant improvement in the induced side force and yawing moment reduction.

20 Distribution/Availability of Abstract [X] unclassified/unlimited [ ] same as report [ ] DTIC users	21 Abstract Security Classification Unclassified

22a Name of Responsible Individual Richard M. Howard	22b Telephone (Include Area code) (408) 646-2870	22c Office Symbol AA/HO

DD FORM 1473, 84 MAR   83 APR edition may be used until exhausted   security classification of this page

All other editions are obsolete

The Effects of Forebody Strakes on Asymmetric Vortices on A
Vertically Launched Missile

by

Yuan, Chih-Chung
Lieutenant, Republic of China Navy
B.S., Chinese Naval Academy, 1986

Submitted in partial fulfillment of the requirements for
the degree of

MASTER OF SCIENCE IN AERONAUTICAL ENGINEERING

from the

NAVAL POSTGRADUATE SCHOOL
September 1990

Author: _____
Yuan, Chih-Chung

Approved by: _____
Richard M. Howard, Thesis Advisor

_____
J. Val Healey, Second Reader

_____
E. R. Wood, Chairman
Department of Aeronautics and Astronautics

ABSTRACT

Wind tunnel tests were conducted on a vertically launched surface-to-air missile model to investigate the effects of forebody strakes on the side forces and yawing moments induced by nose-generated asymmetric vortices at high angles of attack. The effects of body configuration and a turbulent flowfield on the induced side forces and yawing moments were also examined. Test angles of attack ranged from 0° to 90° at a Reynolds number of 1.15×10^5 based on the model diameter, and at a Mach number of 0.11. Three forebody configurations, two body configurations and two flowfield conditions were investigated. The flowfield with a turbulence length scale on the order of the vortex scale was found to have no significant influence on the induced side forces and yawing moments. The change of body configuration had no strong effects on the side forces and yawing moments either. The "4 STRAKES" forebody demonstrated dramatic results in the yawing moment alleviation; the ranges of angle of attack in the induced side forces and yawing moments were also decreased by this modification. The "8 STRAKES" forebody gave no significant improvement in the induced side force and yawing moment reduction.

TABLE OF CONTENTS

LIST OF TABLES

LIST OF FIGURES

NOMENCLATURE

α	=	angle of attack
AOA	=	angle of attack
α_{sv}	=	the AOA at which steady symmetric vortices are formed.
α_{av}	=	the AOA at which steady asymmetric vortices are formed.
α_{uv}	=	the AOA at which unsteady vortices are formed.
d	=	base diameter of the missile body
A_m	=	missile reference area (cross section area)
l_n	=	nose length
l_n/d	=	nose fineness ratio
L_l	=	missile length
L_d	=	missile diameter
L_u	=	dissipation length scale of turbulence
M	=	Mach number
Re_d	=	Reynolds number
N	=	normal force (measured from balance)
S	=	side force (measured from balance)
A	=	axial force (measured from balance)
l	=	rolling moment (measured from balance)
m	=	pitching moment (measured from balance)
n	=	yawing moment (measured from balance)
C_N	=	normal force coefficient, $\dfrac{N}{q A_m}$
C_Y	=	side force coefficient, $\dfrac{S}{q A_m}$

C_A = axial force coefficient, $\dfrac{A}{q\,A_m}$

C_l = rolling moment coefficient, $\dfrac{l}{q\,A_m\,d}$

C_m = pitching moment coefficient, $\dfrac{m}{q\,A_m\,d}$

C_n = yawing moment coefficient, $\dfrac{n}{q\,A_m\,d}$

U_∞ = freestream velocity

q = dynamic pressure

Δp = static pressure difference (between settling chamber and test section of wind t·nnel)

ε = blockage correction factor

ACKNOWLEDGEMENTS

I. INTRODUCTION

A. BACKGROUND

In the past few years, the Vertical Launch Surface-to-Air Missile (VLSAM) system has been developed and deployed on Navy ships (U.S.A., U.K., and U.S.S.R.) because of its several advantages over the conventional surface-to-air missile (SAM) system. [Ref. 1]

First, the VLSAM has a higher target engagement rate, up to one missile fired per second (Martin Marietta Mark 41 vertical launcher system). Also the VLSAM can guide itself to its target after firing, while the conventional SAM needs a trainable launcher to provide a firing elevation and azimuth so that it can be fired into guidance beams directing it to the target. This significant feature should allow the ship to defend against multiple air targets successfully.

Secondly, the VLSAM saves valuable ship space. A trainable launcher needs a wide clear space for its own rotation and the blast of firing SAMs in different directions. The VLSAM uses a canister container which stores and launches the missile, and the blast is concentrated in the immediate area of the launcher. Thus, the design of the missile container/launcher in the VLSAM system saves both storage room and firing space.

Thirdly, the container/launcher module of the VLSAM system has a more rapid and easier replenishment than the conventional systems, because each launch module can be shipped and installed as an individual unit. For instance, there are two groups of Mk 41 Mod. 0 vertical-launch systems in

1

current deployment on the guided missile cruisers of the US Navy (CG 52-73), and each group consists of eight modules which have two rows of launch cells for each module. In each group, one of the eight-cell modules is replaced by a five-cell strikedown module which has a three-cell space occupied by a retractable loading crane, in order to replenish the launcher magazine at sea.

Fourthly, the 360° coverage is provided without interference from the superstructure of the ship. The conventional launcher usually has some specific directions in which the SAM cannot be fired due to the location of the ship superstructure. The VLSAM system eliminates this limitation so the ship can fire the missile to any trajectory regardless of the target's position.

However, the VLSAM faces problems not encountered with the conventional SAM system. A missile launched vertically into the open ocean environment is exposed to potentially significant crosswinds while its velocity is still low. The result is a missile flying at a high angle of attack with a low Mach number during the launch phase [Ref. 2: page 22-24]. In the missile search/acquisition and homing phase, it also maneuvers in high angles of attack to track the target. These high angle of attack flight phenomena may cause the formation of asymmetric vortices around the missile nose and afterbody. The potential induced side force and yawing moment caused by the asymmetric vortices may lead to control and stability problems for the VLSAM during the launch and push-over phases.

The characteristics of out-of-plane forces and moments, caused largely by asymmetric vortex shedding on a slender body at high angles of attack, have been investigated for many years. Much of the research to date has attempted to model or predict the flow about such bodies and to examine the effect of

2

design changes, such as the use of nose strakes or nose blunting, on the observed flow. Some previous investigations will be discussed later in this chapter. Several experimental techniques such as force and moment measurements, flowfield pressure measurements and flow visualization have been applied to analyze both the cause and effect of these asymmetric vortices. Force and moment measurements were used in this thesis research to give information on the magnitude of the induced forces and moments.

Additionally, the launch environment may have some turbulence caused by both the atmospheric boundary layer and the airflow over the ship superstructure; also, the missile could fly through shear turbulence in the atmosphere. The model of the turbulent flowfield, generated by installing a grid screen in the wind tunnel, has been developed by Roane and employed in the Naval Postgraduate School (NPS) low speed wind tunnel. [Ref. 2]

The goal of this thesis was to experimentally investigate the effects of strakes, installed on the forebody tip, on the asymmetric vortex induced forces and moments on a VLSAM model, in an attempt to reduce their magnitude. Other considerations which have influence on the asymmetric vortex system, including the flight body-wing configurations and a turbulent flowfield, were also investigated and will be described in the subsequent sections.

B. AERODYNAMICS OF ASYMMETRIC VORTEX SHEDDING

Many investigations of the aerodynamic characteristics of missiles and aircraft at high angle of attack have been made and reported. A "vortex system" has been found to exist in the leeward flowfield of these bodies. These observations have determined that the pattern of this vortex system depends on angle of attack (AOA), nose geometry (bluntness, fineness ratio,

etc.) and roll angle, crossflow Mach number and Reynolds number, lifting surfaces, freestream turbulence, surface roughness, acoustic environment and vibration [Ref. 3-12]. Most of these factors mentioned above will be discussed later in this chapter.

1. Formation of the Vortex System on a Slender Cylinder

A slender cylinder with a pointed forebody experiences four distinct flow patterns that reflect the diminishing influence of the axial flow component when pitched through the AOA range from 0° to 90° for a typical flight Reynolds number range. These four regimes are shown in Figure 1 and are described below: [Ref. 13: page 246-247]

a. Regime I $(0° \leq \alpha \leq \alpha_{sv})$

The axial flow component dominates and the flow is attached in this low AOA regime.

b. Regime II $(\alpha_{sv} \leq \alpha \leq \alpha_{av})$

At this intermediate AOA regime, the crossflow pushes the boundary layer to the leeward side where it separates and rolls up into a symmetric vortex pair. More pairs of symmetric vortices are formed along a longer body. The number and strength of the symmetric vortices increase with AOA.

c. Regime III $(\alpha_{av} \leq \alpha \leq \alpha_{uv})$

At high angles of attack, the crossflow starts to dominate and to shed asymmetric vortices which induce side forces and yawing moments at zero sideslip on the body. These asymmetric vortices are relatively steady, but may change from side to side as the AOA increases, causing the side forces and

yawing moments to change signs. The maximum side force occurs when the vortices are the most asymmetric.
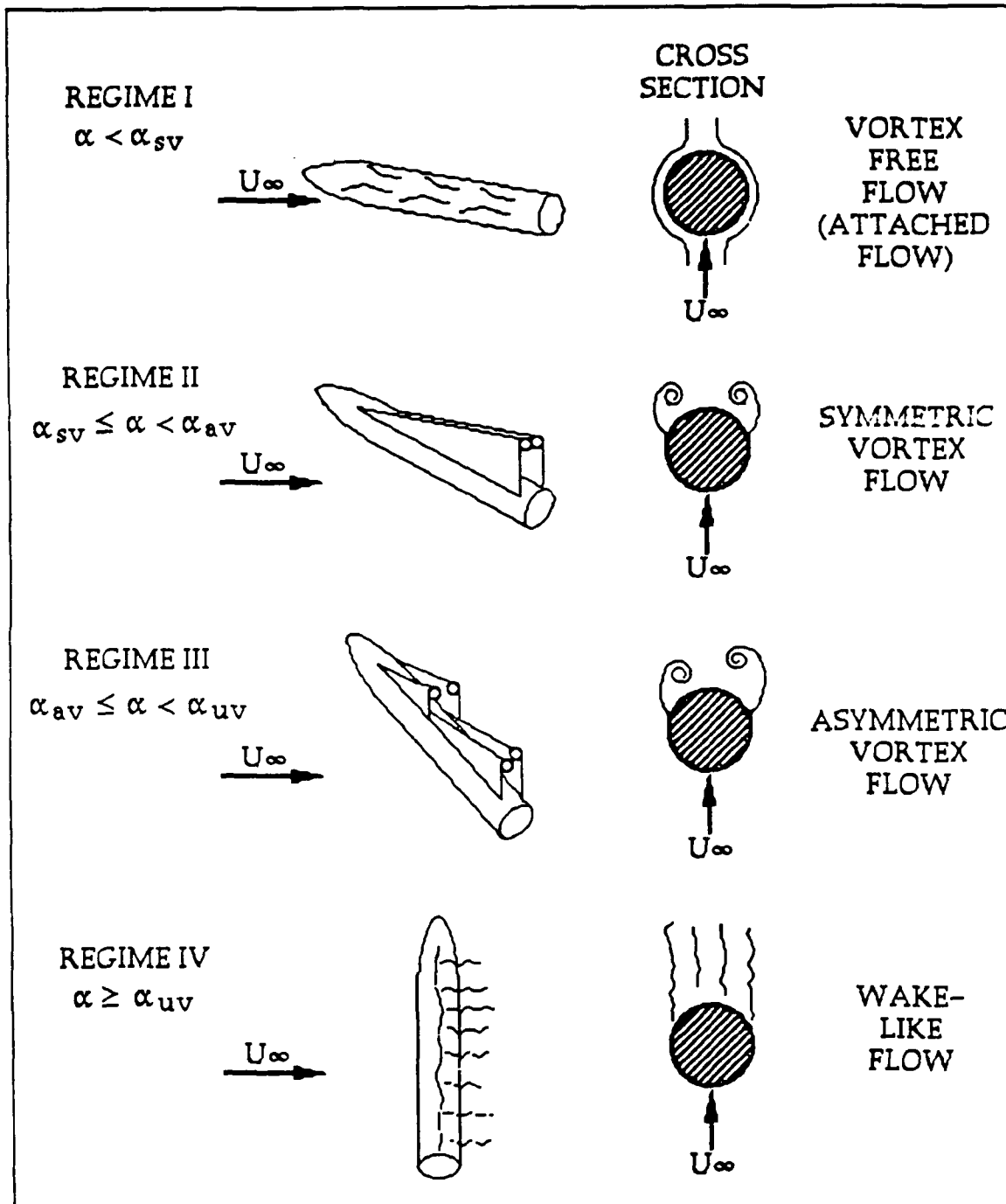
Figure 1. Vortex Generation Regimes [Ref. 13]

d.   Regime IV ($\alpha_{uv} \leq \alpha \leq 90°$)

At very high angles of attack, the crossflow dominates completely and the vortex shedding converts to the unsteady type or a random wake dependent on the Reynolds number. The normal force will decrease from the maximum, and the side force and yawing moment will decrease to zero as the AOA increases in this regime.

Of particular interest is Regime III, where the forces and moments on the slender body are strongly effected by the asymmetric vortex system. The typical boundary AOA values for the above regimes are $\alpha_{sv} \approx 5°$, $\alpha_{av} \approx 20°$, and $\alpha_{uv} \approx 60°$. [Ref. 14]

The behavior of the asymmetric vortices is well documented for numbers of models, but their cause is still not well understood. One suggested cause of vortex asymmetry at high angles of attack is the (inviscid) hydrodynamic instability in the initially symmetric vortex formation and the interaction of the vortices (which increase in strength with incidence) with the surrounding potential flowfield [Ref. 11 and 15]. The boundary layer (viscous) asymmetries due to transition and separation differences on opposite sides of the body, especially in the critical/subcritical Reynolds number region (from 2×10^5 to 5×10^5), is considered as another proposition for the vortex asymmetry [Ref. 13 and 15].

2.   Two Dimensional Crossflow

Airflow over the missile body can be divided into normal and axial components. Essentially, the crossflow is a two dimensional flow normal to a cylinder, and the axial flow follows along the missile body. In Regime III, the effective Reynolds number on a cylinder essentially equals the crossflow

Reynolds number [Ref. 16]. Thus, the sectional characteristics of a missile body should be similar to those of a two dimensional cylinder.

The mechanisms behind boundary layer transition and separation provide an explanation for flow separation and subsequent asymmetric vortex generation effects. The crossflow Reynolds number is the primary factor which influences the separation point of the boundary layer, so the Reynolds number may have a great effect on the vortex asymmetry. A cylinder in incompressible crossflow experience four distinct flow regions, which depend on the Reynolds number, each with a different type of flow separation, as shown in Figure 2. [Ref. 13]
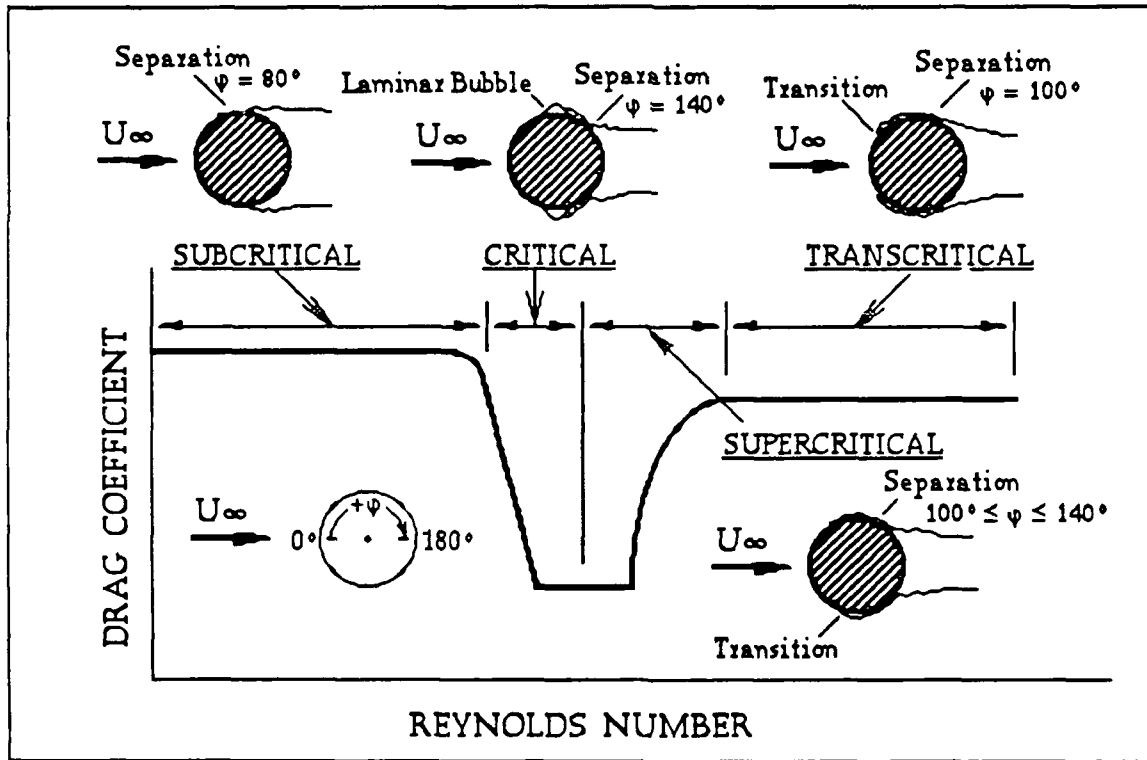
Figure 2. Flow Regions for a 2D Cylinder [Ref. 13: page 248]

In the subcritical Reynolds number region, the boundary layer is laminar, and flow separation occurs near the lateral meridian at $\varphi \approx 80°\text{-}90°$, where φ is defined as the angle from the direction of the crossflow. The side force will become noticeable if the laminar separation on both sides of the body are not exactly at the same angle φ near the lateral meridian.

When the Reynolds number increases to the critical range, the laminar boundary layer separates from the body at $\varphi \approx 90°$, followed by the formation of a laminar separation bubble and a more energetic turbulent reattachment which separates again at $\varphi \approx 140°$. The result is a reduction in wake width and drag.

As the Reynolds number increases into the supercritical region, transition moves forward of the lateral meridian without the formation of a laminar bubble and turbulent reattachment. The separation occurs at $100° \leq \varphi \leq 140°$, in response to the thickening of the turbulent boundary layer. The drag increases with this wake growth.

Finally, in the transcritical range, the laminar transition point moves towards $\varphi \approx 0°$ and turbulent separation occurs at $\varphi \approx 100°$. The drag coefficient increases and reaches a constant which is lower than the value at subcritical conditions.

The description above provides an explanation for the induced side force by the asymmetric vortex formation. The separation point is sensitive to the small change of Reynolds number, especially in the adjacent critical/ subcritical region. An asymmetry is observed in the generated vortex pair when a critical separation occurs at one side of the cylinder with a subcritical separation at the other side. The pressure difference on opposite sides of the

8

lateral meridian produces the side force. For the largest difference in φ of two opposite separation points, the vortices experience the maximum asymmetry and a maximum normalized side force results as shown in Figure 3. The asymmetric vortices may alter back and forth, even in opposite directions, causing a direction change of the induced side forces. No attempt was made to determine if the Strouhal number of the model wake was the same as for a real missile in the atmosphere.

In Figure 3, a logical progression of asymmetric vortex separation with increasing Reynolds number shows how C_Y/C_N has both maximum and minimum values in the critical Reynolds number region.
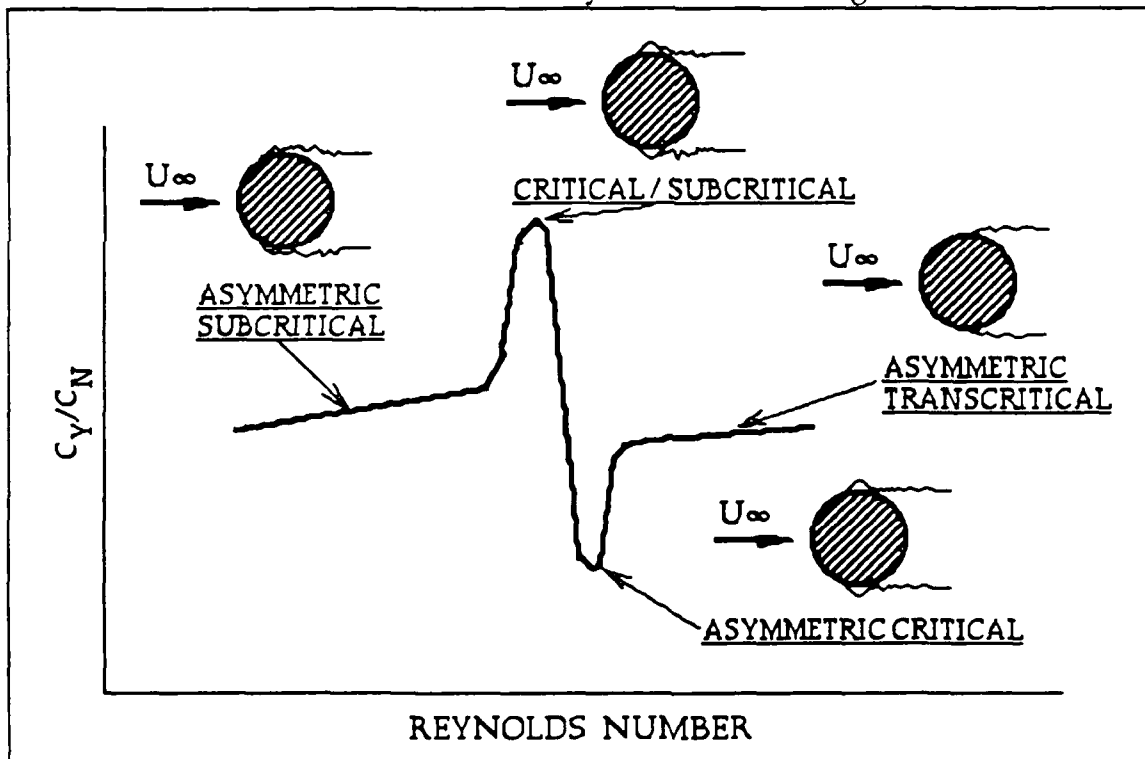
Figure 3. C_Y/C_N for a 2D Cylinder [Ref. 13: page 260]

A moderate side force is produced by an asymmetric separation near the 80°~90° meridian in the subcritical Reynolds number range. Once the

critical Reynolds number is reached, critical/subcritical separation can occur. This gives the maximum differential position between the two separation locations on the opposite sides of the body, and the maximum suction pressure differential at the lateral meridian, where there is the most effective area to produce a side force. The C_Y/C_N peak is sharp, because a relatively small increase in Reynolds number may induce an asymmetric critical separation with nearly equal suction pressures at the lateral meridian; thus, the separation asymmetry only affects the pressure at $\varphi \geq 140°$, where it is not very effective in producing a side force, and the C_Y/C_N drops to a minimum. In the results of Ref. 6, it can also be seen that there is a sharp change of sign in C_Y in the critical/subcritical region. While the Reynolds number increases through the supercritical region to the transcritical region, the flow separation asymmetry moves back to the lateral meridian where it is efficient in producing a side force again.

3. Three Dimensional Crossflow

The 3D missile model is a nose-afterbody combination, and the nose geometry of a missile, which includes the bluntness, fineness ratio, and nose roll angle, plays a great role in vortex generation and disposition [Ref. 3, 5, 9, 13, and 15]. Missile noses are dimensionlized for comparison by the nose length to base diameter ratio, defined as fineness ratio (l_n/d). Two kinds of nose shape were considered: cones and ogives, both pointed and blunt.

Two kinds of asymmetric vortex shedding are observed on cylindrical slender bodies, depending on the nose bluntness, and they are illustrated in Figure 4. On a pointed nose, the vortex asymmetry usually begins at the nose, and vortices are shed at a relatively rapid rate to give alternating side-

force cells along the slender body; thus, the side force is generated along the body length with a probable instability in direction. A slightly blunted nose delays the asymmetric-vortex initiation to the rear of the nose due to the separation bubbles which prevent the vortex to form. The alternating vortex shedding does not occur as rapidly; the side force is smaller and more stable in direction. When the asymmetric vortices are initiated at a slender forebody, they are not affected by the afterbody vortices, although the afterbody vortices still contribute to the overall magnitude of induced side forces. [Ref.13]

Thus, a small nose bluntness reduces the effects of vortex asymmetry and the induced side force. [Ref. 3, 9, and 15]

(a) Blunted nose   (b) Pointed nose
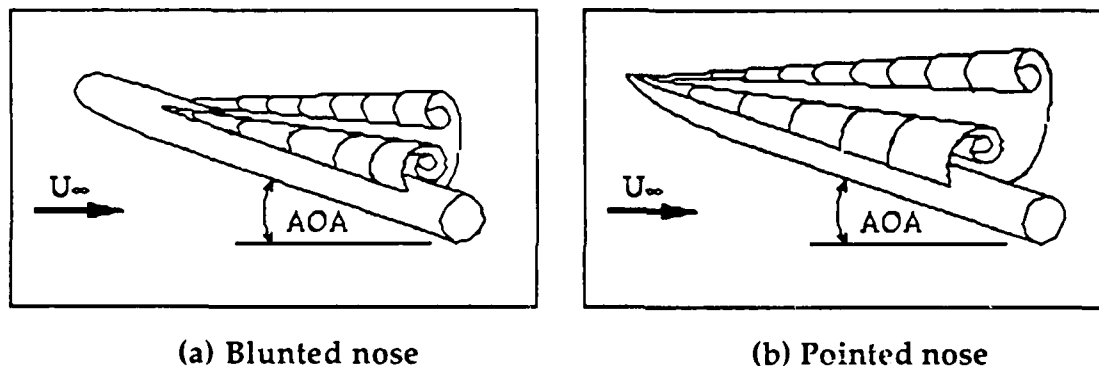
Figure 4. Vortex Flow About 3D Cylinder [Ref. 2]

For pointed conical and ogive noses, observations indicate that α_{av} is a function of the semi-apex angle θ_A [Ref. 13]. At all Mach numbers, the asymmetric vortex shedding begins when the AOA is greater than the nose apex angle; this results in $\alpha_{av} \approx 2\,\theta_A$. This suggests that increasing the nose apex angle delays the onset of asymmetric vortices to higher angles of attack, as verified by Keener and Chapman in Ref. 3.

For a conical nose, the θ_C denotes the apex internal angle of a circular cone; therefore:

$$\theta_A = \frac{\theta_C}{2} \qquad (1)$$

For a tangent ogive nose:

$$\theta_A = \text{Tan}^{-1}\left[\frac{l_n/d}{(l_n/d)^2 - 0.25}\right] \qquad (2)$$

An approximation for a slender body for equation (2) is:

$$\theta_A \approx d/l_n \qquad (3)$$

The nose apex angle is therefore a function of the fineness ratio. As the fineness ratio decreases, the nose apex angle increases and the onset AOA of asymmetric vortices will increase. Keener observed that fewer pairs of asymmetric vortices (and lower side forces) were generated on a nose of smaller fineness ratio [Ref. 15]. Thus, a smaller fineness ratio forebody would have a higher α_{av} with a smaller magnitude of side force, which is desirable.

But in supersonic flight, a blunt nose or pointed nose with small apex angle, i.e. fineness ratio, will produce a relatively stronger and detached curved shock wave which creates higher drag, while a pointed nose with large fineness ratio produces a weaker and attached oblique shock wave which generates a lower drag. Thus, a pointed forebody with high fineness ratio is a normal design for a supersonic flight vehicle.

The other factor of nose geometry is the nose roll angle (about the body longitudinal axis). Varied nose roll angles are known to cause different vortex asymmetry patterns, different side force magnitudes and α_{av} [Ref. 5, 11, and 17]. This phenomenon strongly depends on small surface imperfections near the apex and deviations in the nose axisymmetric geometry [Ref. 3, 7, and 11].

4. Effects of Other Variables in a Vortex System

The vortex system generated around a missile is also effected by the variables described below.

a. Mach Number

As the Mach number is increased, the compressibility effects in the inviscid flowfield intervene to eliminate the "drag bucket" in a 2D flow. When M_∞ falls between 0.4~0.5, the flow around the lateral meridians of the cylinder starts to become supersonic locally. This local supersonic region is terminated by a shock wave. Once M_∞ exceeds 0.5, this shock wave provides a strong adverse pressure gradient to separate the boundary layer whether it is laminar or turbulent, and Reynolds number has a less significant effect on drag generation. In a 3D flow, the crossflow Mach number, M_n, is $M_\infty \sin\alpha$. M_n shows effects similar to M_∞ in 2D flow; at $M_n > 0.4$, strong terminal shocks in the crossflow on the inclined slender body cause flow separation, which eliminates the Reynolds number sensitivity and the possibility of critical flow. Thus, the C_Y/C_N ratio peak is eliminated. [Ref. 13]

Generally, in the subsonic Mach number range, the magnitude of the side force decreases with an increasing Mach number [Ref. 3]. The longitudinal locations of the regions of primary transitional and turbulent separation, as well as vortex shedding, move rearward with increasing Mach number [Ref. 15].

The maximum C_Y reduces to a negligible magnitude for super-sonic crossflow Mach number. When the Mach number enters the transonic range (M≈0.9), the unsteady vortex shedding no longer originates from the body but rather from the wake neck in the leeward flow. The same vortex

13

pattern is observed in the supersonic Mach number region. Thus, the vortex induced side forces will not act on the missile body in the transonic and supersonic regions. [Ref. 13]

b. Lifting Surfaces

The complete vortex structure around a missile body is a super-position of the individual vortices of the body, wings, and tails.

Missiles usually use low aspect ratio wings. But in some cases, the wing span may approach the body diameter of the missiles. Wings interfere with the nose generated vortex in the wing-body junction region. The vortex is deviated from its original direction, moves closer to the body, and generally loses its well defined structure. The net effect of the wing-body combination increases the α_{av} and reduces the side force. [Ref. 4]

The strakes added in the front of wings provide more lift by generating a strake-vortex [Ref. 18]. Thus, the strakes may complicate the interaction between nose-generated vortices and the airflow over the wings. They may lessen the effect of asymmetric body vortices since the strakes interfere with the crossflow component around the body.

Generally, the tails of a missile have relatively little influence on the flowfield around the body. But the wing and/or body vortices affect the flow around the tail, especially for the missile with a long afterbody. Thus, most tail controlled missiles have short afterbodies and low aspect ratio wings with long root chords. [Ref. 19: page 172]

Most missiles have cruciform strake-wings in an "x" or "+" configuration in flight. The results in Ref. 12 for the missile being studied shows that the side forces and yawing moments remain significant in

magnitude in both wing configurations. But the asymmetric vortices are closer to the body for the "+" wing configuration, while the "x" wing configuration has a similar flowfield to that of a slender body without wings. [Ref. 12]

c. *Turbulence*

Turbulence is defined as an irregular, random, and small-scale velocity fluctuation, by comparison to the mean freestream velocity. Turbulence strength is usually represented by a "turbulence intensity" and a "turbulence length scale." [Ref. 20]

Turbulence intensity is the measure of the relative magnitude of velocity fluctuations in the flowfield. For one-dimensional flow, the relative turbulence intensity is simply the ratio of the root-mean-square value of the velocity fluctuations to the mean velocity. A higher turbulence intensity indicates a more turbulent flow.

The dissipation length scale of turbulence, L_u, is a measure of the dimension of the velocity fluctuation. The dissipation length scale used in this research, based upon the spatial decay of turbulence, is defined in Ref. 21, and is not the Kolmogroff length scale. The length scale itself is not very important, but rather the ratio of the length scale to a characteristic body dimension such as body length (L_l) and body diameter (L_d), i.e. L_u/L_l and L_u/L_d. A turbulence with a length scale on the order of the missile body diameter, so called "vortex scale turbulence," has the greatest influence on the formation of the vortex system around the missile at high angles of attack [Ref. 8]. Also, a smaller turbulence length scale of the size of the boundary

layer thickness would affect the boundary layer transitional behavior on the missile nose and therefore the formation of asymmetric vortices.

Previous research reveals some conclusions of the turbulence effects on the side force generation on the missile body. Slightly increasing the turbulence intensity and length scale reduces the side forces. Further increasing the turbulence intensity and length scale increases or maintains the side force magnitudes with a more steady vortex, and a higher side force onset AOA. [Ref. 8] The results in Ref. 8 show that grid#3 had the largest effect on maintaining side force magnitudes, due to its length scale being near the vortex scale. Therefore grid#3 was chosen as the turbulence generating grid used in this experiment.

C. FOREBODY MODIFICATIONS IN VORTEX ASYMMETRY REDUCTION

A number of forebody modifications have been made to reduce or to manipulate the formation of asymmetric vortices around a missile body, such as strakes, boundary-layer trips, beads, nose blowing ports, nose booms, and an elliptic nose tip. These methods are relatively simple to implement, both in design and in the experimental work, and generally have resulted in a successful reduction of vortex generated side forces and/or yawing moments. But they may or may not work in combination, and they do not always give consistent results, even under similar test conditions. [Ref. 3, 5, 6, 7, 9, 10, 22, and 23] Also, these design changes may induce some other adverse effects on other important factors, such as lift and drag. Some experiment results will be summarized below to provide an overview of the efforts and concepts that have been considered for mitigating the asymmetric vortex shedding.

1. Strakes

The strake is probably the simplest and the most favorable modification that has been made up to the present time. Strakes on the forebody can force the flow to separate at different positions from the usual separation points of the flow field around the slender nose. The asymmetric vortices in the leeward flow of a missile, and so the induced side forces and/or yawing moments, can be minimized or even eliminated by installing small strakes at the appropriate location on the forebody to control the flow separation point.

Results of experiments showed that properly designed strakes successfully minimized, and even eliminated, the side forces for certain configurations [Ref. 3 and 22]. Wind tunnel tests conducted on a full size vertical launch ASROC model demonstrated that the strake configuration on the nose cap reduced the mean maximum yawing moments induced by asymmetric vortices at high angles of attack [Ref. 23].

These previous studies reached several conclusions. The size of the strakes should be large enough to fully influence the flow separation location throughout the AOA range of interest; the higher the angle of attack, the thicker the strakes required to work. It was found that the length of the strakes has a more significant influence than the height (which is measured from the body surface). The primary separation point on a slender nose was found to be the most effective strake position. Finally, the radial positions of the strakes on the forebody can be manipulated to produce or to eliminate a yawing moment; this result provides a new control consideration. It should be noted, that if there is only one pair of symmetric strakes installed on the

17

nose tip, they would produce mixed results when the missile was rolled and yawed since the position of flow separation is forced by the strakes in this condition to be asymmetric; thus, multiple pairs of strakes might be expected to provide further improvement. [Ref. 3, 22, and 23]

2. Other Modifications

The purpose of the boundary-layer trip is to cause boundary-layer transition to turbulent flow, desirable because the separation point for turbulent flow is much farther around the body than for laminar flow. Experiments showed that the appropriate length strips attached at the proper position on the nose reduced the magnitude of the side force significantly. [Ref. 3]

The "helical trip" is a design in which a spiral trip is attached on the nose surface along the longitudinal axis. The principle of operation is quite simple. The flow is essentially forced by the helical trip to separate at varying peripheral locations along the forebody. This results in a different vorticity distribution preventing the shed vorticity from concentrating into discrete two-dimensional cores. Thus, the asymmetric vortices are replaced by an less coherent wake and the induced side force is suppressed. Experimental results have proven this design. [Ref. 5]

The bead has been used on the forebody tip as a surface protuberance because the vortex shedding strongly depends on the smoothness of the nose surface. Tests displayed results showing that the force asymmetry can be forced in a specific direction by the existence of a surface perturbation if it is sufficiently large relative to the local body diameter. A bead placed near the tip about 140° from the direction of crossflow was found to be most effective,

but the effectiveness is decreased with decreasing bead size and distance from the tip. [Ref. 7 and 9]

Since the nose geometry has a great effect on the vortex asymmetry, varying-cross-section noses have been designed and tested. The typical varying cross-section forebody has an elliptic tip with a circular base. The magnitude of side force associated with the roll angle rotation was not significantly alleviated by the elliptic tip. But the elliptic tip with rotation replaced the normally random behavior of the nose side force as a function of nose tip orientation with a predictable and generally sinusoidal distribution, and in this manner, would be considered as a device to give additional directional control for the vehicle. A fixed elliptic ogive nose was shown to have a significantly lower onset AOA for induced side forces than that of the corresponding circular ogive nose with the same fineness ratio. [Ref. 3 and 10]

The nose boom is another change of nose geometry. Many aircraft use a nose boom extending ahead of the fuselage to mount pitot-static pressure systems and systems that measure the flow angle, but it is unusual to be seen in a missile derign. The tests made on the forebodies with nose booms gave good results in which the magnitudes of side forces were greatly reduced. [Ref. 3 and 5]

All of the modifications and devices discussed above are static and passive. Some dynamic and active devices have also been introduced. One example is the "rotating tip." This idea originated from the observation that the side forces varied with nose roll angle. The cyclic variation of the side force with roll angle suggested that the tip rotating at an appropriate rate

should subject the body to the time average of the side force, which is hopefully zero. With the rotation of the tip, the vortices may not have enough time to fully develop in the flowfield before switching to a new pattern, thus preventing the strength of the vortex from being adequate to induce side forces and/or yawing moments. It was reported that a nose with a tip rotating at a constant spinning rate had a dramatic reduction in the side force. [Ref. 5]

The other dynamic device for forebody control is the jet blowing port. The ports are installed on the forebody to generate side forces and yawing moments. The magnitudes and directions of the side force and yawing moment could be controlled by the port location, blowing direction (normal or tangential, forward or aft) and blowing rate. [Ref. 18 and 22]

D. VLSAM LAUNCH ENVIRONMENT

1. Marine Environment

Conditions in the marine atmospheric environment may have a significant effect on the VLSAM. The atmospheric boundary layer (ABL) is the result of the interaction of the atmospheric flow over the land or sea surface. This layer is characterized by a turbulent transfer of momentum, heat and mass (water vapor) and their associated gradients.

The surface layer, the lowest 10% of the ABL, is approximately 50 meters high. It is characterized by turbulence, produced mechanically from the ocean surface roughness and friction, with nearly constant vertical fluxes of momentum, heat and mass.

The lowest portion of the surface layer is called the roughness layer and is where the surface has the greatest effect on generating turbulence and

influencing fluid motion. Naturally, the mean flow in the roughness layer is nonhomogeneous and three-dimensional. Small scale turbulence dominates the flow near the surface. As the altitude increases, small scale turbulence decreases rapidly as large scale turbulence formed by convective conditions prevails. The mean flowfield becomes almost horizontally homogeneous and two dimensional at further higher altitudes. [Ref. 24]

The roughness length, Z_0, is a measure of the surface roughness as a function of the mean wind velocity at various elevations above the surface. Surface turbulence length scale and intensity are empirically determined by combining the roughness length with the altitude and wind speed. For the largest mean wind speed about 25 m/sec ($\approx$ 49 knots) at a 10 meters elevation and a typical open ocean roughness range, $10^{-3} < Z_0 < 10^{-2}$ meters, the turbulence intensities are on the order of 13% to 17% with a turbulence length scale in the range $80 < L_u < 90$ meters (or $262 < L_u < 295$ feet). [Ref. 25]

As mentioned previously, the turbulence length scale to body dimension ratio is an important factor for flowfield behavior. Thus, for a typical missile with a 1.1 foot diameter in the atmosphere conditions stated in the last paragraph, the turbulence length scale to missile diameter ratio is about $L_u : L_d \approx 280 : 1$, and would have little effect on its boundary layer development. But this initially large length scale turbulence and crosswind would be distorted, by interacting with the ship's superstructure, to vortex scales which might influence the generated vortices, and to boundary layer scales which could affect the boundary layer of the flowfield around the missile [Ref. 17].

2. Launch and Crosswind Velocities

A typical VLSAM launched with a 10g acceleration reaches an altitude of about 56 feet, 0.2 seconds after leaving the launcher, with a vertical velocity of approximately 164 fps. The VLSAM is still in the surface layer environment (about 164 feet above the surface) and is subjected to crosswind and turbulence effects. For instance, for a ship moving at 20 knots (≈34 fps) with a mean crosswind speed of 20 m/sec (≈66 fps) [Ref. 24: page 64], the maximum combined crosswind speed is about 74 fps. In a two-dimensional system, this crosswind velocity and missile vertical velocity will give the resultant wind speed of approximately 180 fps at an angle of 24.4° from the missile direction. This places the missile in Regime III, the asymmetric vortex regime, almost right after its tail clears the launcher. [Ref. 2]

An effective AOA up to 50° may be reached by a VLSAM when it pitches over towards the target [Ref. 26]. These examples indicate situations for the apparent possibility of asymmetric vortices formed on a VLSAM during both launching and maneuvering phases.

3. Ship Airwake

The hull and superstructure of the ship drastically change the freestream flowfield and turbulence conditions. The airwakes of most ships are highly turbulent, recirculating flows with very steep velocity gradient. The typical sharp edges of the boxy-configurations of most ships act as a very effective turbulence generator.

4. Additional Considerations

There are many factors which affect the aerodynamics of a VLSAM during the launching phase. These factors can be divided into two categories.

One category is due to the design of missile itself, such as jet effects of the missile engine, blast effects of the vented exhaust gas, and activation of the flight control systems. Another category is due to the launch platform, such as the rolling, pitching and yawing motions of the ship.

The VLSAM is launched directly from its canister (launcher). In this way, large amounts of exhaust gas would be constrained in the canister. The large adverse pressure gradient forces the exhaust flow to be turned upstream into the annular gap between the missile and the launcher wall. These hot gases may severely interact with the flowfield around the missile and cause critical heat-transfer problems. [Ref. 27]

Also, the uncontrollable motions of the platform would be transmitted to the VLSAM before it clears the launcher, and add to the complexity of the initial velocity vector of the missile. An attempt could be made at an analysis of a missile launch from an ideal platform, which would cause no significant change to the statistics of neutral atmospheric winds. The properties of the latter are well known.

These considerations briefly described above show the multiple factors which may influence the VLSAM flowfield and complicate an understanding of the launch flowfield during the launch phase. These factors make a fully comprehensive flowfield analysis of the VLSAM more difficult, and are beyond the range of this research to quantify.

II. EXPERIMENT AND PROCEDURE

A. APPARATUS

The experimental investigation was conducted at the Naval Postgraduate School low-speed wind tunnel test facility. The VLSAM model was mounted on a six-component strain gage balance and sting support assembly. The turbulence generating grid and the test facility steady-state data acquisition hardware/software complete the experimental apparatus to be discussed in this section.

1. Wind Tunnel

The low-speed tunnel used for this experiment is located in the Naval Postgraduate School wind tunnel test facility and shown in Figure 5. The power section of the tunnel is comprised of a 100 hp electric motor coupled to a three-bladed variable pitch fan by a four-speed Dodge truck transmission. The fan is operated in a duct of essentially constant cross-sectional area; thus, its effect is to increase the pressure of the air rather than the velocity. A set of stator blades directly follows the fan to straighten the flow. Turning vanes are installed at each corner to reduce the turning losses in the air flow. Two fine wire mesh screens are installed in the settling chamber to reduce any flowfield turbulence in the test section. The contraction cone between the settling chamber and test section accelerates the air, and has an approximate ratio of 10:1. The diffuser following the test section converts the kinetic energy of the air into pressure, and a heavy wire mesh

screen at the end of the diffuser is used to prevent any foreign object damage to the fan.
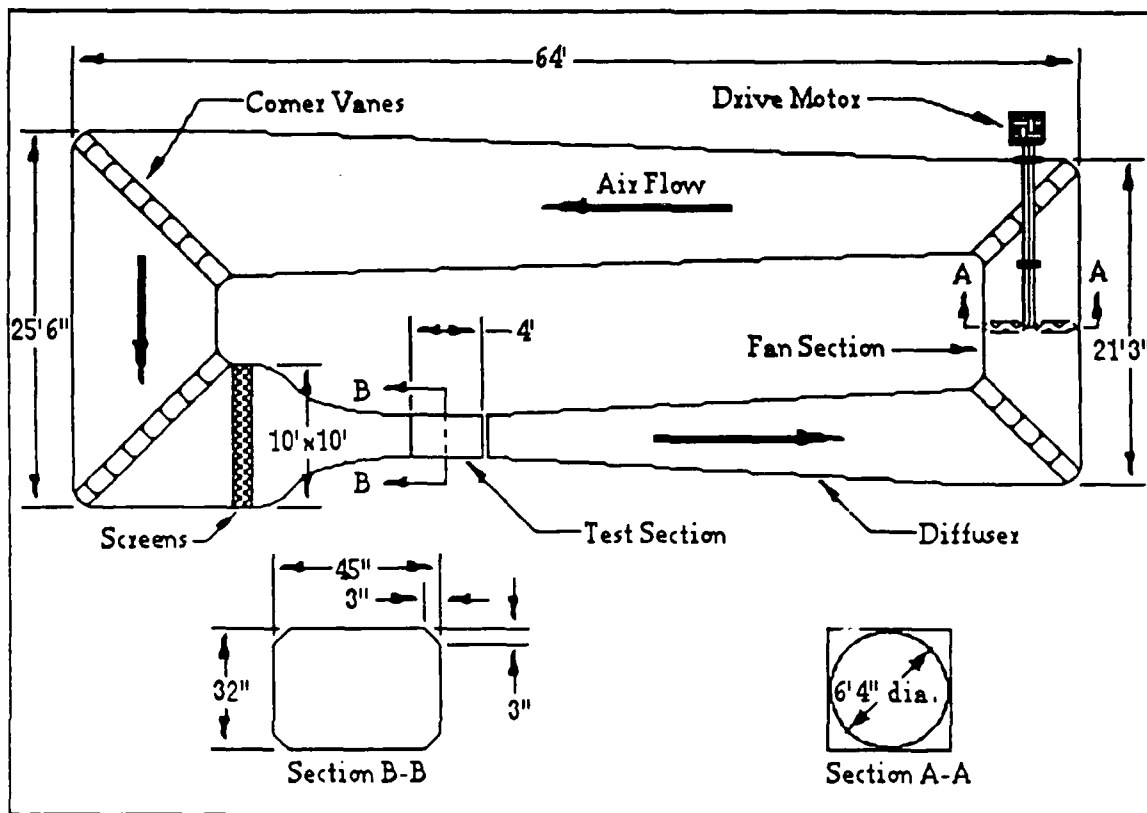
Figure 5. Naval Postgraduate School Low Speed Wind Tunnel

The test section measures 45 by 32 inches, and was modified with frosted-light glass corner fillets to provide illumination of the test section and reduce the boundary layer effects at the wall intersections.* Immediately downstream of the test section is a breather slot of 5% tunnel-diameter width which extends completely around the tunnel, and allows air to enter and

---

* The fillets reduce the area of the test section from 10 ft^2 to 9.875 ft^2. Fillets without lights are employed throughout the wind tunnel at wall intersections

leave the tunnel for compensating the leakage losses and ensuring an uniform test section pressure. A reflection plane located 4 inches above the floor in the center of the test section provides a horizontal surface to the flowfield, and a flush turntable at the center allows the operator to change the angle of attack of the model during wind tunnel operation.

Temperature in the wind tunnel is measured by a dial thermometer extending into the settling chamber. Dynamic pressure, q, is obtained by measuring the static pressure difference, Δp, between the test section and the settling chamber using a water-filled micromanometer. Four static pressure taps, one on each wall in the settling chamber, are used to measure the static pressure; the test section has similar static pressure taps, one on each wall, upstream of the test section to preclude interference from the model. The pressure taps at each section are connected via a common manifold prior to feeding into the manometer. The manometer measures the pressure difference in cm H_2O, which can be used with a calibration factor to determine the test section dynamic pressure. [Ref. 28: page 11-14]

2. VLSAM Model

The VLSAM model was designed to be representative of a cruciform tail-control missile with four very low aspect ratio wings. This model was fabricated from aluminum alloy by Naval Postgraduate School personnel.

Four major parts form the model. The body section is a hollow cylinder with locating pin attachment points for the balance, sleeve, wings and tails. The body mounts on the balance which attaches rigidly to the sting mount. The body can be rolled to obtain two test body-wings configurations: "+" and "x". The nose portion attaches to the body forward of the balance.

The nose roll angle can be varied in 45° increments independent of the body orientation. The nose is a tangent ogive* following by a short constant diameter section, which has the same diameter as the body section and provides an interference-free interface between the ogive and the body. Four low aspect ratio wings with strakes comprise the cruciform wing section and are mounted equilaterally in fixed positions along the model axis. Four tail control fins are mounted aft of each wing, and are also fixed. All parts are rigidly connected to the model body by countersunk machine screws.

Detailed dimensions of the VLSAM model are shown in Figure 6, and some of the key dimensions are listed below:

$$\text{Total length, } L_l = 22.85 \text{ in.}$$

$$\text{Body diameter, } L_d \text{ or } d = 1.75 \text{ in.}$$

$$\text{Length/diameter ratio, } L_l/L_d = 13.06$$

$$\text{Ogive nose length, } l_n = 4.0 \text{ in.}$$

$$\text{Ogive radius} = 9.58 \text{ in.}$$

$$\text{Nose fineness ratio, } l_n/d = 2.29$$

$$\text{Wing span/root chord} = 3.11 \text{ in. } / 13.455 \text{ in. } = 0.231$$

$$\text{Tail span/root chord} = 5.51 \text{ in. } / 1.70 \text{ in. } = 3.241$$

$$\text{Moment center of balance, } x_m = 13.375 \text{ in. aft of nose tip}$$

$$\text{Moment center/total length, } x_m/L_l = 0.585$$

---

* A tangent ogive nose is constructed from an intersection of two constant radius arcs.
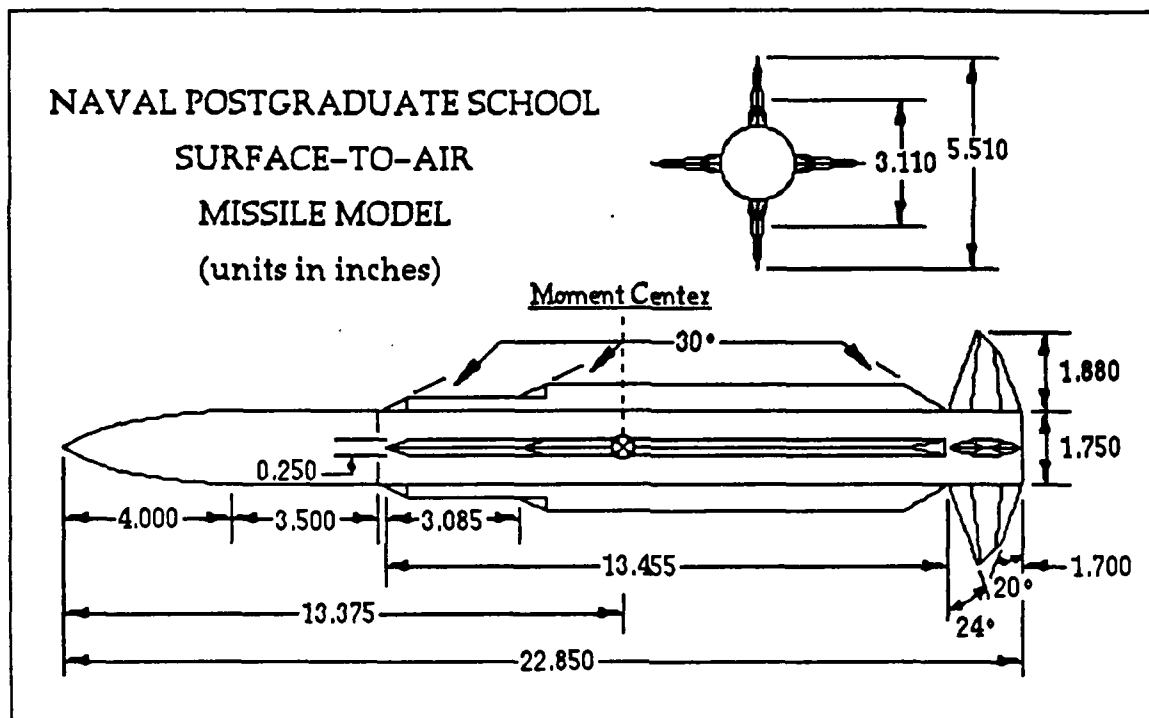
Figure 6. Drawing of VLSAM Model

3. Strake

The brass strake was designed to investigate its function, by fixing the separation point of the air flow from the forebody, to eliminate or reduce the asymmetric vortices generated at the missile nose, in order to decrease the magnitude of the side force which might cause the missile to miss its target. The curvature of the strake is based on the curve shape of the ogive nose of the model; the strake lies on the nose surface with a nominal constant height, h, measured perpendicular to the nose surface. Due to the curvature, the actual strake height measured from the nose surface and perpendicular to the model axis decreases from 0.038 in. to 0.036 in. The strake tip was pointed. Its dimensions are shown in Figure 7 and are listed below:

$$\text{Height, h} = 0.035 \text{ in.}$$

$$\text{Height/body diameter ratio, h/D} = 0.02$$

28

Thickness, t = 0.025 in.

Length, l = 1.25 in.

Length/body diameter ratio, l/D = 0.71
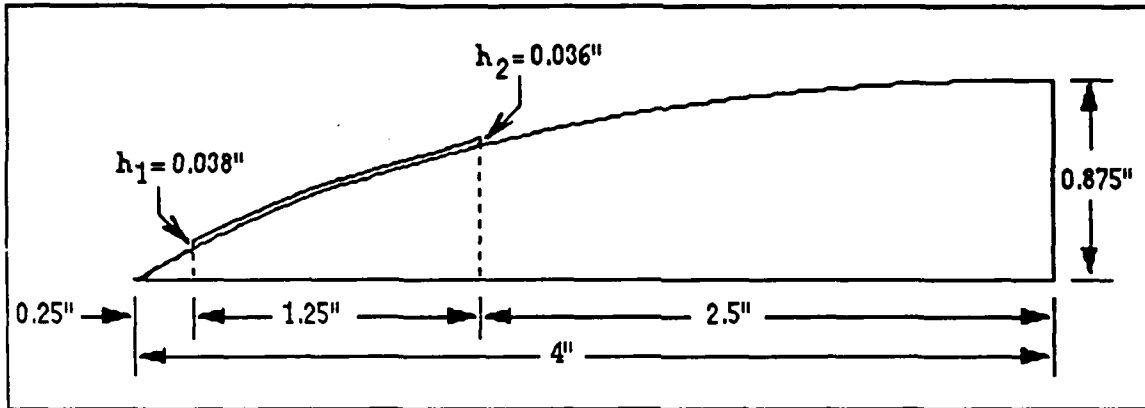
Figure 7. Drawing of Strake on Model Nose

4. Balance

Force and moment measurements were taken with a one-inch diameter, six-component strain-gage precision balance. The balance was borrowed from NASA Ames Research Center under the Navy-NASA Joint Institute of Aeronautics in 1987. It was calibrated by NASA Ames personnel; the calibration data, data conversion values, maximum channel loads and percent accuracies (based on maximum load) are listed in Appendix A [Ref. 29]. Each channel has a wheatstone bridge circuit to measure positive and negative strain of a specific direction. The output consists of two normal force (N1,N2), two side force (S1,S2), one axial force (A), and one rolling moment (R) channels. The output directions are relative to the model axes. A 21-foot cable which is comprised of several very fine gage wires with a woven nylon sheath, was used to transmit the balance output to the signal conditioner in the data acquisition system.

A machined sleeve provided a close tolerance fit between the balance and the interior of the VLSAM model. One locating pin was used to seat the model to the balance. The balance was supported by a hollow sting which was connected to the mounting arm and secured by two pins.

5. Model/Balance Support

The VLSAM model and balance support assembly was rigidly fixed in the wind tunnel test section by the reflection plane turntable at the base and by an aluminum reinforced clear acrylic section at the top. By rotating the turntable, the sting mount changed the model pitch in the horizontal direction with the pivot point at approximately the moment center of the balance. The sting mount had a small cross-section (2.8% maximum at AOA = 90°) to the air flow for all AOA to reduce blockage effects. Thus, sting interference corrections were ignored. The reflection plane turntable sits on a heavy-weight pedestal to prevent deflections and vibration. This entire assembly was driven via a chain gear drive powered by an electric motor. The pitch angle and pitch rate are controlled by the operator with the motor controller. A photograph and a illustration drawing of the sting mount with model set-up in the test section are shown in Figures 8 and 9.
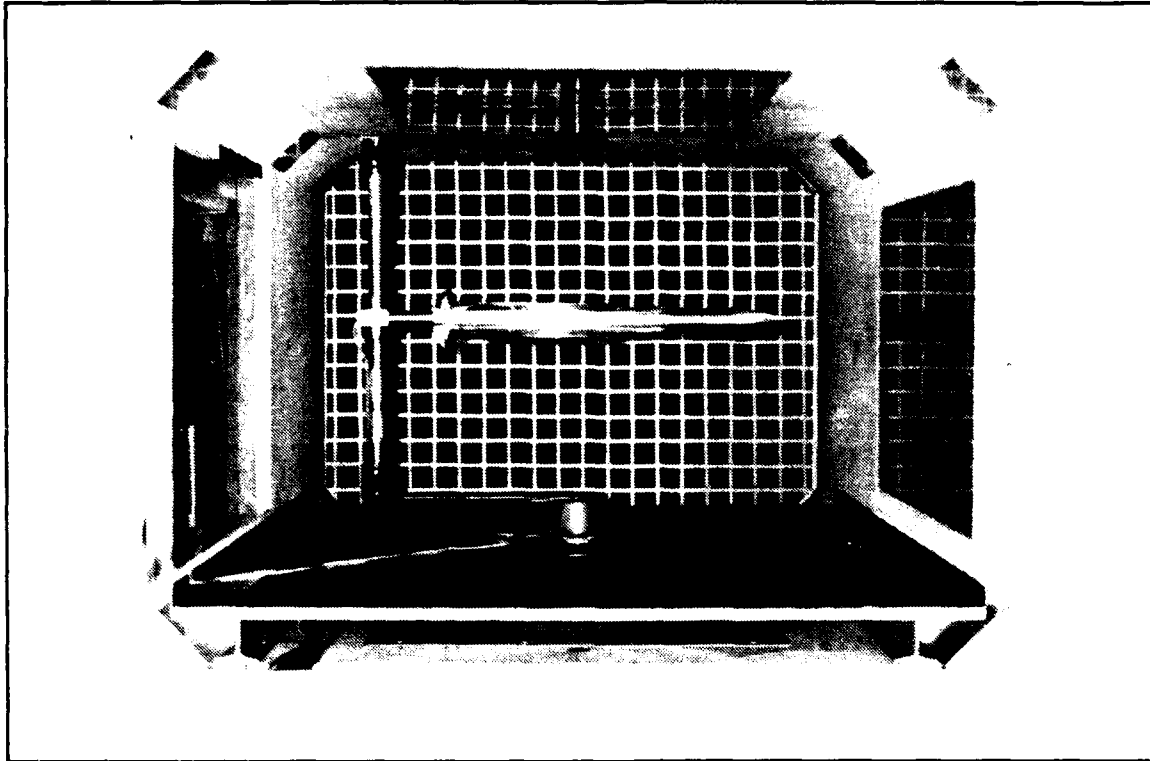
Figure 8. Photograph of VLSAM Model in Test Section
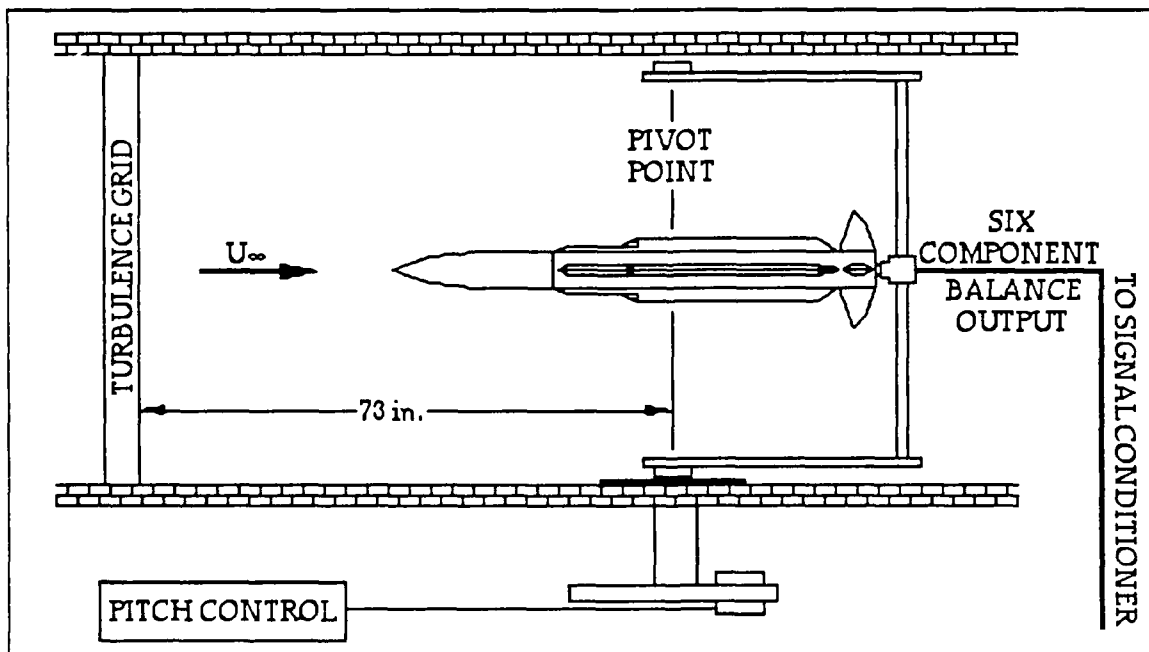
Figure 9. Illustration Drawing of VLSAM Model in Test Section

31

6. Turbulence Grid

The turbulence grid was designed to generate nearly isotropic homogeneous turbulence in the low speed wind tunnel. The biplanar wooden grid was of a 0.5-inch square bar, 2.5-inch square mesh design, and was installed 73 inches upstream of the model sting mount pivot point. At the pivot point, the turbulence intensity was determined to be 1.88% with a 1.08 in. length scale. The grid used in this thesis investigation was grid#3 used in Ref. 2; the dynamic pressure used in Ref. 2 was 16.38 lb/ft^2 which is close to the dynamic pressure used in this thesis, 16.55 lb/ft^2, which was used to keep a Reynolds number $\approx$ 110,000. The method used to determine the turbulence intensity and length scale is described in Ref. 2. The turbulence intensities and length scales downstream of the turbulence grid along the center line of the wind tunnel are plotted in Figures 10 and 11. [Ref. 2: page 44-49]

The location of the turbulence grid in the wind tunnel can also be noted in Figures 8 and 9.

At the test section, the grid generated turbulence-length-scale to model-length ratio is 0.047, and the length-scale/model-diameter ratio is 0.62. These values suggested that the turbulence effects on the flowfield and vortices may be due to boundary layer scale and/or vortex scale turbulence.

The turbulence conditions for changing length scale at constant intensity and changing intensity at constant length scale are not possible with the present grid turbulence geometries. Furthermore, no information is available for the spectra of the velocity fluctuations.
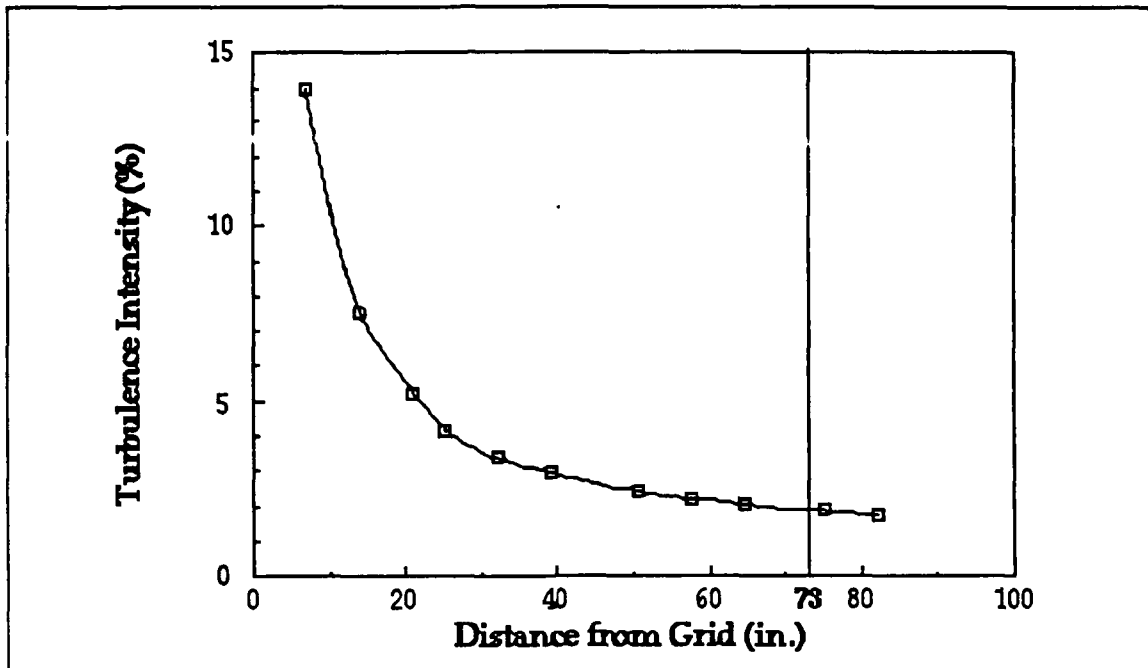
Figure 10. Grid-Generated Turbulence Intensity Curve [Ref. 2]
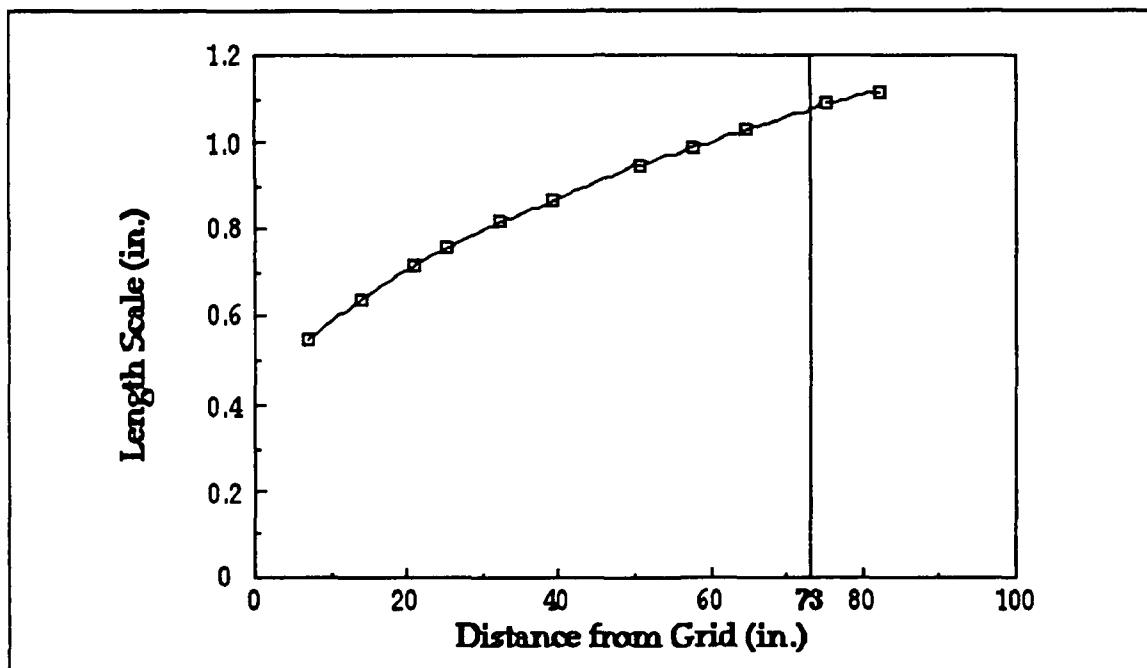
Figure 11. Grid-Generated Length Scale Curve [Ref. 2]

33

7. Data Acquisition Hardware

The data acquisition hardware consisted of the test facility components to operate the precision balance in the wind tunnel and to record data.

First, the six channels were connected to a signal conditioner. Each strain-gage in the balance was supported by a signal conditioning circuit which supplied the excitation voltage and allowed for zeroing and calibration of the balance circuit.

Second, the output of each channel from the signal conditioner was fed into the Hewlett-Packard PC Instruments 61011A relay multiplexer which sequentially sampled each signal of six channels. The channel selection of the relay multiplexer was automatically controlled by the PC Instruments software in the data acquisition software. [Ref. 30]

Third, in order to improve the resolution for small magnitude signals, the sequentially-sampled signal was fed through a low-noise amplifier with an adjustable gain up to 1000. The amplifier was zeroed and calibrated by adjusting two screws on the front panel. [Ref. 31]

Fourth, the signal was sent to the Hewlett-Packard PC Instruments 61013A Digital Multimeter (DMM) which measured the amplified D.C. voltage signals. The DMM has a 4 1/2 digit Analog-to-Digit converter to convert the analog signals into digital signals for use by the data acquisition program. It automatically selects the optimum voltage range for measuring the signal, and was set to take measurements continuously at 2.5 readings/second rate to obtain higher accuracy. The DMM is under the control of the PC Instruments software. [Ref. 30]

34

Finally, an IBM-AT microcomputer executed the data acquisition software and stored the collected data. A Hewlett-Packard Interface Card installed in the microcomputer provided the connection to the DMM and relay multiplexer.

Additionally, the wind tunnel measurement apparatus is also a part of the data acquisition hardware. The components are shown in Figure 12.
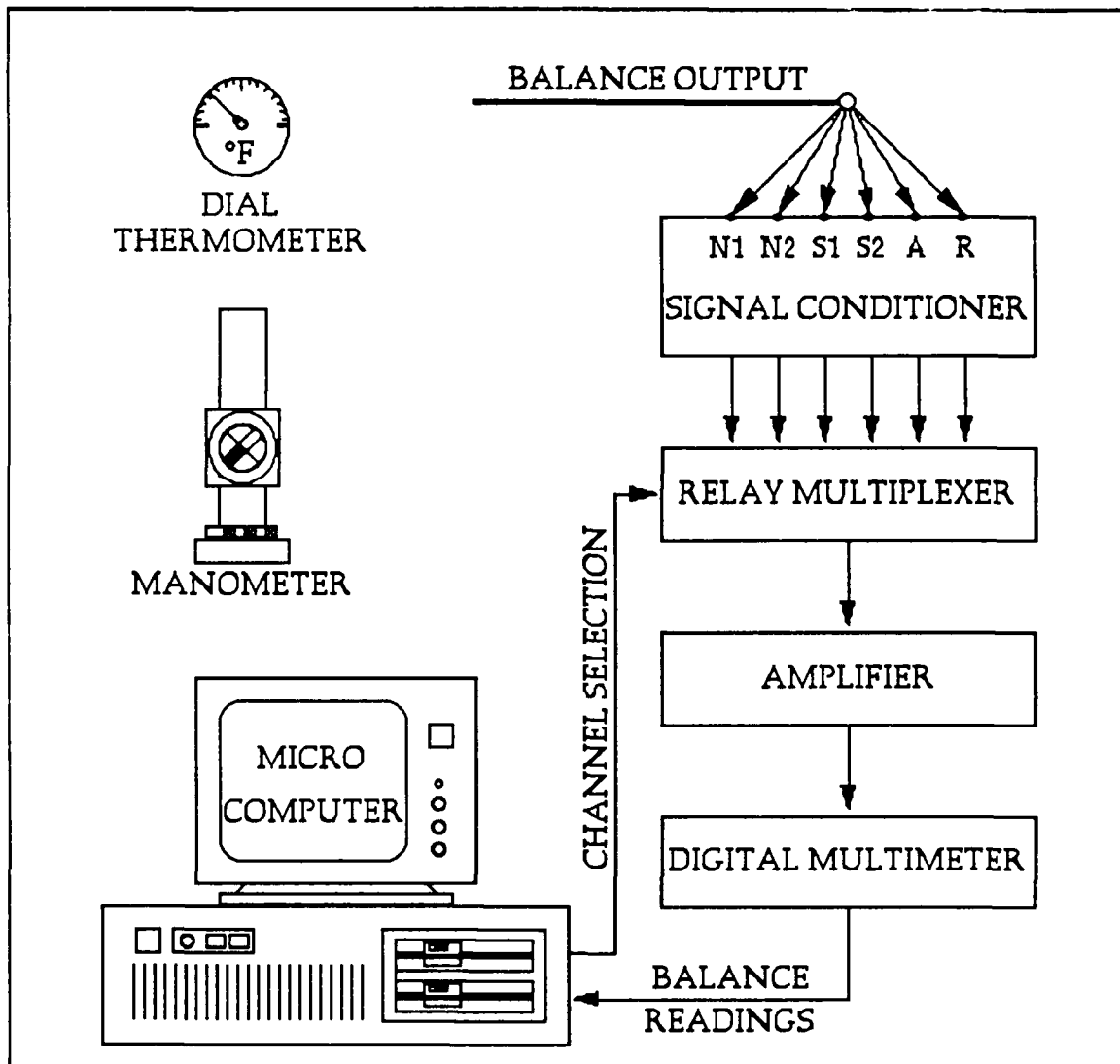
Figure 12. Data Acquisition Hardware

8. Data Acquisition Software

The data acquisition software consists of three computer programs:

a. PANELS Program

The PANELS program enables all the functions of the Hewlett-Packard PC Instruments, and provides a video readout on the computer screen for the operation of each instrument. In this thesis project, PANELS was used to operate the DMM and relay multiplexer for adjusting the excitation voltage of each of the six balance channels, and for calibrating/balancing the amplifier and the bridge circuitry of each channel. [Ref. 30]

b. READ.BAS Program

The READ program, written in BASIC, is embedded within the SHELL program that also controls the DMM and relay multiplexer. The READ.BAS sampled the six amplified/digitized channel output voltages ten times by the sequential action of the relay multiplexer. Then, the readings were averaged and combined with the appropriate balance calibration constants and conversion factors (listed in Appendix A) to yield the force and/or moment reading for each channel. Calculations were performed by using force and moment readings of each channel to obtain normal, side and axial force measurements in pounds and the pitching, rolling and yawing moment measurements in foot-pounds. The taring data, obtained at the beginning of execution of READ.BAS without any dynamic forces in the wind tunnel, were subtracted from these measurements to deduct the static forces and moments not zeroed out during balance zeroing. The final data were stored in files on both hard disk and floppy disk. This program also recorded

the test conditions to be discussed in the next section. The listing of this program is provided in Appendix B.

c. COEFF.BAS Program

The COEFF program, also written in BASIC, translated the force and moment values into dimensionless coefficients based on the model parameters, test conditions and blockage corrections. It also provided a hardcopy of the reduced data, which included the test conditions, force and moment values, and dimensionless coefficients. The listing of this program is shown in Appendix C.

B. EXPERIMENTAL CONDITIONS

There are many variables which could affect flow separation and vortex structure at high angles of attack. In order to concentrate on the purpose of this project, the experimental conditions were simplified by keeping the following variables as constant as the situation would allow:

- Reynolds number $= 1.15 \times 10^5$.
- Test section dynamic pressure $= 16.55$ psf.
- Test section velocity $= 111 \sim 114$ fps.
- Test section Mach number $= 0.11$.

The settling chamber temperature was kept in a 20°F range above the starting temperature for each run, so that the test section air density could be kept as constant as possible. If the temperature exceeded the maximum allowable value, the runs were interrupted; before operation was resumed, the tunnel air was exchanged by running the tunnel at low speed, in order to cool the air down to within 5°F of the starting temperature.

The vibration of the wind tunnel itself during operation was not controllable. Also, the dynamic vibration and deflection of the sting mount due to the air flow were beyond control. Once the turbulence generating grid was installed in the wind tunnel, higher energy in the air flow was required to keep the desired dynamic pressure; thus, more severe dynamic vibration was observed in the air flow.

Three main test conditions–wind tunnel condition, body configuration, and forebody configuration–were investigated and will be discussed in this section. These three different test conditions were kept unchanged for each individual test, but were varied for different tests to compare the results. In each test, the angle of attack was varied from -5° to 90°, in order to see the traces of coefficients for specific experimental conditions. The actual test conditions of each experiment are listed in Appendix D.

1. **Wind Tunnel Test Condition**

The turbulence-generating grid installed in the wind tunnel was used to simulate flowfield turbulence of a scale of the nose-generated vortices. Thus, a "turbulent" test condition was obtained by installing the turbulence-generating grid in the wind tunnel, while the wind tunnel without a grid gave a "non-turbulent" test condition (an ambient value of 0.2%).

Ideally, the static pressure difference (Δp) between the settling chamber and the test section is directly related to the dynamic pressure (q) at the test section. In general, the relationship between q and Δp should be essentially linear. Additionally, a turbulent flow generated by the grid in the wind tunnel greatly decreases the dynamic pressure in the test section, and the grid framework causes wall boundary layer separation interfering with the test

38

section static pressure ports. Thus, an experiment was necessary to examine the relationships between q and Δp for both "non-turbulent" and "turbulent" wind tunnel conditions. This experiment was conducted with an ambient temperature = 60°F and a 29.92 in.Hg ambient pressure. A pitot-static tube was placed in the center of the test section without any other objects in the test section in order to eliminate any interference. At the location of the tube, 70 inches ($\approx$ 30 mesh diameter) downstream of the grid, the flow should be nearly isotropic and homogeneous [Ref. 32]. While the wind tunnel was running, with a grid and without a grid, the output of the pitot-static tube equalled the dynamic pressure in the test section, and the static pressure difference was read from the manometer. No attempt was made to correct the static pressure reading for possible errors due to the transverse turbulent fluctuations. Several measurements were recorded and are listed in Table 1, and plotted in Figures 13 and 14. Two linear equations were obtained from the experiment data; both q and Δp are in units of cm. H_2O:

$$q = -0.027 + 1.115\,\Delta p \qquad \text{(non-turbulent)} \qquad \{4\}$$

$$q = 0.019 + 0.696\,\Delta p \qquad \text{(turbulent)} \qquad \{5\}$$

These are actually the wind tunnel correction factors for two different wind tunnel test conditions. The dynamic pressure in this research experiment was kept constant at 16.55 psf. (8.09 cm. H_2O). The corresponding manometer readings calculated from equations {4} and {5} are 7.28 cm. H_2O for "non-turbulent" and 11.60 cm. H_2O for "turbulent" wind tunnel test conditions. The manometer reading was set at the above value, depending on the test wind tunnel condition, and was kept constant by adjusting the pitch angle of the fan through one test run.

TABLE 1. EXPERIMENTAL DATA FOR WIND TUNNEL CALIBRATION FACTOR

WITHOUT GRID (NON-TURBULENT)		WITH GRID (TURBULENT)	
Δp (cm. H_2O)	q (cm. H_2O)	Δp (cm. H_2O)	q (cm. H_2O)
0.00	0.00	0.00	0.00
3.11	3.43	2.76	1.96
5.07	5.61	4.94	3.45
8.27	9.12	7.10	4.98
9.87	11.05	10.29	7.16

$$q = -2.6749\,e\text{-}2 + 1.1149\,\Delta p$$
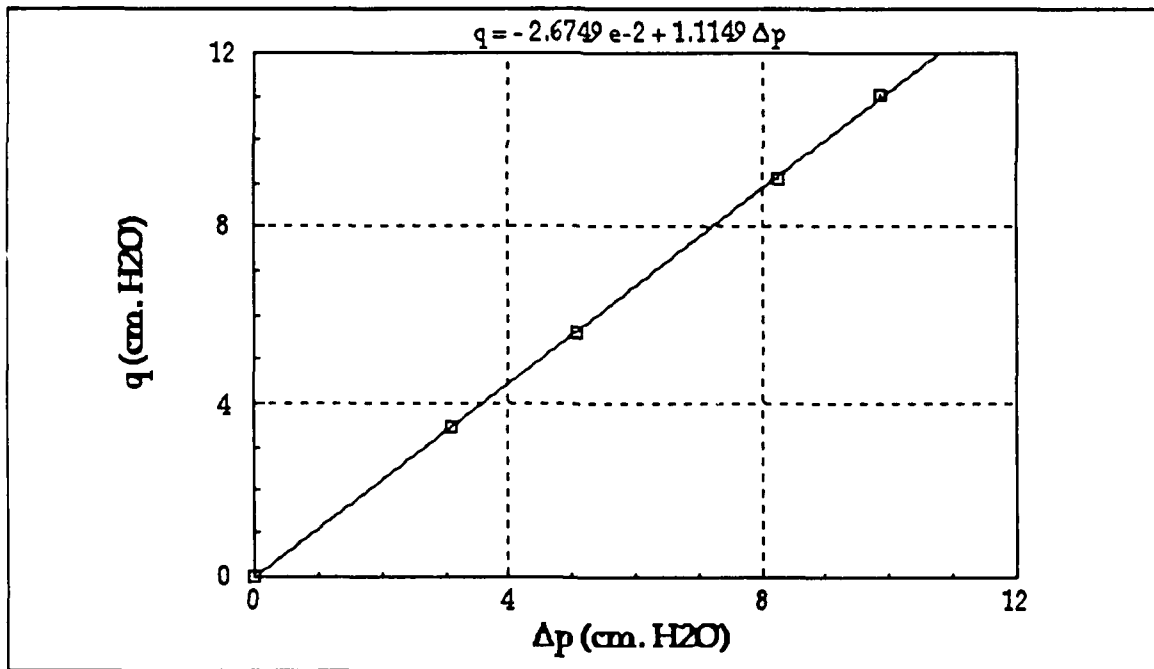
Figure 13. Calibration Factor Plot for "Non-turbulent" Wind Tunnel
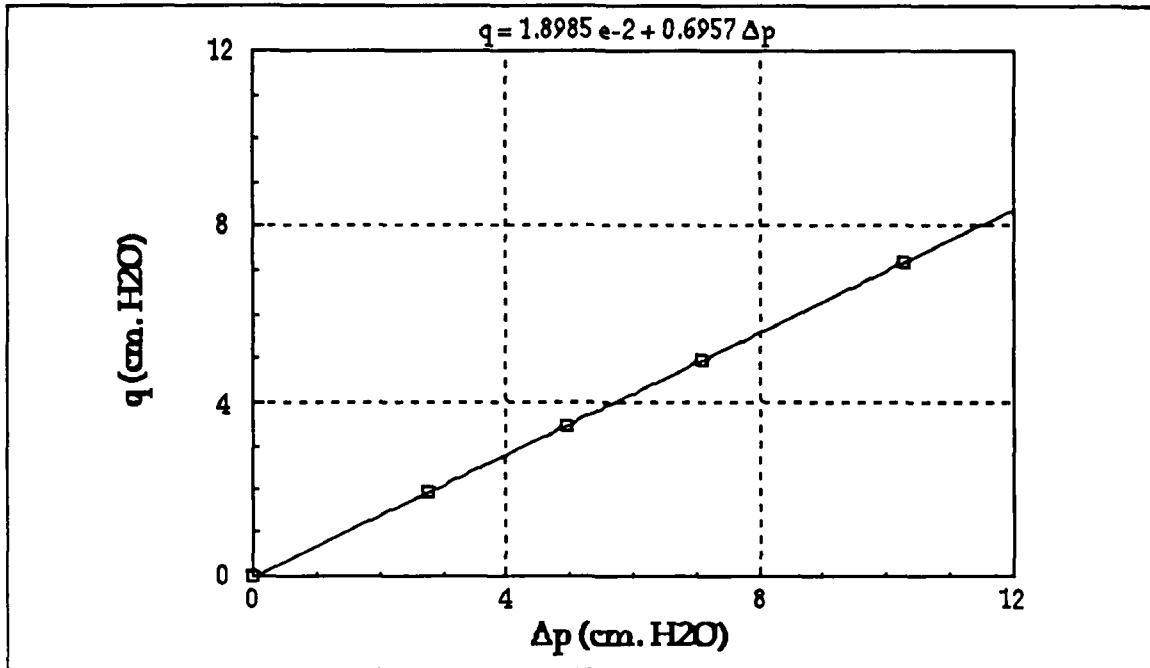
Figure 14. Calibration Factor Plot for "Turbulent" Wind Tunnel

2. Body Configuration

Three different VLSAM model body configurations were used; one without wings was used in preliminary runs only, and the other two with wings at different roll angles were chosen to examine the effects of the wings on the asymmetric vortices. They are shown in Figure 15.

"BODY 0" has no wings, but has four tail surfaces due to the difficulty of removal with the balance in place. It was decided that the effects of the tails on the nose-generated vortex system were minimal and the same for all cases. The body-tail configuration has a right roll angle $\phi_R = 45°$. This configuration was used in the preliminary runs to examine the forebody roll angle which exhibited the maximum side force coefficient.

"BODY 1" is a complete body-wing-tail configuration with a zero roll angle, and the wing-tail forms a "+" configuration.

Another complete body-wing-tail configuration is "BODY 2" whose roll angle is set at ϕ_R = 45° with wing-tail in an "x" configuration.

In all cases, as the body roll angle changed, the forebody roll angle remained fixed. "BODY 1" and "BODY 2" were chosen and fixed in each test to compare the effects of different body configurations.
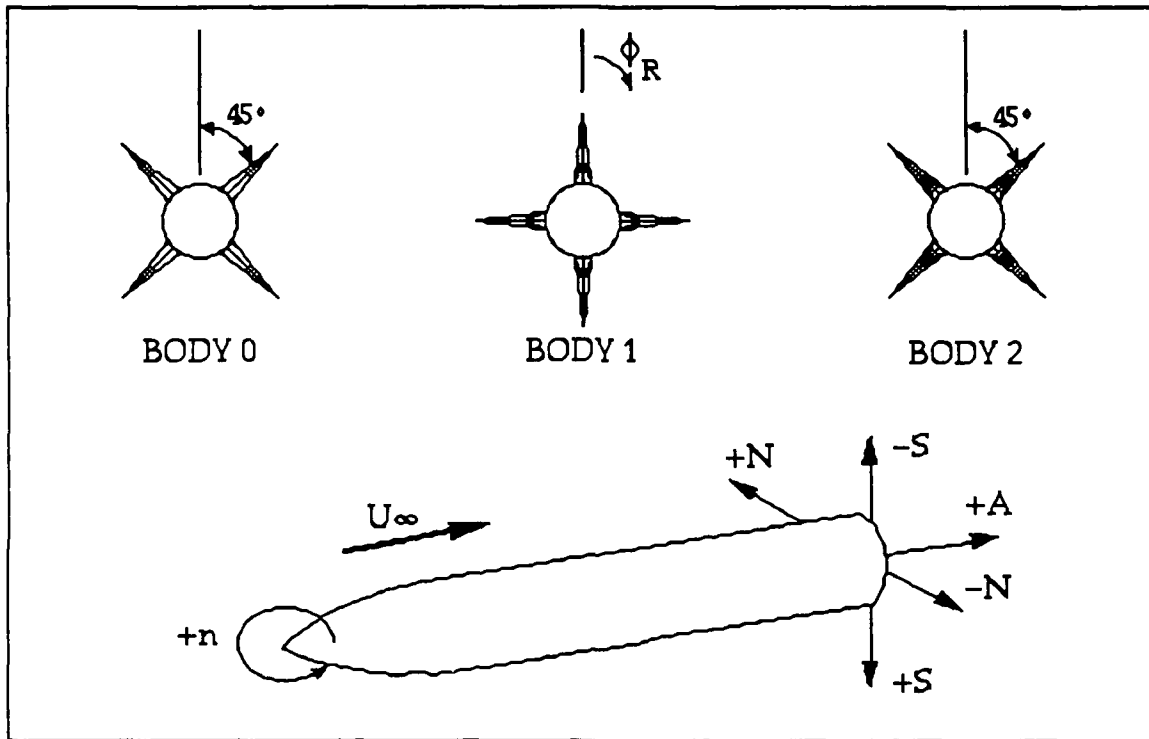
Figure 15. Body Configuration and Reference System

3. Forebody Configuration

The main goal of this experiment was to determine the influence of the forebody strakes on the high angle of attack aerodynamics of the VLSAM model, in particular the effect on the magnitudes and directions of side force and yawing moment.

Four and eight strakes installed symmetrically on the forebody were tested. In order to investigate the effects of strakes on the asymmetric

42

vortices, the number of strakes was fixed in each test, and the results were compared with the clean configuration without strakes.

The clean forebody, "NO STRAKE" nose, was tested in the baseline runs to generate the baseline traces for certain body-wing-tail configurations and wind tunnel conditions.

"4 STRAKES" had four strakes on the forebody in the "+" configuration without roll angle with respect to the reference plane. This configuration is shown in Figures 16(a) and 17(a). The nose roll angle was fixed at that which exhibited maximum side force in the preliminary runs. The strakes were secured on the forebody with grooved slots and epoxy; thus, a forebody with 4 strakes in the "x" configuration could not be tested.

"8 STRAKES" adds four strakes in the "x" configuration with a 45° roll angle on the "4 STRAKES" nose, and is shown in Figures 16(b) and 17(b).
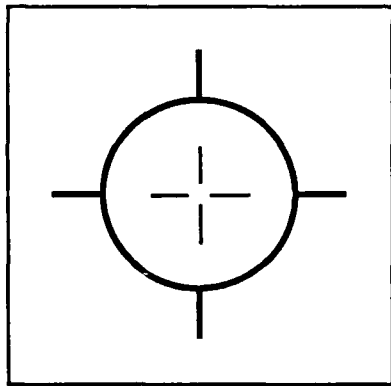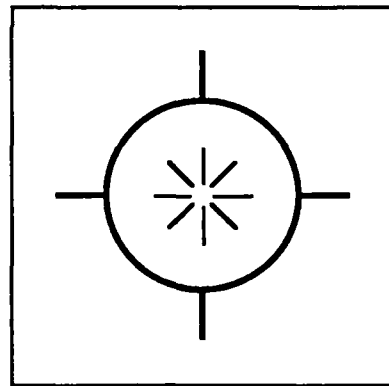
(a) "4 STRAKES" Forebody   (b) "8 STRAKES" Forebody

Figure 16. Forebody Configuration with "BODY 1"
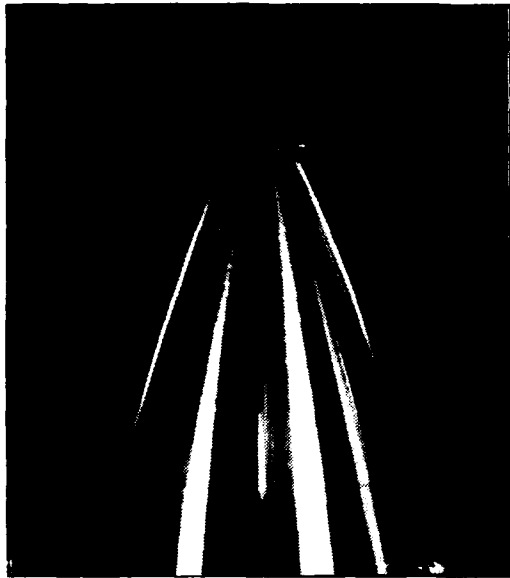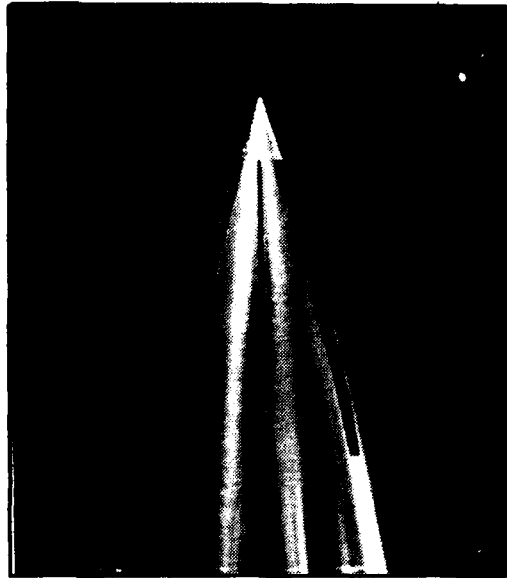
(a) "4 STRAKES" Forebody   (b) "8 STRAKES" Forebody

Figure 17. Photographs of Forebody Configuration

C EXPERIMENTAL PROCEDURE

1. Experiment Matrix

Three types of runs were conducted in this experiment in the following sequence.

a. Preliminary Runs

Previous experiments showed that variations in nose roll angle would alter the asymmetric vortex structure, thus changing side force magnitude and direction [Ref. 17: page 37-39]. A new nose was made for this research, which had the same dimensions of the original nose. Preliminary runs were made to determine which nose roll angle produced the largest side force magnitude. Eight nose roll angles 45° apart were tested with the "BODY 0" configuration in 5° increments from -5° to 90° AOA.

44

b. Baseline Runs

Once the nose roll angle which produced the maximum side force was determined, it was chosen as the test nose roll angle for the rest of this experiment. The nose was fixed in the test roll angle with the "NO STRAKE" configuration, and was tested in two wind tunnel conditions and with two body configurations to generate the baseline data which are compared with the data obtained from the subsequent test runs. The AOA was varied in 1° increments from -5° to 90°.

c. Test Runs

After the baseline data runs were made, the forebody was modified to the "4 STRAKES" configuration first and the "8 STRAKES" configuration second. The modified forebody, combined with two body configurations, was tested in two different wind tunnel conditions to examine the effects of strakes on the asymmetric vortices by comparing the results with the data produced by the baseline. The data were collected at each 1° AOA from -5° to 90°.

2. Test Procedure

a. Balance Setup and Calibration

The balance was secured on the end of the sting by tightening four tap screws until the two components were securely fixed together. Then the model was seated on the balance by a locating pin; a sleeve in the interior of the model provided a close fit between the balance and the model, in order to ensure that the balance-measured forces and moments were pure forces and moments acting on the model without any dislocation. Because of the rotation of the turntable in the wind tunnel, the normal force plane of the

balance was aligned parallel to the ground and the side force plane of the balance was set perpendicular to the ground. Prior to securing the balance on the sting, the balance output cable was threaded through the hollow sting with very careful attention. The cable was taped along the mounting arm and the reflection plane and then threaded through the breather slot to the signal conditioner.

Each balance channel was connected to the rear of the signal conditioner via a cannon plug. The order of the wire connection for each channel, starting at the slot on the top of the cannon plug in a clockwise direction and depending on the wire color, is illustrated as follows:
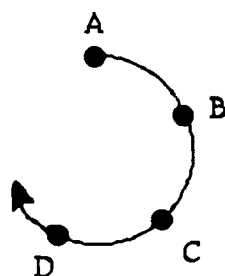
Plug slot	Wire color
A	Black
B	Channel color*
C	Green
D	Red

After the balance assembly was installed completely, the static calibration of the balance was made. The balance was zeroed first as described in the next section, then static weights were hung on the balance to check the balance readings with its calibration specifications. Normal and side force readings were found to meet the accuracy limits. [Ref. 33: page 27-29]

---

* The channel colors are:

N1	N2	S1	S2	A	R
blue	white	gray	yellow	light purple	orange

b. Test Sequence

The test wind tunnel condition, body configuration and strake configuration were determined as pre-work for each run. The data acquisition system was energized for an hour to warm up prior to each run.

Three stages were proceeded in each run by the following sequence: [Ref. 17: page 33-35, Ref. 33: page 28-29]

(1) Balance zeroing. The PANELS program was used in this stage. One co-axial cable transmitted the span output of the signal conditioner to the DMM, which allowed the excitation voltage for each channel to be set to 5.0 ± 0.003 VDC via the signal conditioner.

Then, the relay multiplexer video readout was monitored on the computer screen. Channels 2 to 8 of the relay multiplexer corresponded to the N1, N2, S1, S2, A and R channels of the balance, and the amplifier respectively. Each of the channels was zeroed starting with channel 8, the amplifier channel.

Channel 8 was selected and the amplifier gain was set to one. The voltage was set to 0.0 ± 200 μV by adjusting the "zero out" screw on the amplifier. The gain was then selected to 1000. Because of the instability of the amplifier around zero volts at the 1000 gain setting, a 200 mV offset voltage was added. Thus the voltage reading was set to 200 ± 0.5 mV by adjusting the "zero in" screw on the amplifier. The uncertainties were based on the resolution of the different gain settings of the amplifier as specified by the manufacturer in the amplifier manual [Ref. 31].

The model/balance was set at a static condition with a 0° AOA, and channels 2 to 7 were also zeroed with a 200 mV offset voltage. The

potentiometers on the signal conditioner were adjusted to obtain voltage readings as 200 ± 0.5 mV. After all channels were zeroed, the PANELS program was exited. [Ref. 30]

(2) Data acquisition. The READ.BAS program was executed to collect data. The taring data were taken first before the wind tunnel was operated. The wind tunnel was operated with a constant Δp setting, depending on the wind tunnel condition, by changing the pitch angle of the driven fan. The actual data acquisition began after the wind tunnel started. The missile AOA was manually set and entered with the settling chamber temperature into the data collecting program for each set of readings. The balance readings were reduced to force and moment values and stored in a data file on disk.

The test runs were interrupted during the run cycle to cool the air in the wind tunnel if the temperature reading exceeded 20°F above the start temperature. The air was cooled down to within 5°F of the start temperature by exchanging the air at a low tunnel speed. Then the test run continued from the balance zeroing stage at 4° below the interrupted AOA to overlap readings. Once the desired AOA was reached, the wind tunnel was shut down and one final set of readings was collected in the static condition to check the drift of the instruments. Before exiting the READ.BAS program, the test conditions were also recorded, which included the date, wind tunnel test condition, body configuration, strake configuration, average temperature and static pressure in the data file.

(3) Data reduction. The dimensionless coefficients are more useful than the force and moment data, because they can be analyzed directly

regardless of model size. The COEFF.BAS program read the data file produced by the READ.BAS program and calculated the coefficients based on the experimental information recorded in the force and moment data file.

The force was divided by the dynamic pressure and missile reference area (model cross section area) to give the force coefficient; the mathematical expression for force coefficient is:

$$C_{Force} = \frac{Force}{q\,A_m} \tag{6}$$

where:

$C_{Force} \equiv$ force coefficient

$q \equiv$ dynamic pressure

$A_m \equiv$ missile reference area

The moment coefficient was derived from dividing the moment by the dynamic pressure, missile reference area and missile base diameter; equation {7} is the mathematical expression for moment coefficient:

$$C_{Moment} = \frac{Moment}{q\,A_m\,d} \tag{7}$$

where:

$C_{Moment} \equiv$ moment coefficient

$d \equiv$ missile base diameter

The program also corrected for the blockage which varied with body configuration and AOA (Ref. 17). The coefficient was stored in another data file on disk. The program also can provide a hardcopy including the experimental conditions, force and moment data, and coefficient data. The coefficient data were plotted for comparative analysis and the plots are shown in the results chapter.

D. EXPERIMENTAL CORRECTIONS

Two corrections were made to reduce the final data. One was the blockage correction due to the model in the wind tunnel, and the other one was the drift correction due to the instruments, in particular, the six-component balance.

1. Blockage Correction

The blockage correction is developed from the following equations: [Ref. 28: page 35-38]

$$q = q_d (1 + 2\varepsilon) \qquad \{8\}$$

$$\varepsilon = \frac{1}{4} \frac{\text{model frontal area}}{\text{test section area}} \qquad \{9\}$$

where:

$q \equiv$ actual dynamic pressure on model

$q_d \equiv$ determined test section dynamic pressure (from Δp)

$\varepsilon \equiv$ blockage factor

The AOA of the model was varied during each experimental run, which caused the frontal area to vary. Thus, the blockage factor varied with the AOA. In addition, the blockage factor also changed with the body configuration as shown in Figure 18 [Ref. 17: page 36]. The blockage correction for each configuration was developed as a function of AOA, and is also shown in Figure 18. The equations were implemented in the PANELS program listed in Appendix C.
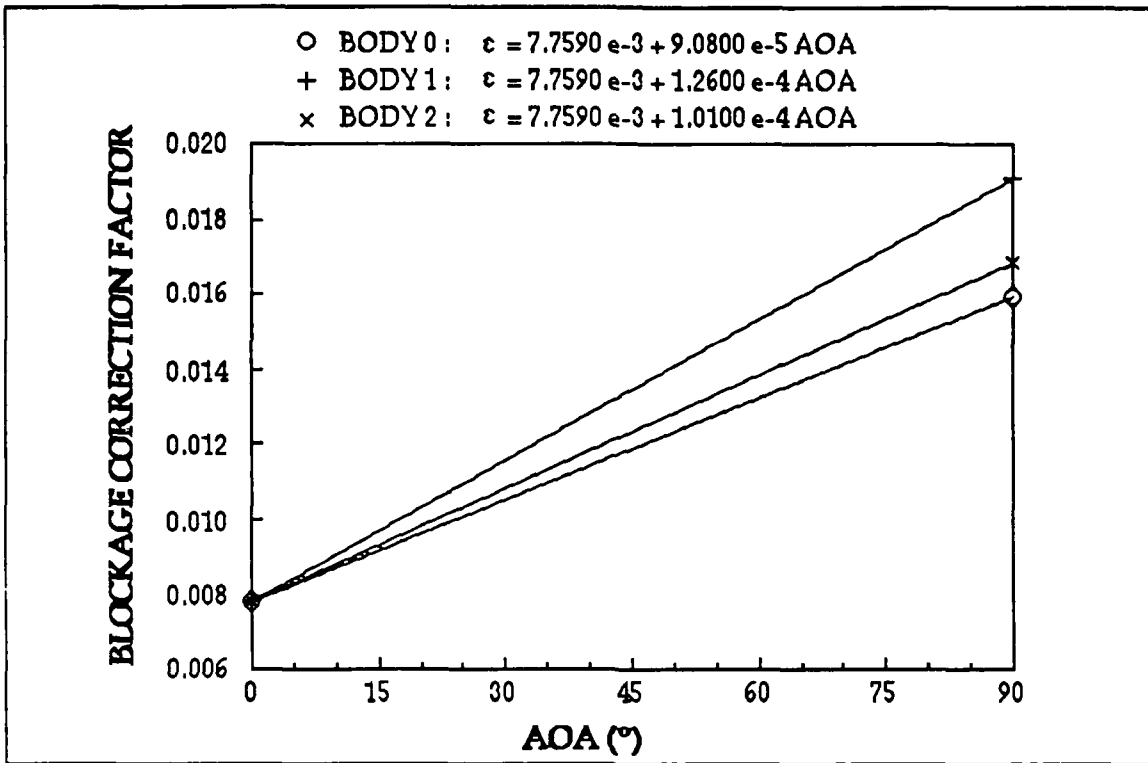
Figure 18. Blockage Factors for Different Body Configurations

2. Drift Correction

The test runs with the non-turbulent wind tunnel lasted about 4.5 hours, and the ones with the turbulent condition took up to ten hours. Hence, the final data for the static condition were made to check the instrumental drift.

The final data showed that one coefficient unit approximately equals 0.28 pound for force data, and one coefficient unit is equal to about 0.04 foot-pound for moment data. Comparison of these values to the accuracies of force and moment specifications as listed for the particular balance was made, and it was noted that one coefficient unit is in the accuracy range. Thus, the decision was made that the correction requirement limitation is ± one

51

coefficient unit, which means a correction would not be justifiable if the final static coefficient is in ± one unit of zero value.

The drift correction for the test runs without the grid in the wind tunnel was straightforward. The instrumental drift was assumed to increase linearly with the AOA as a function of operating time, and the correction was made by applying the equation:

$$C_c = C_u - d\left(\frac{\alpha}{90}\right) \qquad \text{(non-turbulent)} \qquad \{10\}$$

where:

$C_c \equiv$ corrected coefficient

$C_u \equiv$ uncorrected coefficient (direct COEFF output)

$d =$ drift (obtained from the final static measurement)

$\alpha \equiv$ AOA

The settling chamber temperature rose very fast with the turbulence generating grid in the wind tunnel, so the test runs were interrupted several times. The correction requirement limitation and linear drift assumption were applied again. The corrections for each run with the grid in the wind tunnel were divided in several portions depending upon the stop AOAs. But the static condition data of the interrupted AOAs were not recorded. Another assumption was therefore made that the data of the interrupted AOA were more accurate, because the instruments had been zeroed again before the test resumed. The drift values then were taken as the difference between the data of the interrupted AOA and the data of the same AOA in the next portion. The equation was applied to each interrupted portion separately as follows:

$$C_c = C_u - d\left(\frac{\alpha - \alpha_s}{\Delta \alpha}\right) \qquad \text{(turbulent)} \qquad \{11\}$$

where:

$d \equiv$ drift (from the final static measurement or

difference between the data of the same AOAs in

this portion and the next portion)

$\alpha_s \equiv$ interrupted AOA of this portion

$\Delta\alpha \equiv$ the number of AOAs in this portion

The normal force coefficient trends of the "turbulent, body 2, no strake" test

before and after the drift correction are shown in Figure 19, as an example.
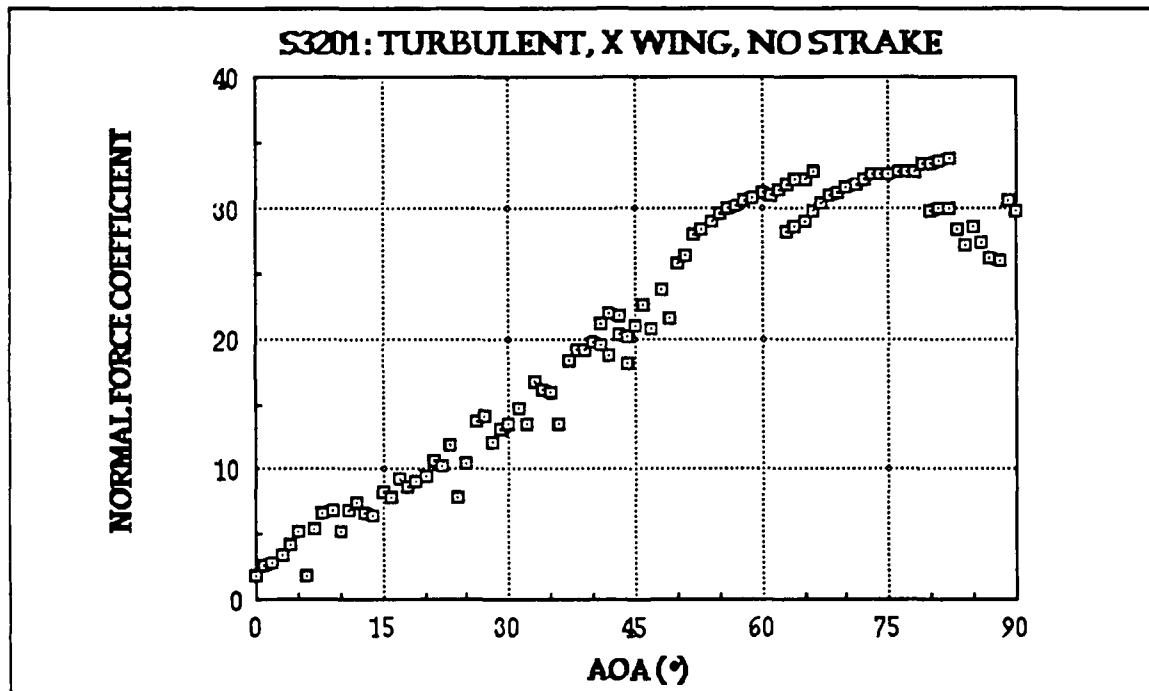
(a) Original Normal Force Coefficient Before Drift Correction

Figure 19. Illustration Sample for Drift Correction

S3201: TURBULENT, X WING, NO STRAKE
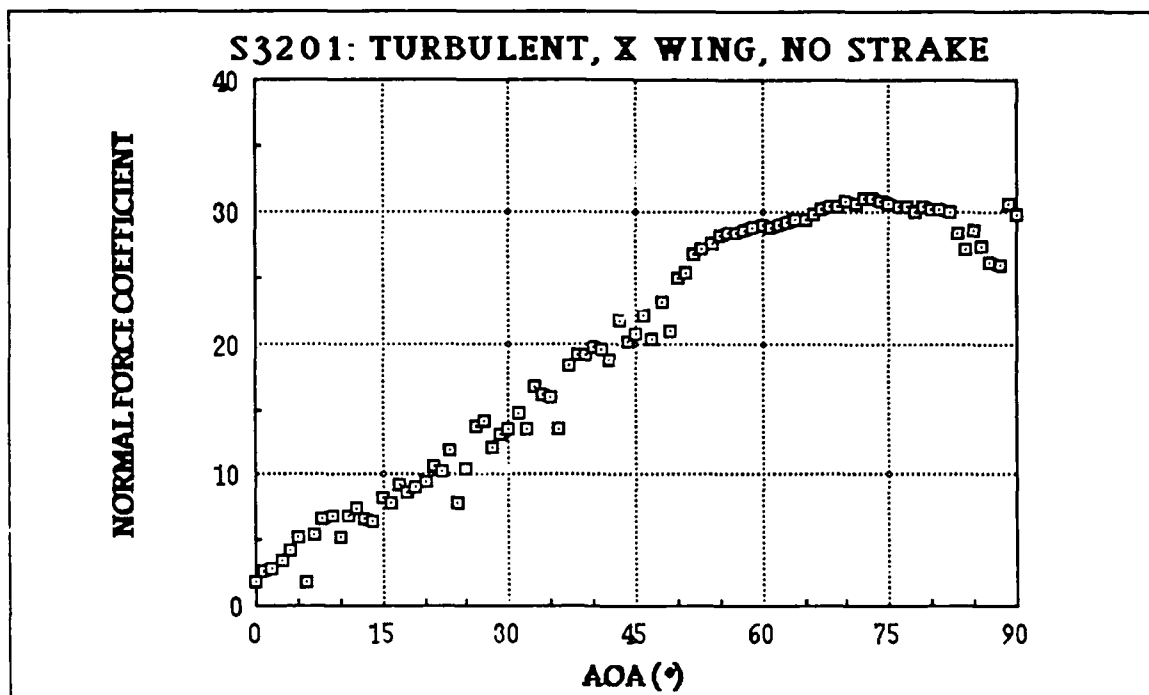
(b) Corrected Normal Force Coefficient After Drift Correction

Figure 19. Illustration Sample for Drift Correction

These drift corrections were made to the output data of the COEFF program. The final data then were graphed and will be analyzed in the next chapter "RESULTS".

III. RESULTS

All the results presented and discussed in the following chapters are expressed in coefficient form, which are dimensionless and can be applied to any size of model. The focus of the results will be concentrated on normal force coefficients (C_N), side force coefficients (C_Y) and yawing moment coefficients (C_n). Conditions for all runs were stated in the previous chapter and are listed individually in Appendix D.

A. PRELIMINARY RUNS

Previous research has shown that variations in nose roll angle altered the vortex shedding structure, and therefore side forces, at high angle of attack [Ref. 17]. The objective of these preliminary runs was to determine the nose roll angle which produced the highest side force magnitude for this new model nose. This nose roll angle was held as the test nose roll angle for all subsequent runs regardless of other test configurations.

Eight nose roll angles, each varied by 45°, were tested for AOAs from -5° to 90° in 5° increments for each run. The test conditions were identical for all runs: the "non-turbulent" wind tunnel, the "BODY 0" configuration, and a q of 16.55 psf. with $Re_d \approx 1.15 \times 10^5$.

Results of C_Y for the preliminary runs are plotted in Figure 20. As expected, the variation of nose roll angle changes the side force magnitudes and directions. The varied side force trends with nose roll angles are due to the nose geometry variation (misalignment, imperfections, machined axis-asymmetry, etc.) "Nose #3" had the highest side force in the positive

direction ($C_{Ymax} \approx 3.6$) at AOA = 50° and was chosen as the test nose in the rest of this research.

The C_Y trends show large changes in magnitude and direction, which are due to the large AOA increment. Because of limitations in the accuracy of the balance at small loads and in the unsteadiness of the leeward flowfield, the scattered results were expected and are acceptable. Smaller AOA increments would give more reliable scatter bands of the data; all subsequent runs were carried out in one degree increments.

The C_N, C_Y and C_n values versus AOA for "Nose #3" are also plotted in Figures 21 to 23 as a "non-turbulent, no wing, no strake" configuration of the model. The plots show that the C_{Nmax} = 18.5 at AOA = 60° and the C_{nmax} = 9.59 at AOA = 65°. All side forces and yawing moments are in the positive direction without any sign change throughout the 90° AOA range. The side force induced at the forebody dominated with this configuration. The reference system of the model shown in Figure 15 indicates that the side forces will dominate over the forebody if the side forces and yawing moments have the same sign; otherwise, the side forces will dominate at the afterbody if the side forces and yawing moments have an opposite sign.
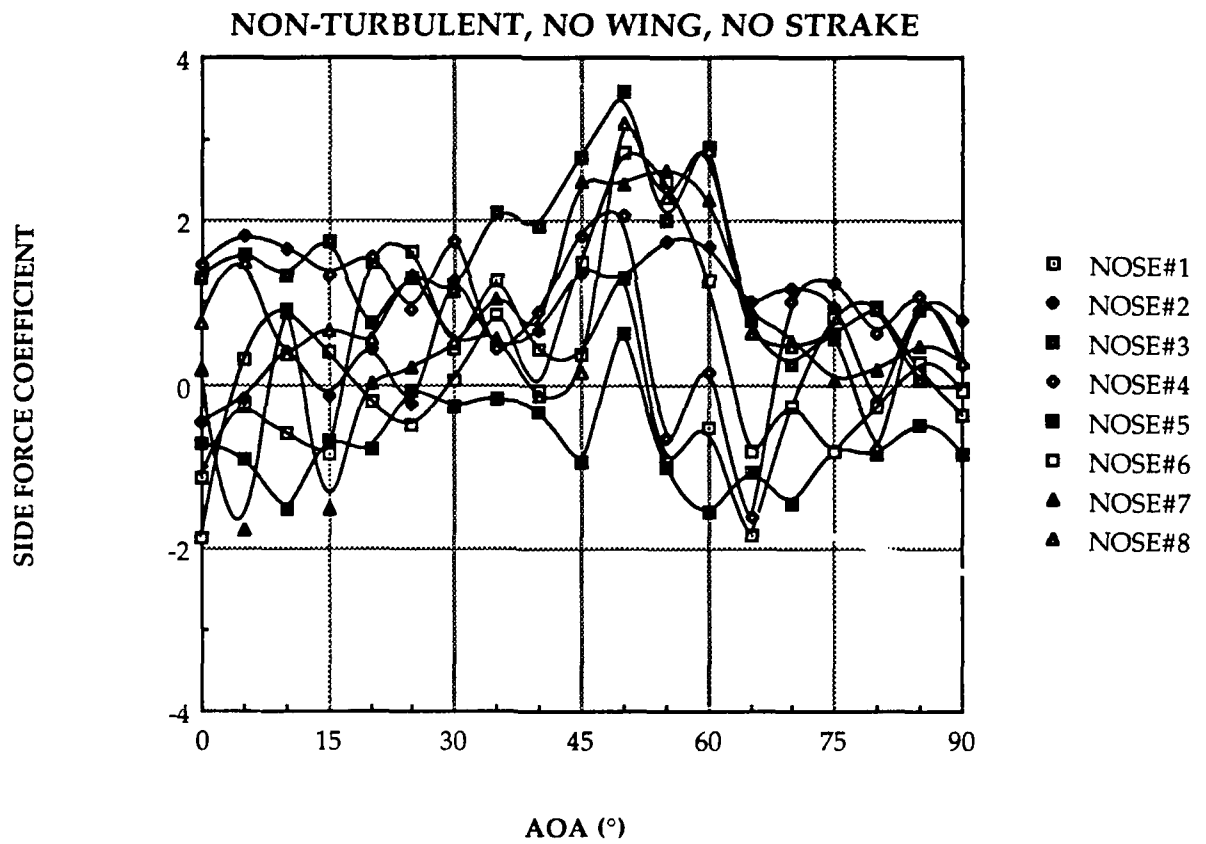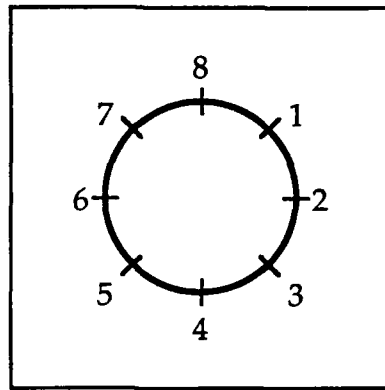
Figure 20. Side Force Variations With Nose Roll Angle: Runs T11 to T81
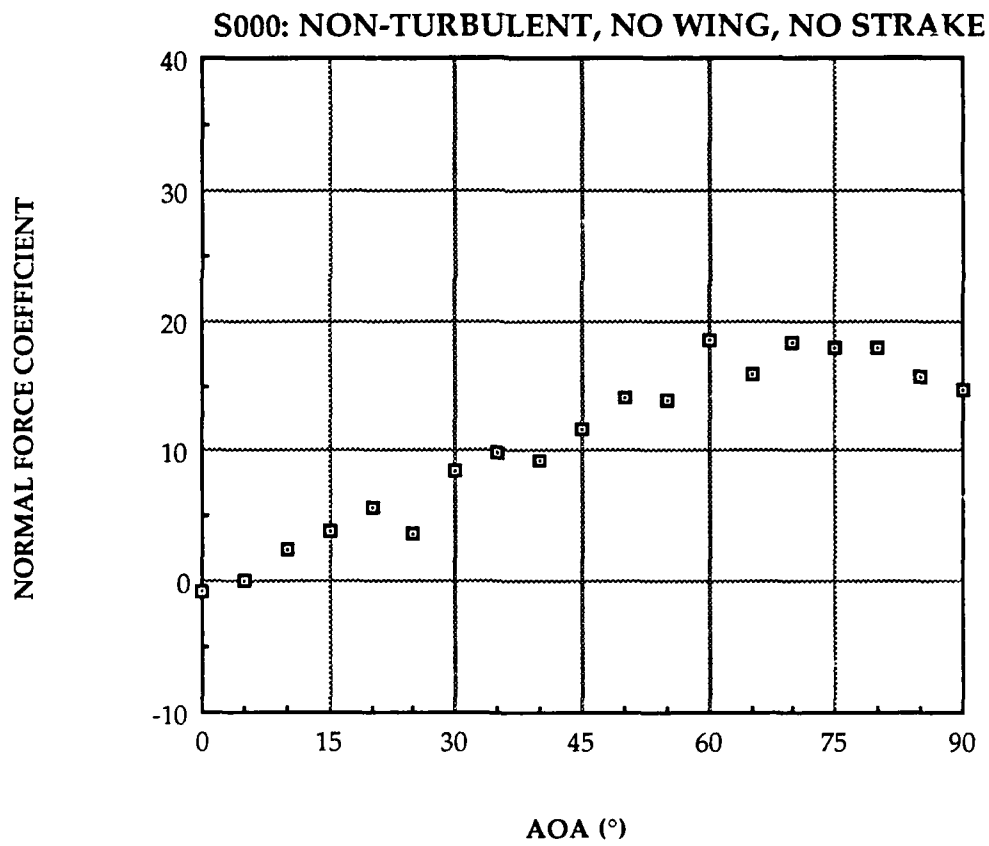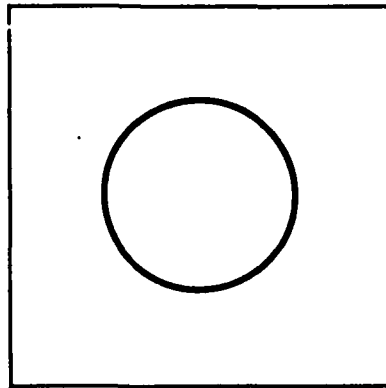
Figure 21. S0000: Normal Force Coefficient

58
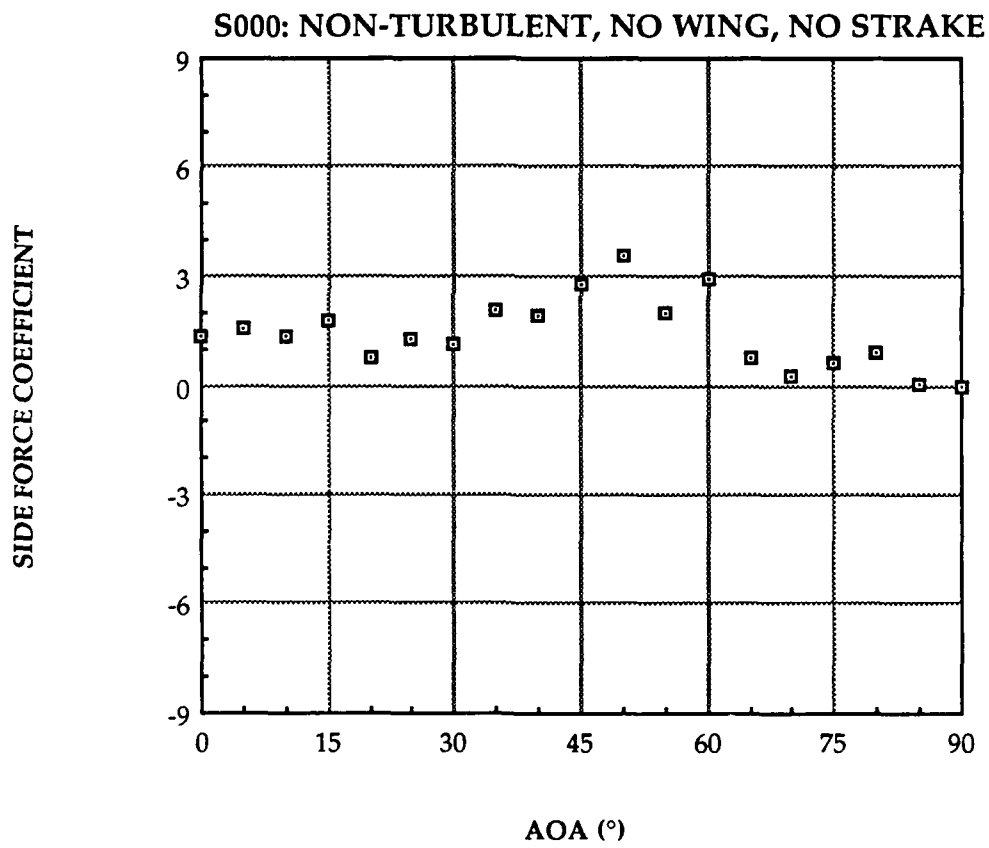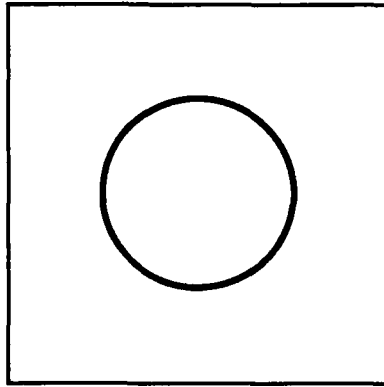
Figure 22. S0000: Side Force Coefficient
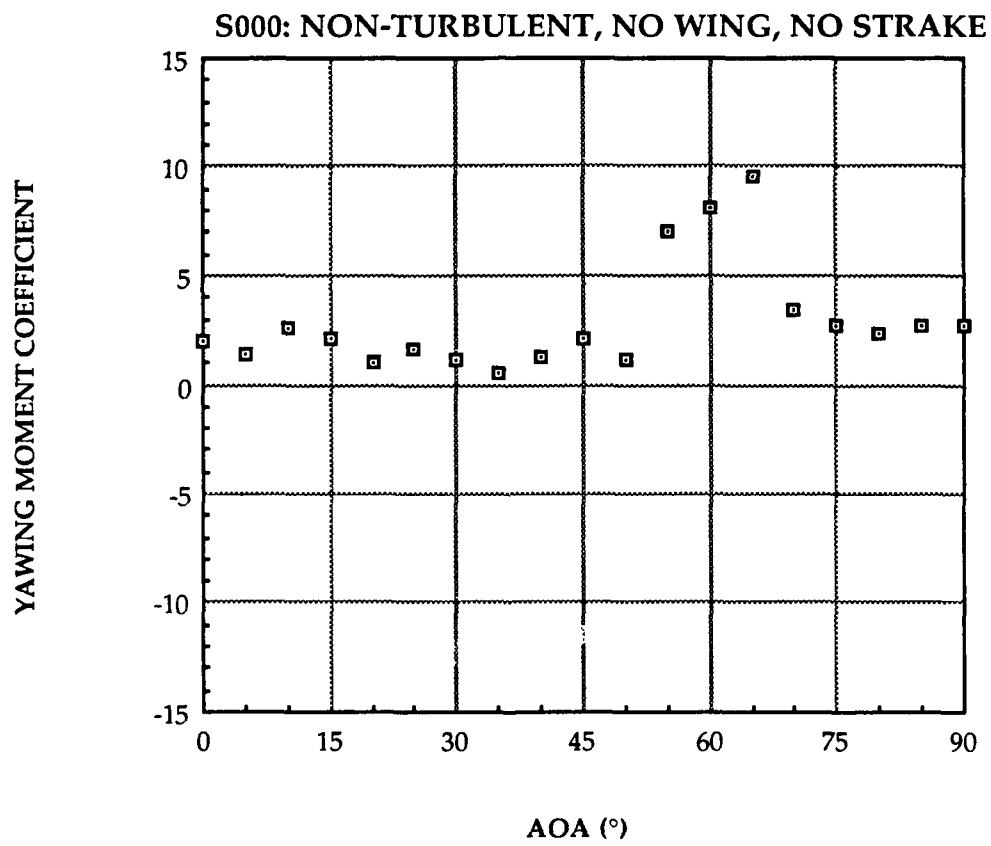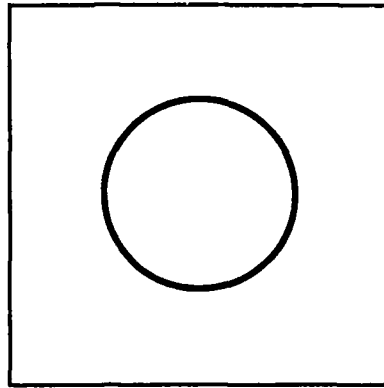
Figure 23. S0000: Yawing Moment Coefficient

B. BASELINE RUNS

The specified nose roll angle "Nose #3" with "BODY 1" and "BODY 2" were tested in non-turbulent and turbulent wind tunnel conditions, to obtain the baseline. The results are plotted in coefficient form in Figures 24 to 35.

1. "BODY 1" Configuration

The results of the "+" wing configuration tests are plotted in Figures 24 to 29. The C_{Nmax} for the non-turbulent condition is 33.3 at AOA = 58° shown in Figure 24, while the C_N trend for the turbulent condition has a C_{Nmax} = 34.5 at AOA = 64° in Figure 25. Both maximum normal force coefficients are approximately twice that of the preliminary run, indicating that the wings provide about half of the normal force in flight at high angles of attack.

The side force coefficient trend for the non-turbulent condition in Figure 26 shows that the induced side force becomes significant at AOA ≈ 25°, and reaches a maximum at AOA ≈ 43° with C_Y = 5.1; it then gradually decreases to about zero at AOA ≈ 73°. The C_Y trend for the turbulent condition in Figure 27 shows that the C_Y grows in the positive direction to a maximum value of 2.7 at AOA ≈ 38° and then tapers off to nearly zero at AOA ≈ 60°. The side force coefficients for both wind tunnel conditions show similar trends with smaller amplitudes in the turbulent condition.

The yawing moment for the non-turbulent condition in Figure 28 starts to increase in magnitude in the negative direction at AOA ≈ 30° and reaches a peak C_n = -4.8 at AOA ≈ 39°. It then increases in the opposite direction, passing through a zero value at AOA = 45° and increasing to a C_{nmax} = 12.1 in a positive direction at AOA ≈ 66°. It then drops back to zero

61

suddenly at AOA ≈ 73°. The C_n trend for the turbulent condition in Figure 29 has similarities to the results for the non-turbulent condition. It also becomes negative at AOA ≈ 30°, reaches a peak C_n = -3.84 at AOA ≈ 38°, then climbs to zero at AOA = 45° and keeps growing to the C_{nmax} = 10.7 at AOA ≈ 70°. It then drops to zero at AOA ≈ 75°. Both conditions switch direction from negative to positive at AOA ≈ 45°.
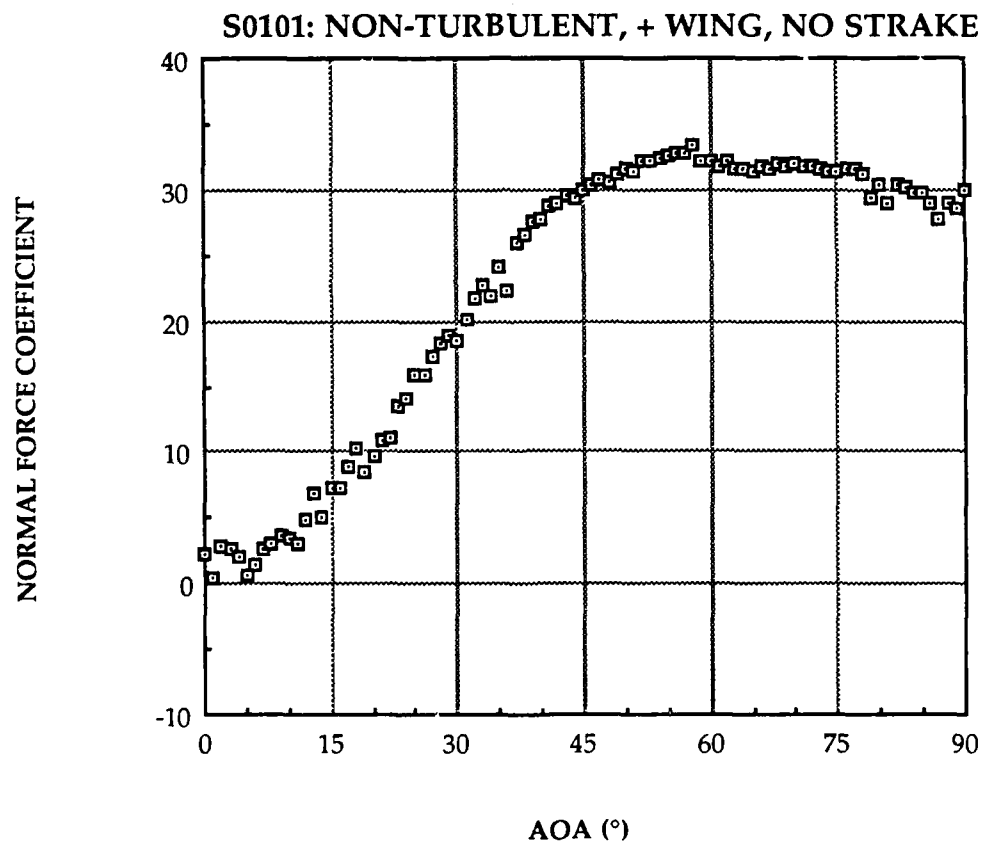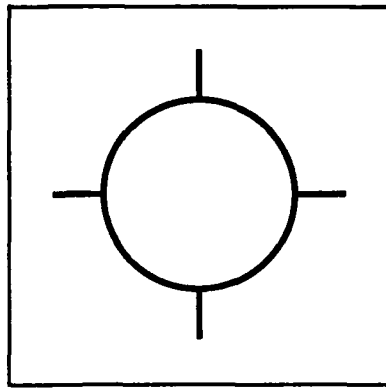
Figure 24. S0101: Normal Force Coefficient

63

S3101: TURBULENT, + WING, NO STRAKE
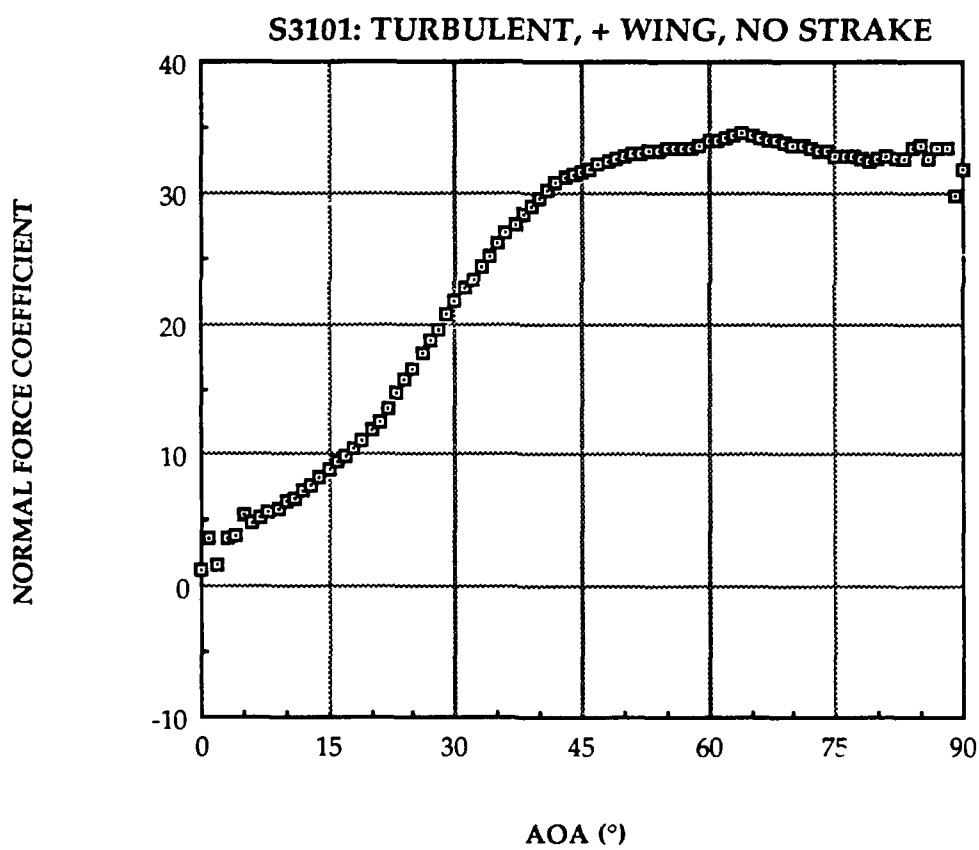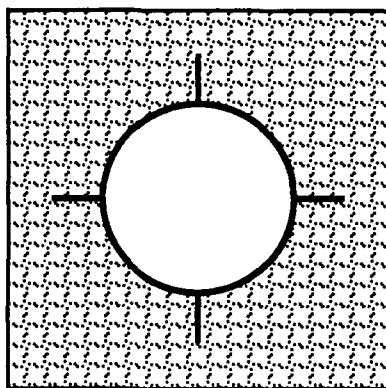
Figure 25. S3101: Normal Force Coefficient

S0101: NON-TURBULENT, + WING, NO STRAKE

Figure 26. S0101: Side Force Coefficient

S3101: TURBULENT, + WING, NO STRAKE

Figure 27. S3101: Side Force Coefficient

S0101: NON-TURBULENT, + WING, NO STRAKE

Figure 28. S0101: Yawing Moment Coefficient

S3101: TURBULENT, + WING, NO STRAKE

Figure 29. S3101: Yawing Moment Coefficient

2. "BODY 2" Configuration

The results of the "x" wing configuration are plotted in Figures 30 to 35. The normal force coefficient trend for the non-turbulent condition in Figure 30 has a $C_{Nmax} \approx 30.7$ around AOA $\approx 75°$, and the C_N graph for the turbulent condition in Figure 31 shows a $C_{Nmax} \approx 30.9$ at AOA $\approx 73°$. The maximum normal force coefficients are slightly smaller and at higher AOAs than those for the "BODY 1" configuration, but they are also approximately twice as large as the ones in the preliminary run. This again indicates that the wings provide approximately half of the normal force in flight at high AOA. The introduced turbulence appears to have an insignificant effect on the normal force.

In Figure 32, the side force coefficient for the non-turbulent condition decreases in the negative direction to a peak $C_Y \approx -2.8$ at AOA $\approx 30°$; it then moves in the positive direction and has a $C_{Ymax} \approx 3.9$ at AOA $\approx 62°$ with a consequent decrease to zero at AOA $= 90°$. The side force shows a direction switch at AOA $\approx 40°$. The scatter for AOA $\leq 15°$ is considered due to the instability of the balance instrument, and therefore the onset AOA is assumed at about 15°. But no attempt was made to measure the natural frequencies of the model/sting/balance combination. The side force coefficient trend for the turbulent wind tunnel condition shown in Figure 33 has a similar trace to the one for the non-turbulent condition, except for the reduction in the AOA range of the induced side forces. The side force starts at AOA $\approx 20°$ and initially grows negatively to a peak $C_Y \approx -2.2$ at AOA $\approx 33°$, switches to being positive at AOA $\approx 45°$ and rises to a $C_{Ymax} \approx 3.9$ at AOA $\approx 70°$, and then decreases to zero at AOA $\approx 85°$.

In Figures 34 and 35, the yawing moment coefficient plots for both the non-turbulent and turbulent conditions have many similarities in that they both increase in a positive direction to peak values around AOA $\approx 30°$, then decrease to negative peak values around AOA $\approx 45°$, then change directions again to become positive and reach the maxima followed by sudden drops to approximately zero. The only significant differences are the maximum C_n values and the AOA range of high induced yawing moments. For the non-turbulent condition, the C_{nmax} is about 12.1 at AOA $\approx 60°$; the C_{nmax} is about 9.0 around AOA $\approx 70°$ for the turbulent condition.

3. Correlations Between C_Y and C_n

The changes of the side force distribution along the model with the angle of attack can be understood by observing the side force coefficient change with the yawing moment coefficient. Generally, if the side forces and yawing moments are of the same sign, the side forces dominate over the forebody; if the side forces and yawing moments have a different sign, the side forces will dominate at the afterbody.

In "BODY 1" configuration tests for the two wind tunnel conditions, the induced side forces are always positive with direction changing yawing moments. For AOA = 30° to 45°, a positive C_Y with a negative C_n shows that the side forces dominate over the afterbody. Once the C_n switches to positive values after AOA = 45°, the positive C_Y indicates that the side forces switch to forebody dominant. The side forces and yawing moments both return to zero at AOA $\approx 75°$. The side forces, therefore, are seen to dominate over the afterbody initially, and then move forward along the body with increasing AOA.

70

The correlations between C_Y and C_n are more complicated for the "BODY 2" configuration. The initial negative C_Y with positive C_n shows afterbody-dominant side forces for AOA $\leq 40°$, while the positive C_Y with positive C_n show forebody-dominant side forces at AOA $\geq 55°$. In the AOA range between 40° and 55°, the yawing moments are always negative for both wind tunnel conditions. The positive side forces dominate at the forebody for the non-turbulent condition. For the turbulent condition, the side forces on opposite sides of the model have apparently the same magnitude but opposite direction to give nearly zero resultant side forces; the negative side forces dominate at the afterbody and the positive side forces dominate over the forebody, producing a negative yawing moment. Also, the side forces dominate at the afterbody and move to the forebody as AOAs are increased.

A general observation for both body-wing configurations in this baseline run is that the side forces initially dominate over the afterbody and move forward with increasing AOA. At some AOAs, the side forces are zero with non-zero yawing moments; this suggests that the side forces on the two sides of missile body are of equal size, but the side force dominant positions on the two sides are not coincident, causing unbalanced yawing moments. Conversely, two unequal and opposite side forces with the stronger side force farther from the moment center may result in non-zero side forces with zero yawing moments. Also, opposite but equal side forces may dominate at the same position to give a balanced yawing moment, yielding both zero side forces and yawing moments. These uncertain situations happen throughout the whole angle of attack range, and preclude a complete description of the

71

force-and-moment behavior. Yet the general observation noted is consistently indicated.
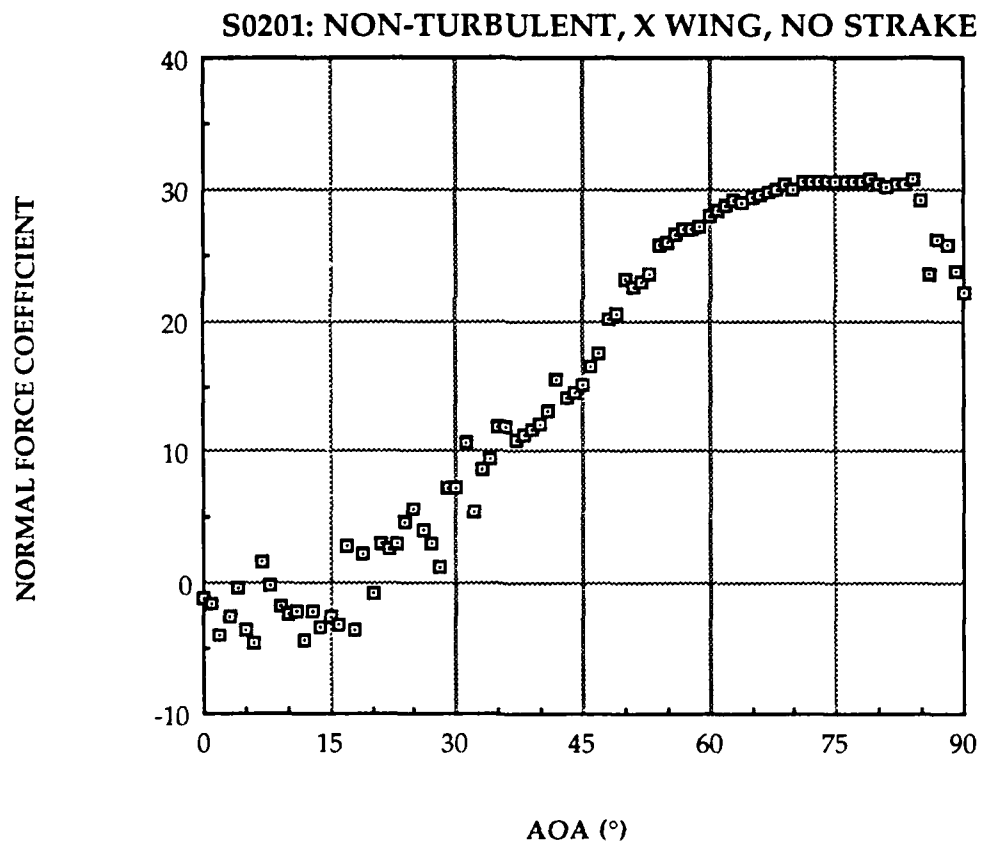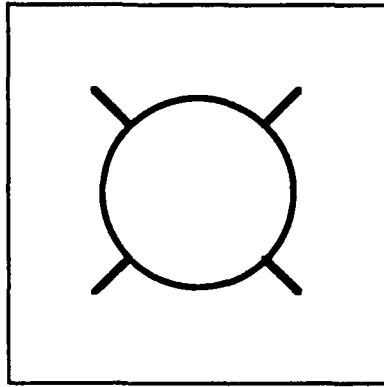
Figure 30. S0201: Normal Force Coefficient

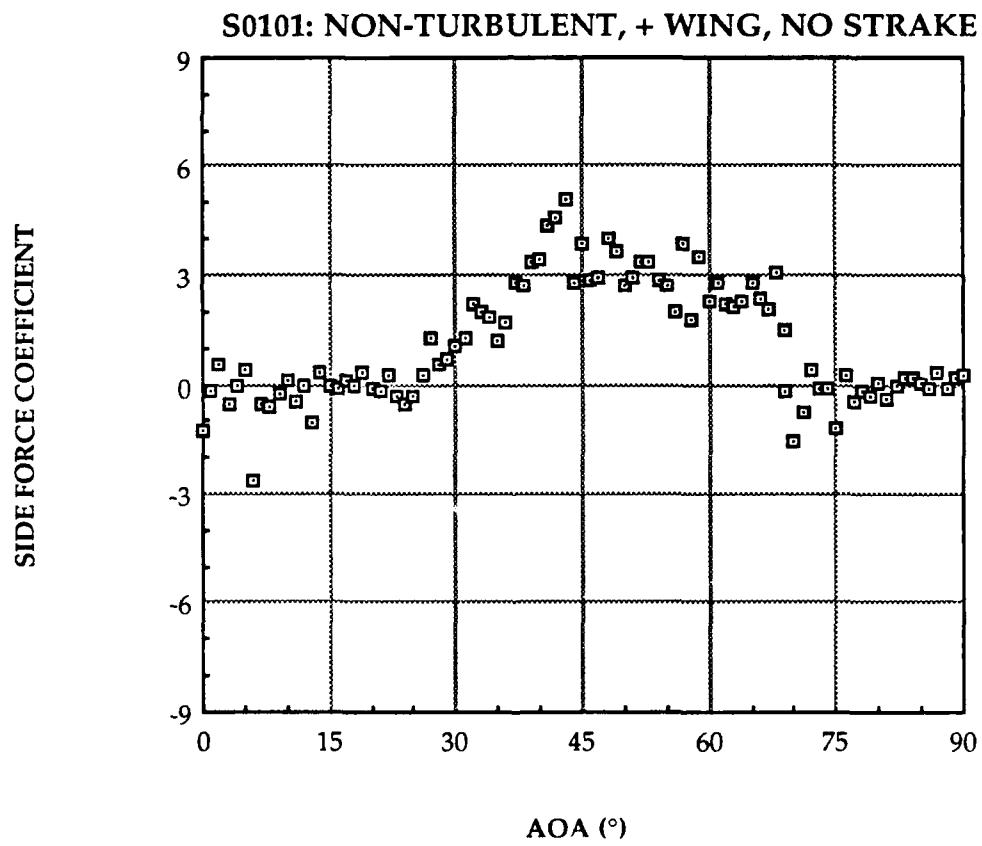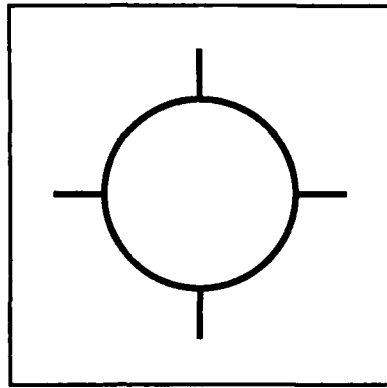73
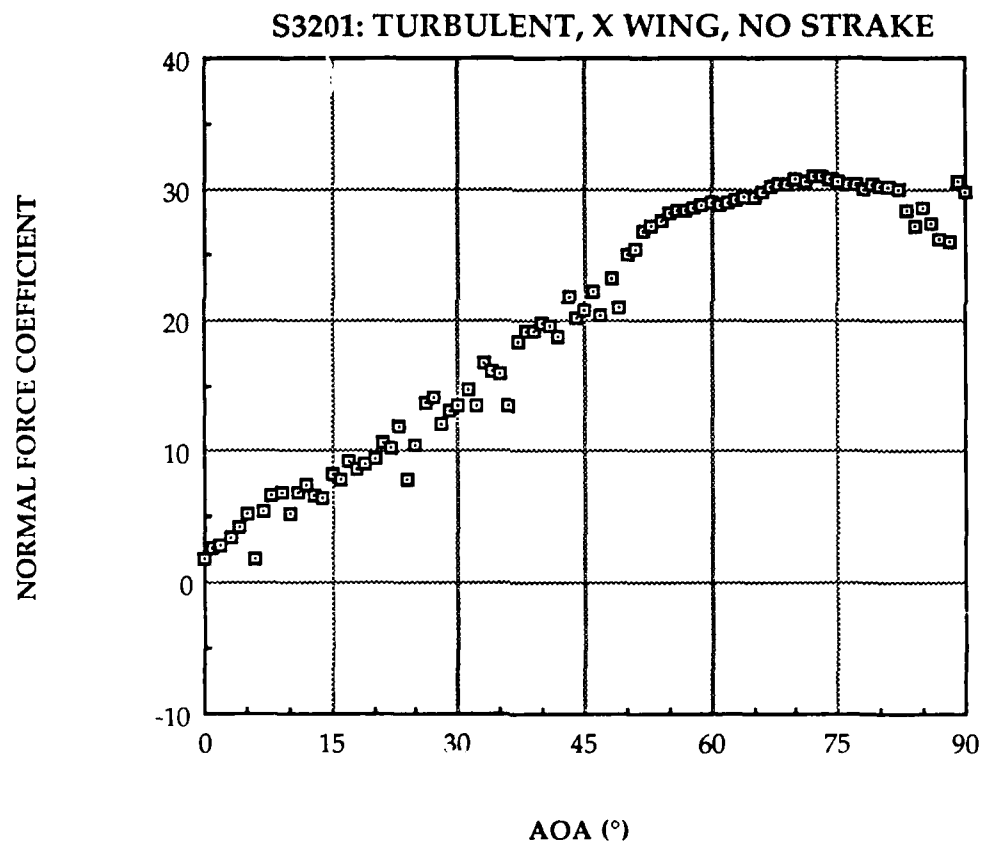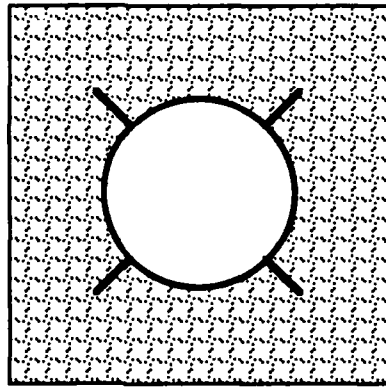
Figure 31. S3201: Normal Force Coefficient

74
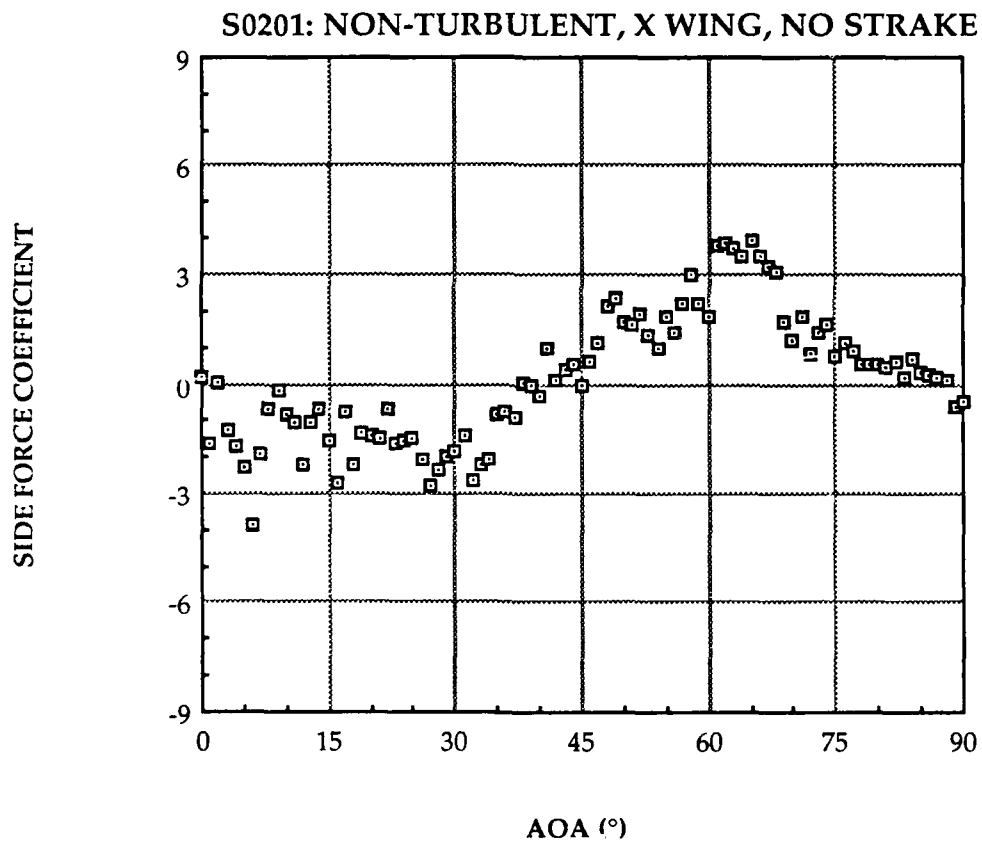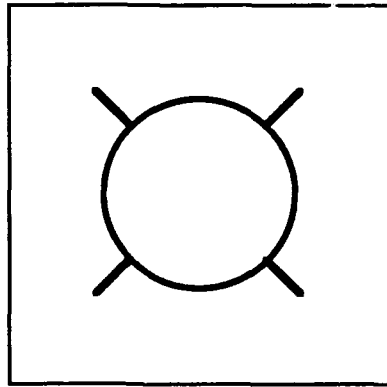
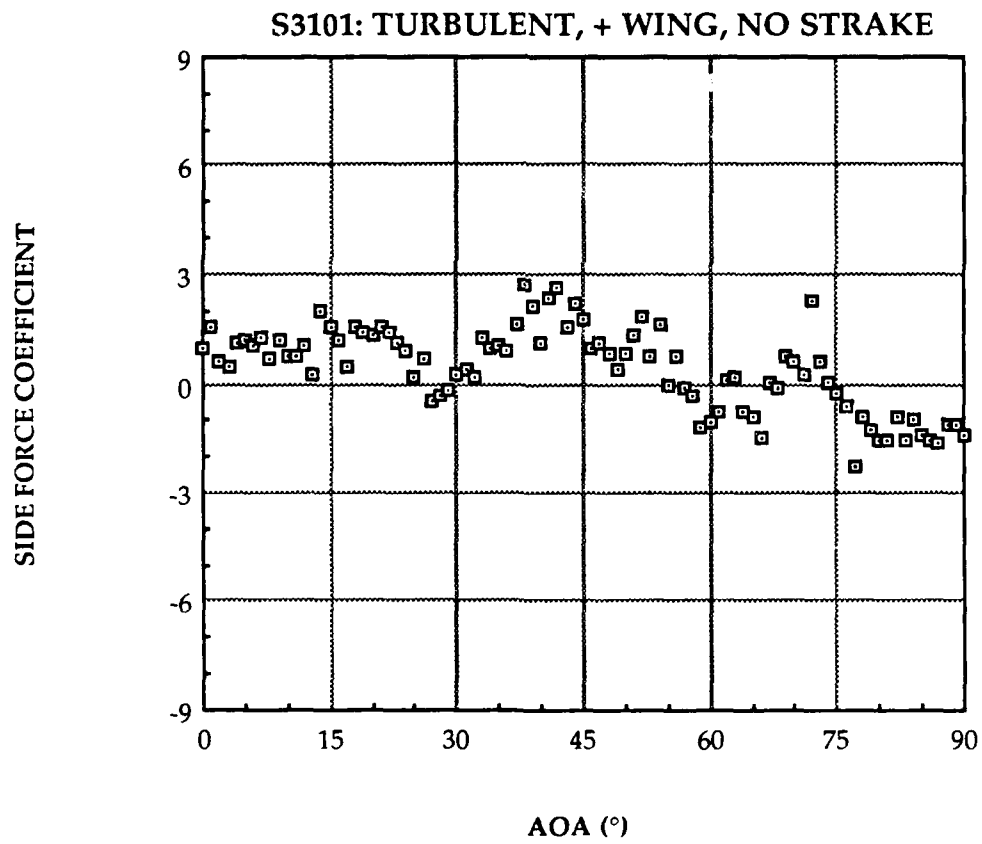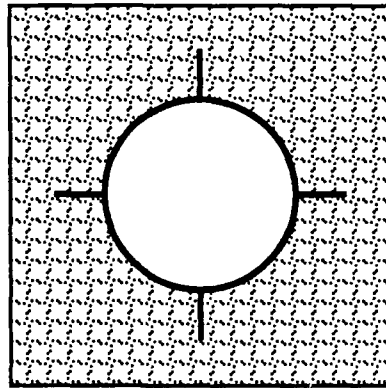Figure 32. S0201: Side Force Coefficient
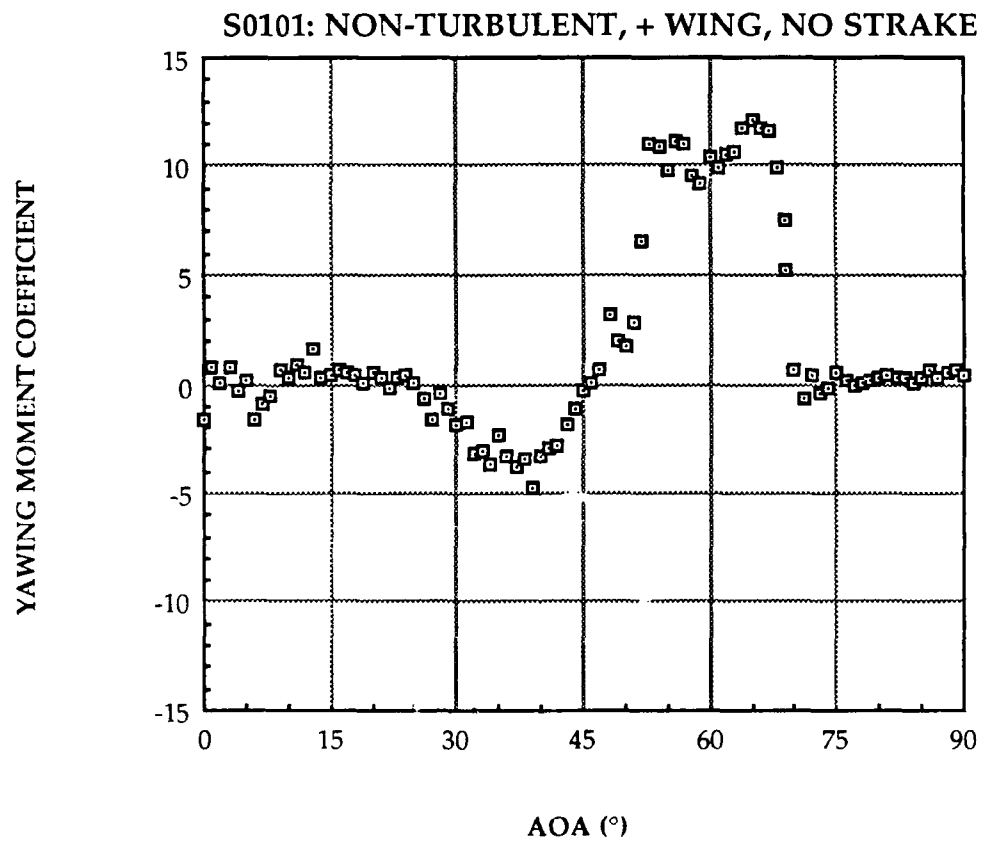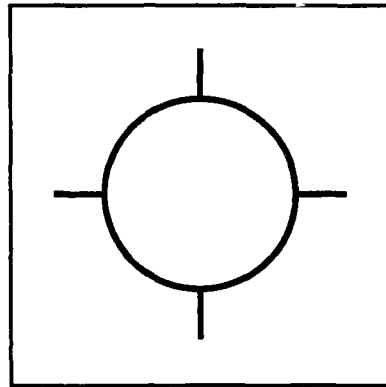
75
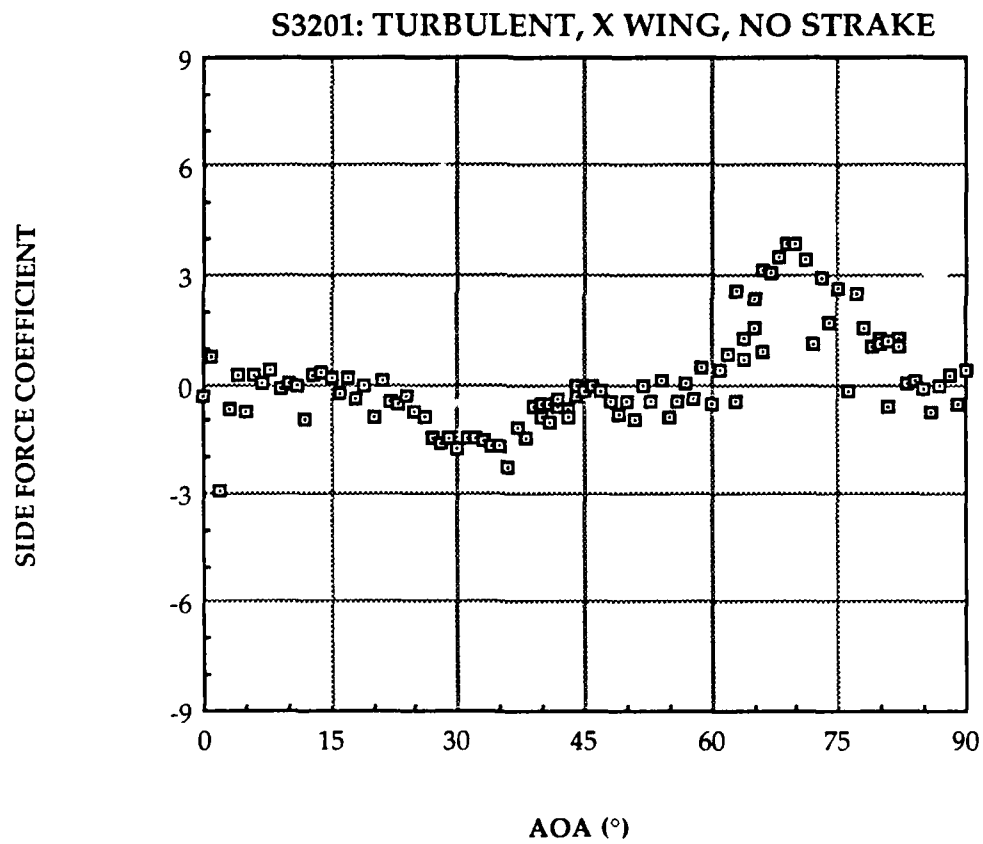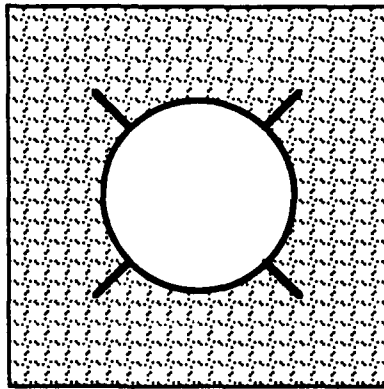
Figure 33. S3201: Side Force Coefficient
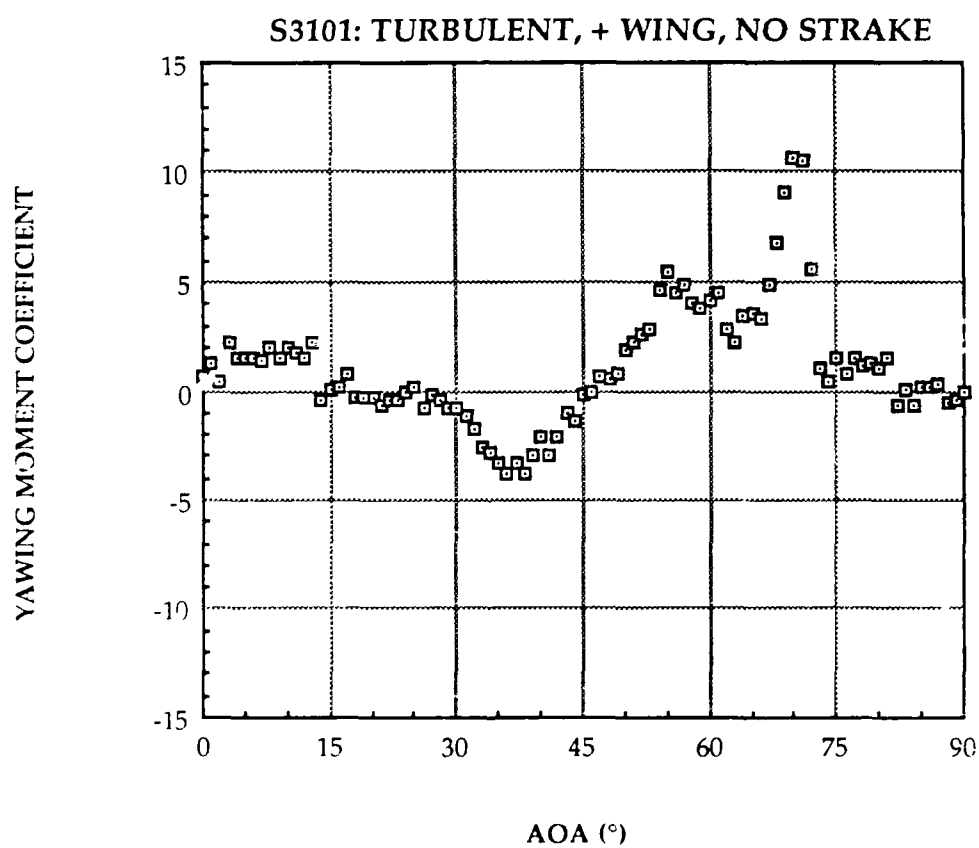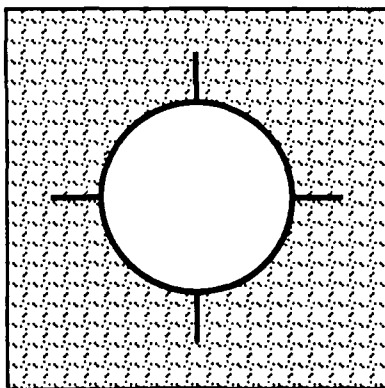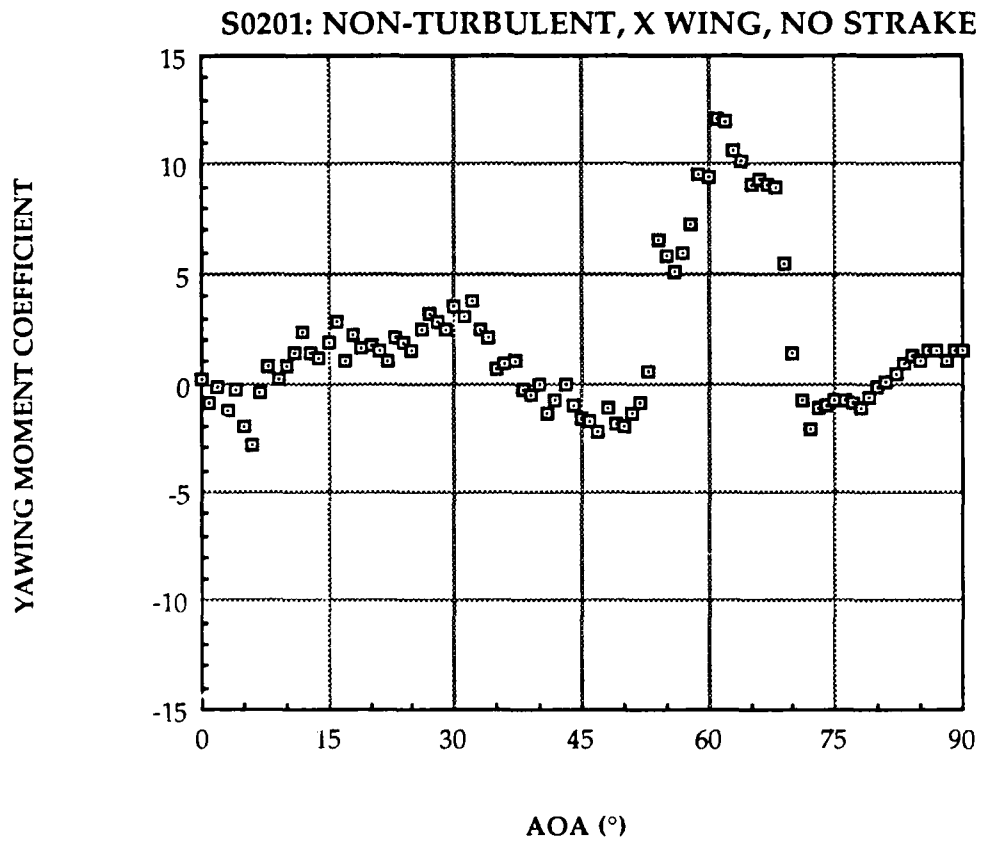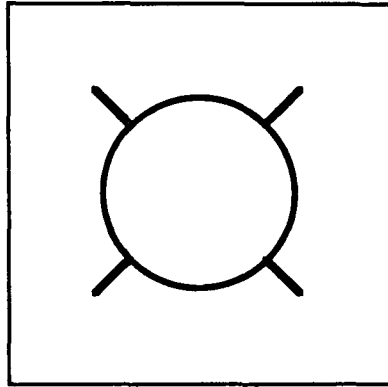
Figure 34. S0201: Yawing Moment Coefficient
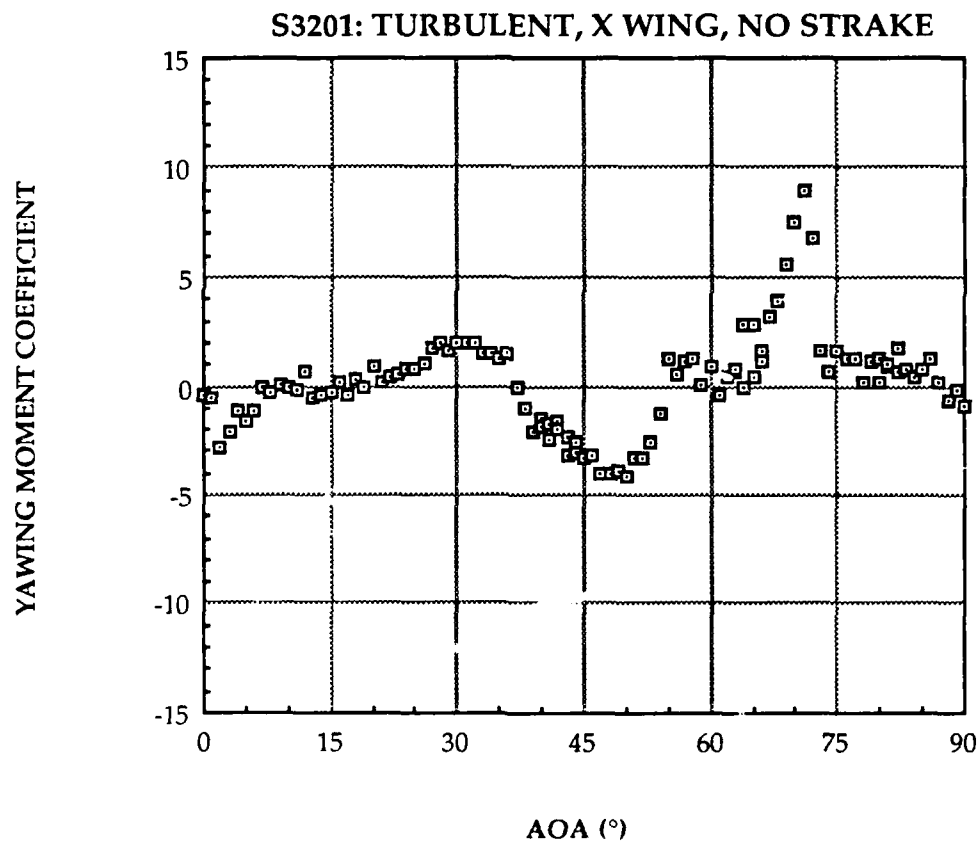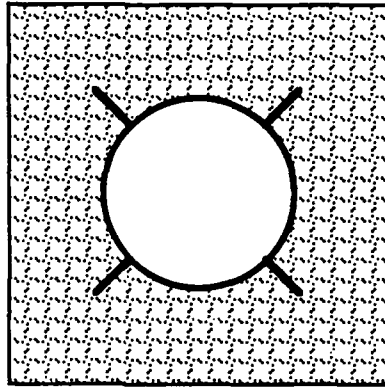
Figure 35. S3201: Yawing Moment Coefficient

C. TEST RUN I (4-STRAKE MODIFIED FOREBODY)

After the baseline runs were finished, the nose was modified by adding four strakes on its tip in the "+" configuration as shown in Figures 16(a) and 17(a). The modified nose was also tested with two body configurations and in two wind tunnel conditions. The results are plotted in Figures 36 to 47.

1. "BODY 1" Configuration

The normal force coefficient graphs for both non-turbulent and turbulent conditions, shown in Figures 36 and 37, are similar to the ones of the baseline runs, but with smaller maxima occurring in the same AOA region. The approximate C_{Nmax} is 29.8 for the non-turbulent case, and is about 32.5 for the turbulent condition. The negative value at zero AOA for the non-turbulent condition indicates a possible shift below actual values, implying that these two maximum values may actually be about the same magnitude.

The side force coefficient results for both wind tunnel conditions have almost identical appearances, shown in Figures 38 and 39, but are different from the ones of the baseline runs. The induced side forces become significant at AOA $\approx$ 30°, and reach the maxima around AOA $\approx$ 40°; they decrease gradually to about zero at AOA $\approx$ 50°. The C_{Ymax} is approximately 5.5 for the non-turbulent condition, and is about 6.5 for the turbulent condition. Again, these two maxima are about the same size; a negative shift at zero AOA for the non-turbulent condition indicates that the represented values may be smaller than the actual values. Both maxima have larger values than the ones measured in the baseline runs, especially for the turbulent condition. They have higher onset AOAs and smaller AOA ranges

79

where the side forces are significant (Regime III). Also, the plots have smaller scatter bands than the ones for the baseline runs. This modification gives no significant indication of a reduction in side forces.

The yawing moment coefficient results shown in Figures 40 and 41 for the two wind tunnel conditions have almost the same appearance. Non-zero yawing moments can be noted for an AOA range from 30°~65°. For AOA $\leq$ 45°, the trends show similar traces to the ones of the baseline runs, with slightly smaller values. For AOA $\geq$ 45°, they have much smaller positive C_{nmax} occurring in a lower AOA region in comparison with the C_{nmax} of the baseline runs. The C_{nmax} is about 2.8 at AOA = 48° for the non-turbulent condition, and is about 4.9 at AOA = 49° for the turbulent condition; additionally, the turbulent case has a negative $C_{nmax} \approx -4.0$ at 37°. This modification has a significant influence on the yawing moment alleviation in the high AOA range.

In this case of the modified "4 STRAKES" forebody with the "BODY 1" configuration, it appears that the " 4 STRAKES" forebody may not be helpful to reduce the side force magnitude, but it did reduce the induced side force AOA range. On the other hand, it did reduce the yawing moment magnitude and the AOA range over which those yawing moments are produced, keeping them to a manageable level.

S0141: NON-TURBULENT, + WING, 4 STRAKES
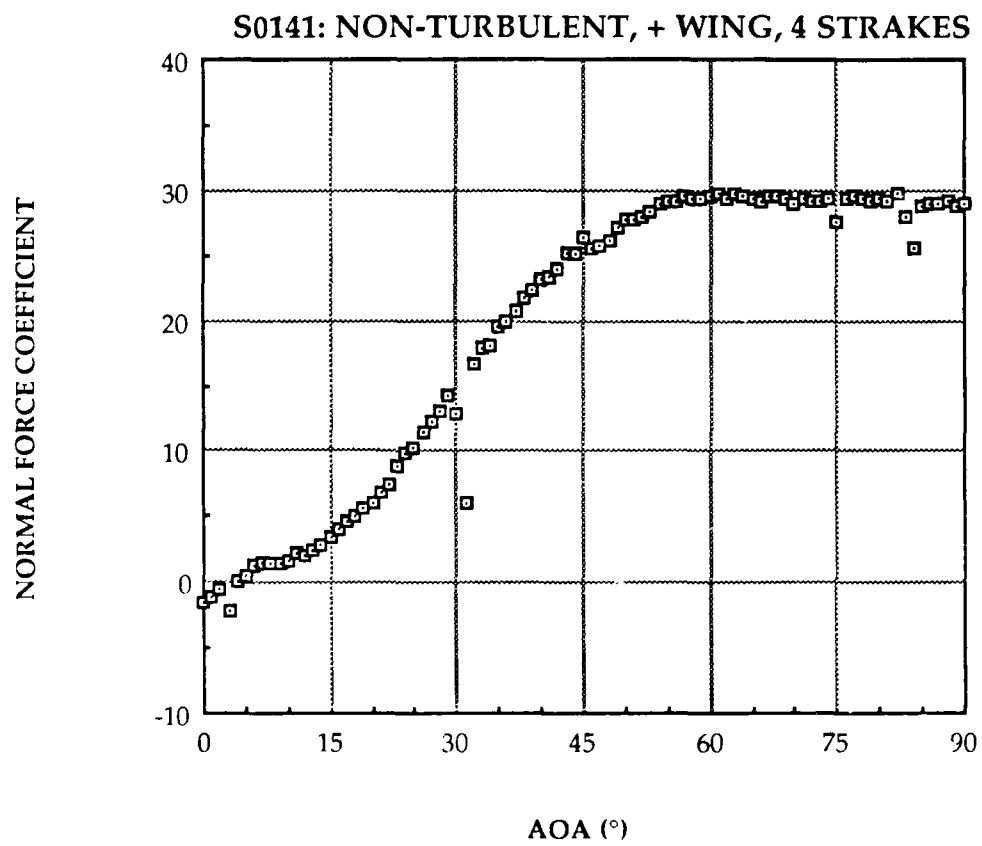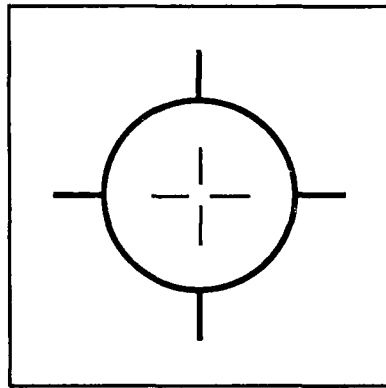
Figure 36. S0141: Normal Force Coefficient

81

S3141: TURBULENT, + WING, 4 STRAKES
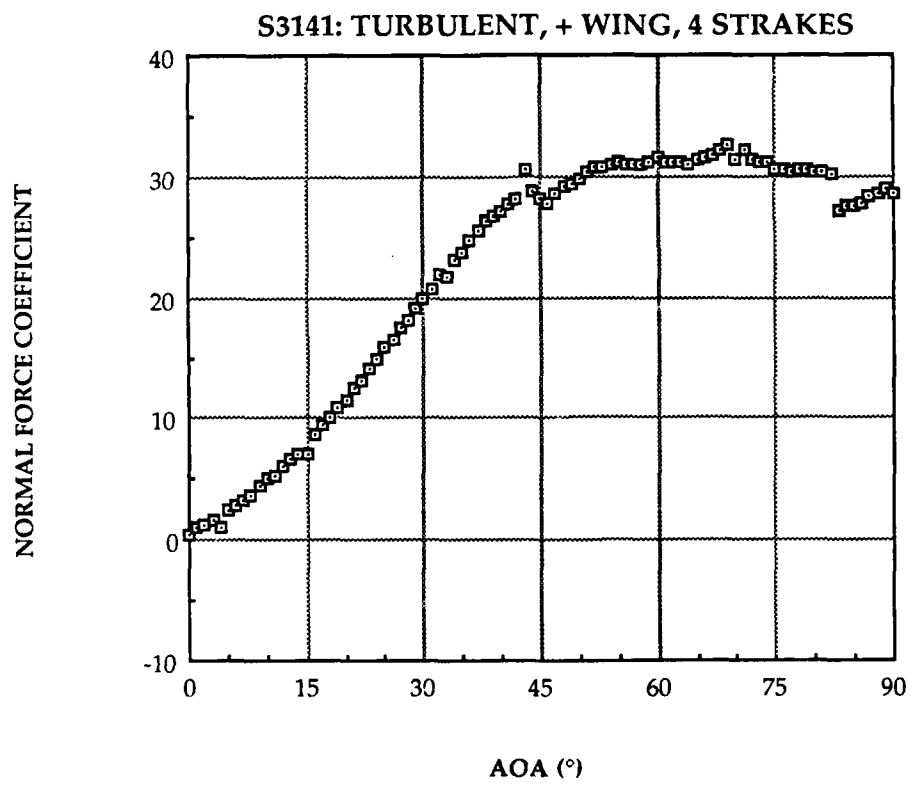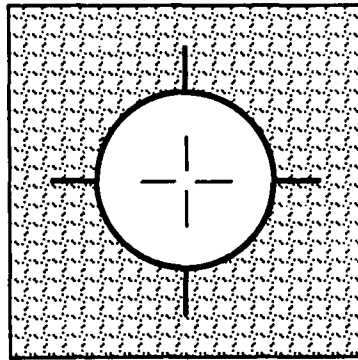
Figure 37. S3141: Normal Force Coefficient

82

S0141: NON-TURBULENT, + WING, 4 STRAKES
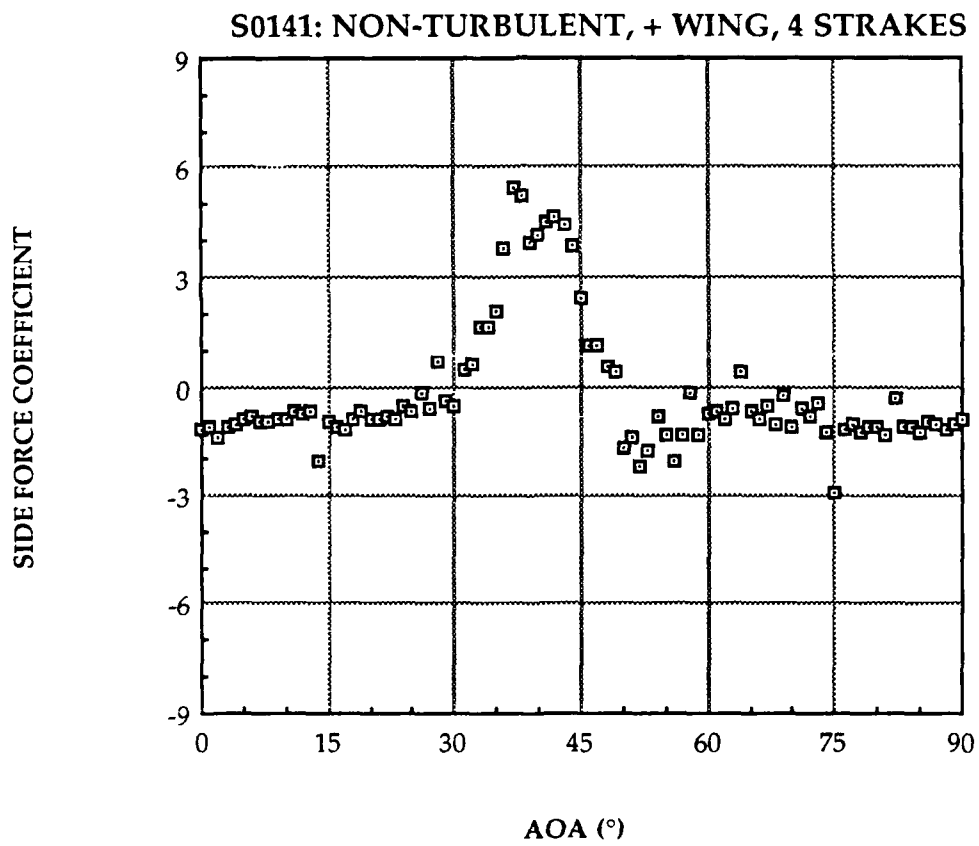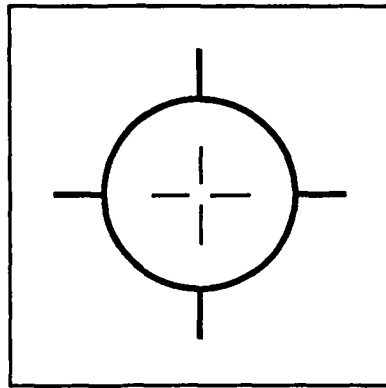
Figure 38. S0141: Side Force Coefficient

Figure 39. S3141: Side Force Coefficient

84

Figure 40. S0141: Yawing Moment Coefficient

S3141: TURBULENT, + WING, 4 STRAKES

Figure 41. S3141: Yawing Moment Coefficient

2. "BODY 2" Configuration

The normal force coefficient curves for the non-turbulent and turbulent conditions, shown in Figures 42 and 43, show smaller C_{Nmax} occurring in about the same AOA region in comparison with the curves of the baseline runs. The C_{Nmax} is about 26.3 at AOA $\approx 70°$ for the non-turbulent condition, and is approximately 27.4 at AOA $\approx 75°$ for the turbulent condition. The plots also indicate the same phenomenon seen in the baseline runs, that the C_{Nmax} of "BODY 2" are smaller than the ones of "BODY 1" with their occurrence at higher AOA.

The side force coefficient results, shown in Figure 44 for the non-turbulent condition and in Figure 45 for the turbulent condition, have similar appearances to each other. They both have an onset AOA $\approx 20°$ followed with an increase in the negative direction to peak values around AOA $\approx 30°$; they then increase in a positive direction to maxima at AOA $\approx 50°$ with a subsequent decrease to zero around AOA $\approx 60°$. The C_{Ymax} is about 2.1 for the non-turbulent condition, and is about 3.0 for the turbulent condition. They have a better performance than the analogous cases in the baseline runs, with a lower C_{Ymax} and a smaller induced side force AOA range. They also have smaller C_{Ymax} values than for comparable results of the "BODY 1" configuration, but a larger AOA range for the induced side forces. The scatter shown in the graph for the turbulence condition for AOA $\leq 15°$ is considered to be caused by a lack of instrument stability. This strake modification works well in a side force reduction in both the non-turbulent and turbulent conditions.

87

The yawing moment coefficient results in Figures 46 and 47 also show improvements over the cases in the baseline runs. The yawing moments become non-zero from AOA $\approx$ 25° and increase in a positive direction to the maxima around AOA $\approx$ 38°, then taper off to zero at AOA $\approx$ 45° followed with scattered results around zero. The C_{nmax} is about 6.1 for the non-turbulent condition and approximately 3.4 for the turbulent condition. The significantly high C_n values at high AOAs shown in the baseline runs are eliminated; by comparison to the results of the baseline runs, the C_{nmax} values are much smaller and move to the intermediate AOA region (about 35°~40°), and the induced yawing moment AOA range is also significantly decreased. This strake modification shows a great alleviation of the yawing moments at the high AOA range.

The "4 STRAKES" nose with "BODY 2" configuration shows more effective results in both side force and yawing moment considerations. This modification reduces the maxima and moves the maxima to lower AOAs; also, it decreases the AOA range over which induced side forces and yawing moments are significant.

3.   Correlations Between C_Y and C_n

In the "BODY 1" configuration tests, the side forces were positive and the yawing moments were negative in an AOA range from 30°~40°, which indicates the side forces are dominant over the afterbody. The side forces then become dominant at the forebody when the yawing moments become positive while the side forces remain positive in the 40°~50° AOA range. The side-force-dominant position moves from the afterbody to the forebody with increasing AOA.

In the "BODY 2" configuration tests, the negative side forces caused positive yawing moments in the 20°~40° AOA range, indicating afterbody-dominant side forces. For AOA ≥ 40°, both side forces and yawing moments were positive but small, indicating forebody dominant side forces. The side-force-dominant position again moves forward with increasing AOA.

In general, the distribution patterns of the domination of side forces observed in the "4 STRAKES" forebody modification case are similar to the ones in the baseline runs. The side forces initially dominate at the afterbody, and move forward to the forebody with higher AOAs.

The "4 STRAKES" forebody reduced the high C_{nmax} in the high AOA region to much smaller C_{nmax} in the intermediate AOA region, and reduced the induced yawing moment AOA range, for both body configurations in both wind tunnel conditions.

S0241: NON-TURBULENT, X WING, 4 STRAKES
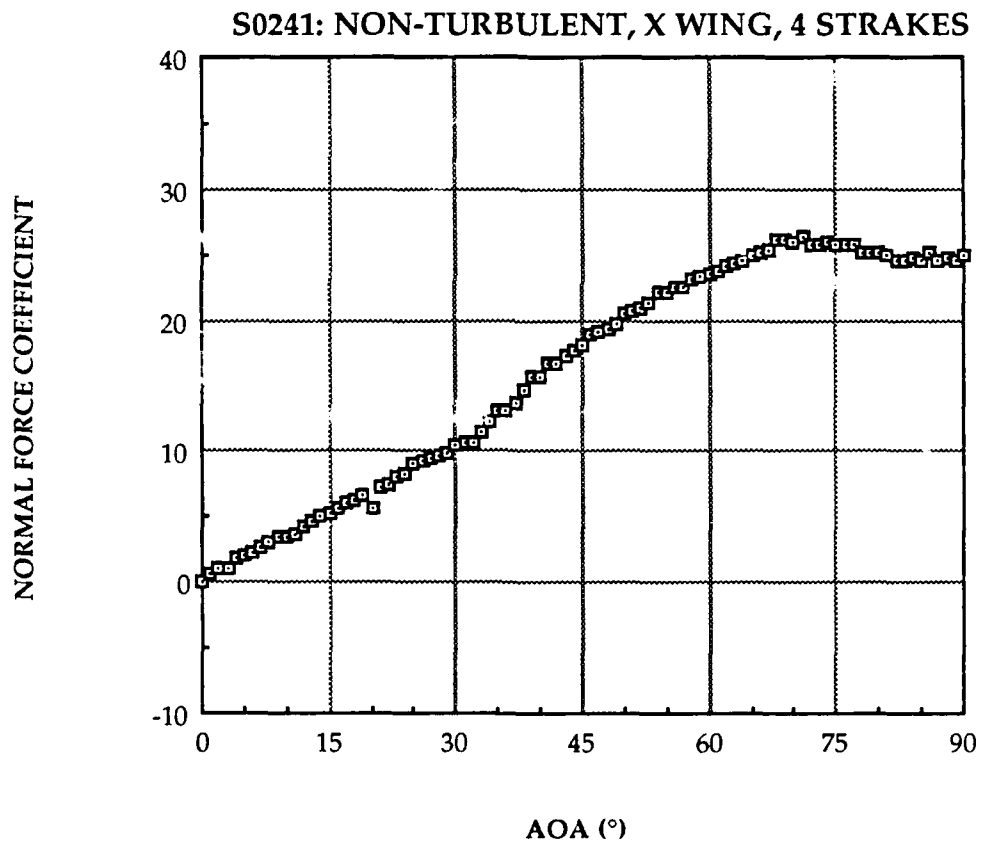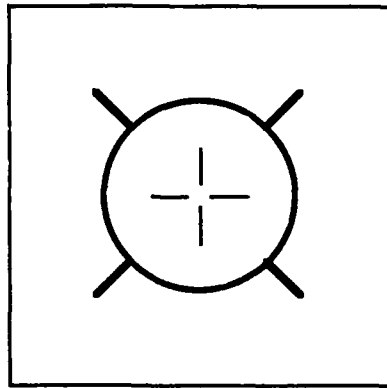
Figure 42. S0241: Normal Force Coefficient

S3241: TURBULENT, X WING, 4 STRAKES
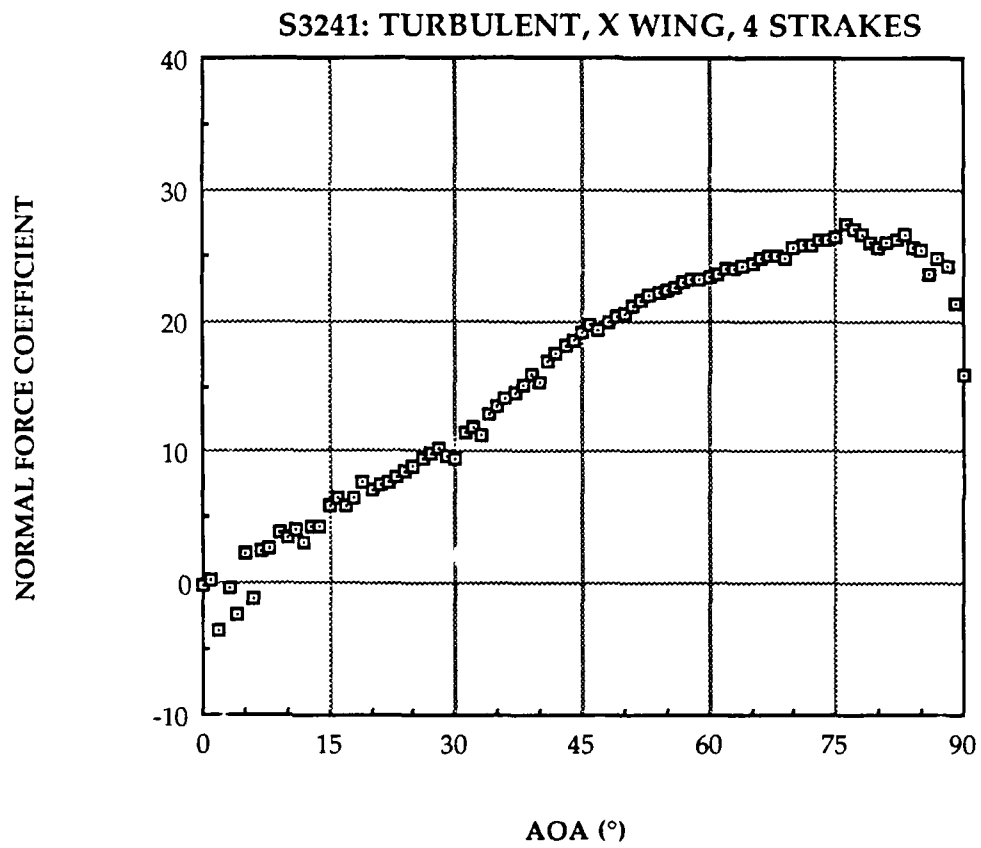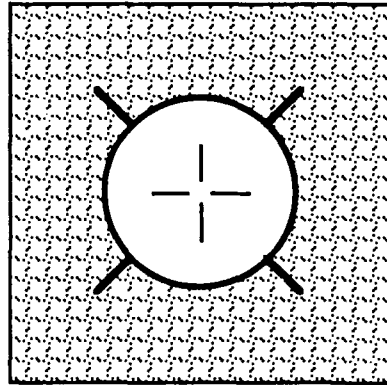
Figure 43. S3241: Normal Force Coefficient

91

S0241: NON-TURBULENT, X WING, 4 STRAKES
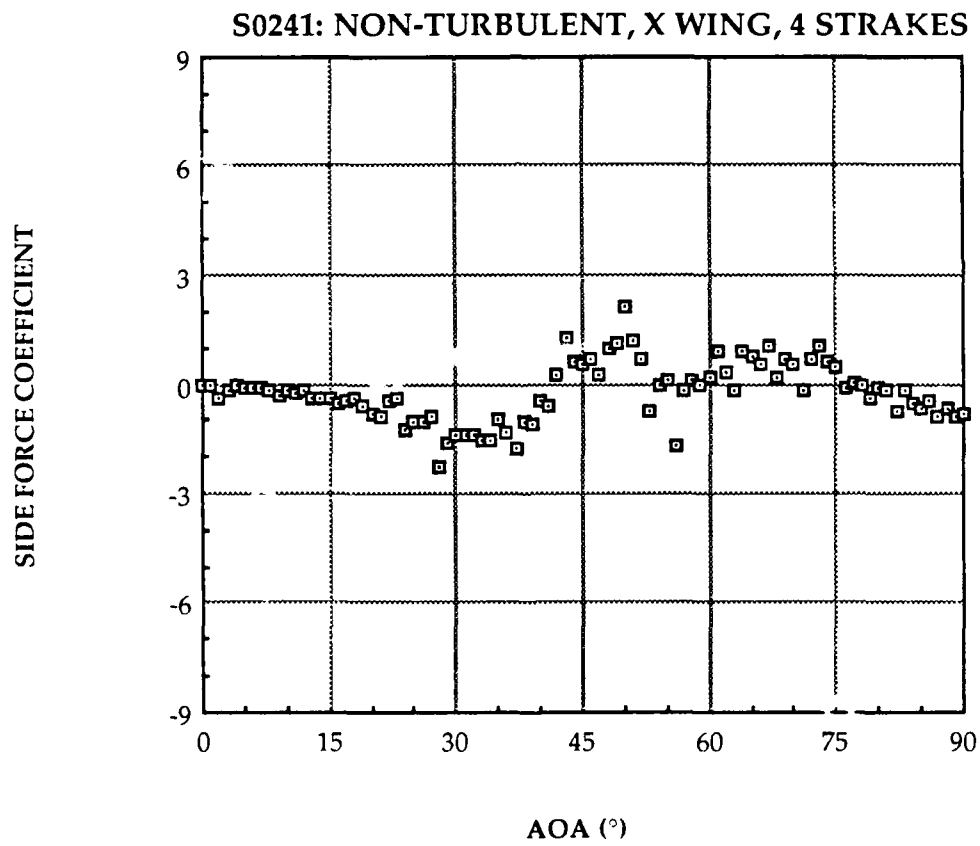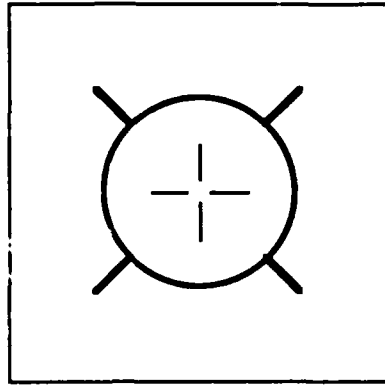
Figure 44. S0241: Side Force Coefficient

S3241: TURBULENT, X WING, 4 STRAKES

Figure 45. S3241: Side Force Coefficient

S0241: NON-TURBULENT, X WING, 4 STRAKES
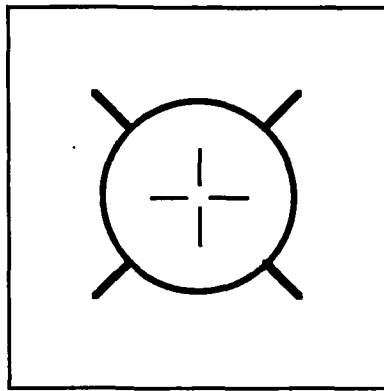
Figure 46. S0241: Yawing Moment Coefficient
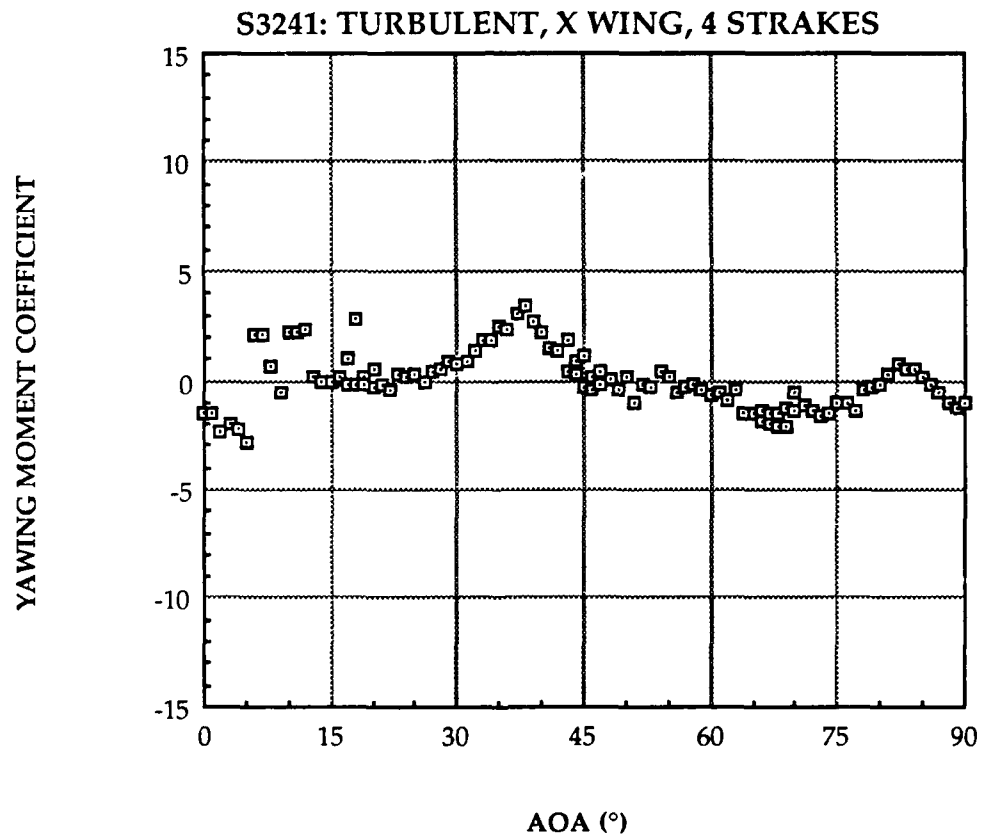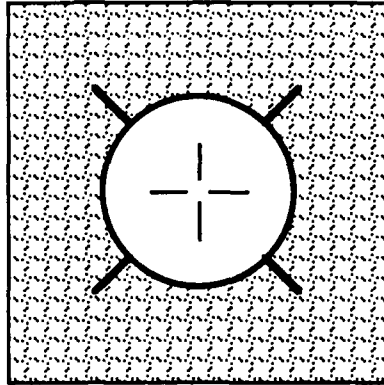
Figure 47. S3241: Yawing Moment Coefficient

D. TEST RUN II (8-STRAKE MODIFIED FOREBODY)

The forebody was further modified by adding four more strakes to the nose tip. The 8-strake modified forebody is illustrated in Figures 16(b) and 17(b). The results of this forebody tested with two body-wing configurations in two wind tunnel conditions are graphed in Figures 48 to 59.

1. "BODY 1" Configuration

The normal force coefficient results for the non-turbulent condition and the turbulent condition are shown in Figures 48 and 49, respectively. They have the usual appearances of the other normal force coefficient trends, and both have maxima about 32.5 at AOA $\approx$ 55°, which are slightly smaller and in a lower AOA region than the comparable cases in the baseline runs.

The side force coefficient curve for the non-turbulent condition, shown in Figure 50, has a similar appearance to, but with more scatter than, the baseline run shown in Figure 26. The onset AOA is about 20°, which is slightly lower than the onset AOA in the baseline run. The curve rises gradually to a $C_{Ymax} \approx 6.3$ at AOA $\approx$ 46°, which is larger than the maximum value observed in the baseline run. Subsequently, it drops with a significant scatter to zero at AOA $\approx$ 75°. The C_Y trend for the turbulent condition in Figure 51 also shows a similarity to that of the baseline run in Figure 27. The onset AOA is delayed to about 25°, and the curve initially increases in the positive direction to a peak $C_Y \approx 2.1$ around AOA $\approx$ 38°. Then it decreases in a negative direction, and reaches a $C_{Ymax} \approx -2.9$ at AOA $\approx$ 52°. Then it switches direction again to another peak at a positive $C_Y \approx 1.6$ around AOA $\approx$ 67°, followed by a drop to zero at AOA $\approx$ 75°. Generally, the C_Y trends for the "8 STRAKES" nose with the "BODY 1" configuration in both wind tunnel

96

conditions are similar to the cases in the baseline runs, with slight differences in peak values at various AOAs and a wider induced side force AOA range. This modification has no significant improvement in side force reduction.

The yawing moment trends in Figures 52 and 53 have similar traces, and are like the cases of the baseline runs shown in Figures 28 and 29 with the exception in the medium AOA region, $45°~60°$. The curves grow initially at AOA $\approx 25°$ in the negative direction to peak at $C_n \approx -3.8$ for the non-turbulent and -2.9 for the turbulent conditions. They then switch direction and go to zero at AOA $\approx 45°$. In the $45°~60°$ AOA region, the C_n values are negative with a peak $C_n \approx -3.3$ around AOA $\approx 52°$ for the turbulent condition, while the C_n remains constant at about 0.8 for the non-turbulent condition. After $60°$, they both jump to $C_{nmax} \approx 10.0$ at AOA $\approx 69°$ which are about the same magnitudes at slightly higher AOAs as the ones of the baseline runs; they then drop back to zero at AOA $\approx 77°$. This "8 STRAKES" modification does not give any significant improvement for alleviating yawing moments.

This case of the "8 STRAKES" forebody with the "BODY 1" configuration shows no significant improvement, either for the alleviation in magnitude of side forces and yawing moments, nor for the reduction in the induced force and moment AOA range.
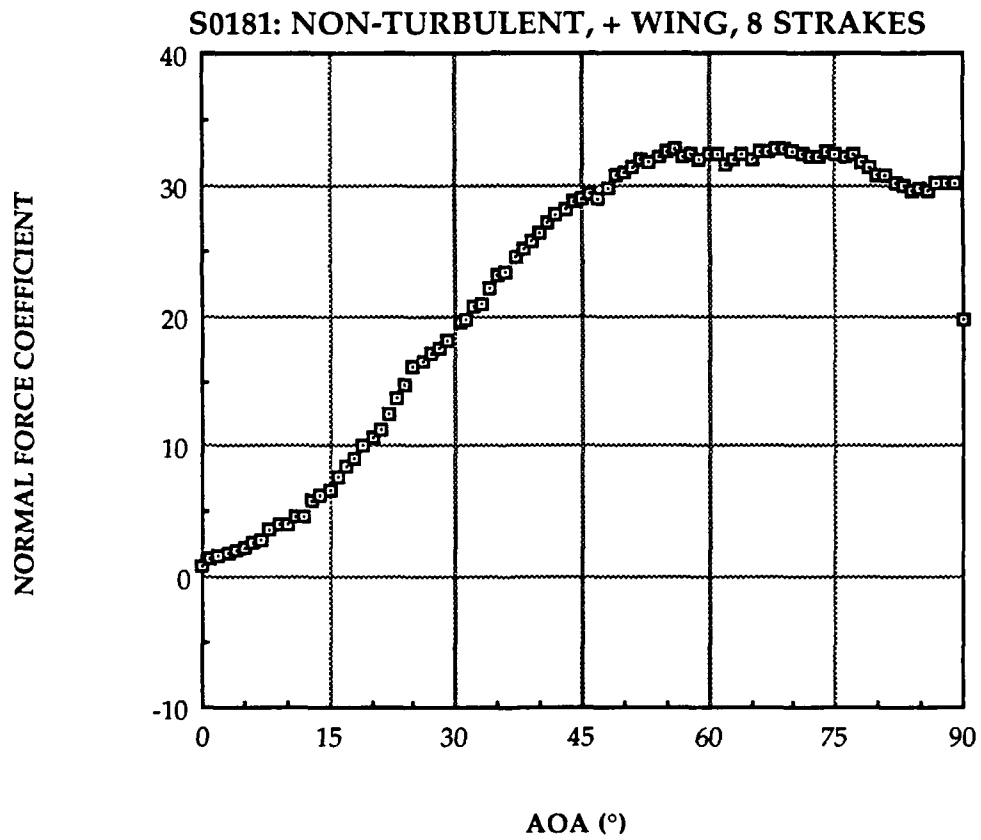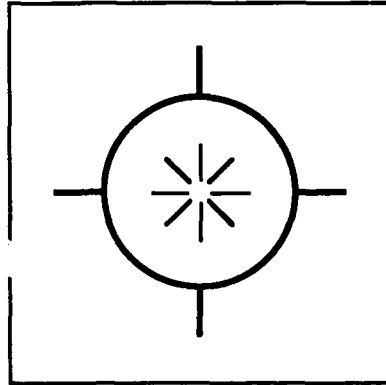
Figure 48. S0181: Normal Force Coefficient

S3181: TURBULENT, + WING, 8 STRAKES
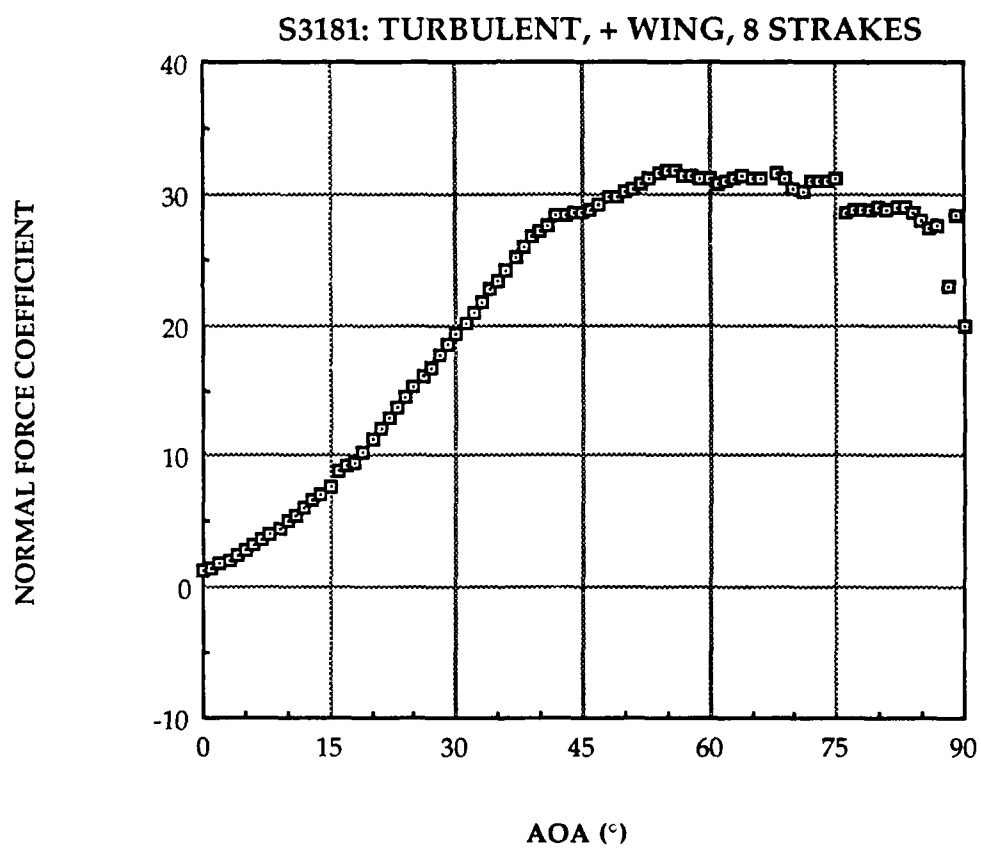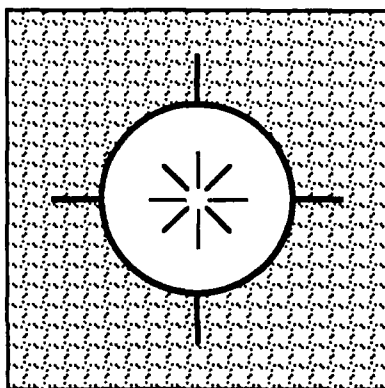
Figure 49. S3181: Normal Force Coefficient
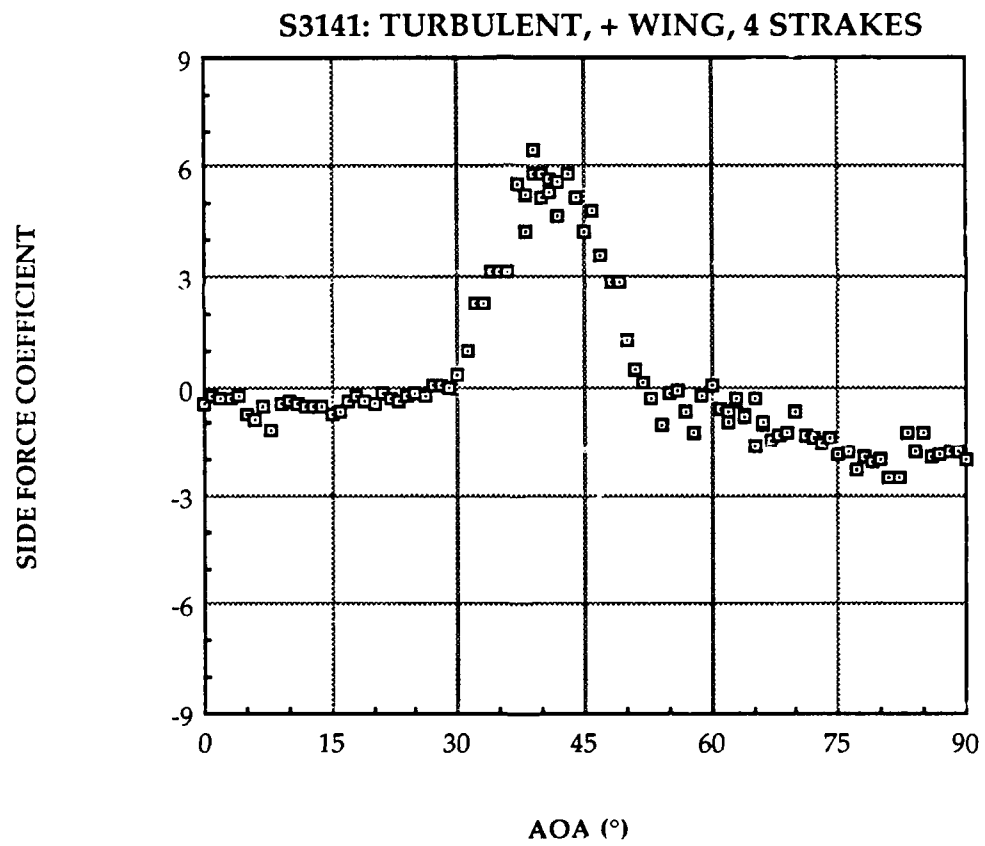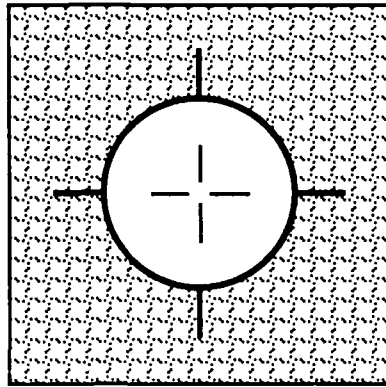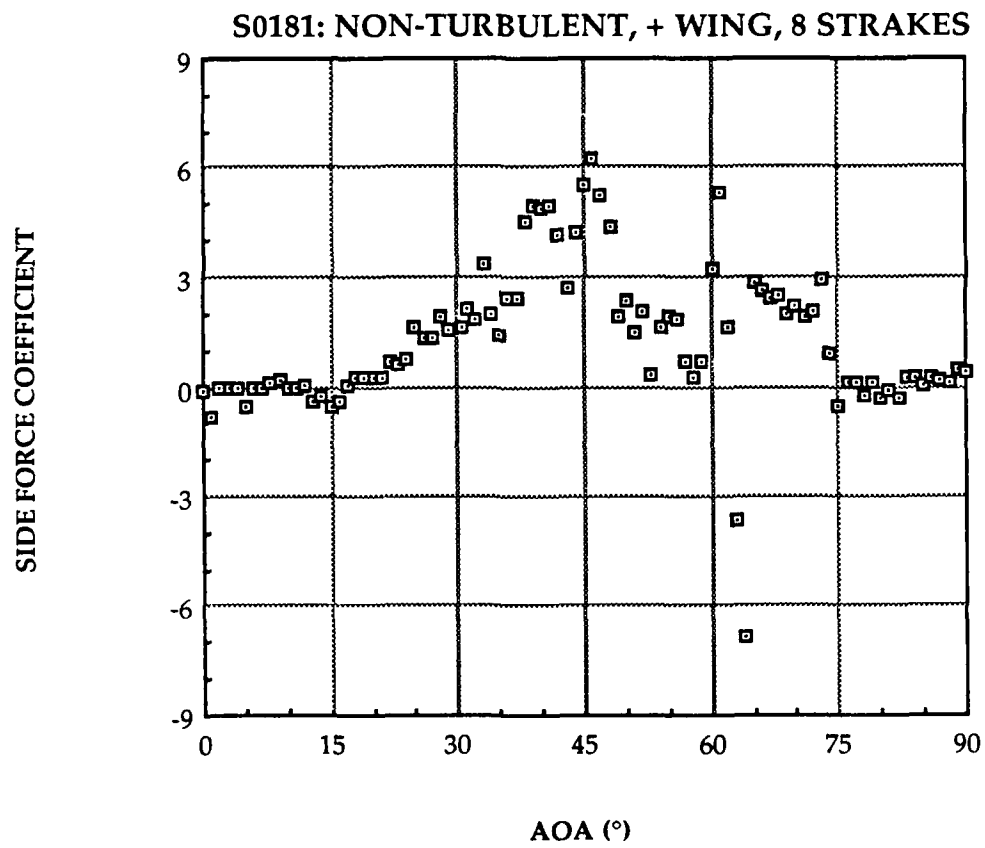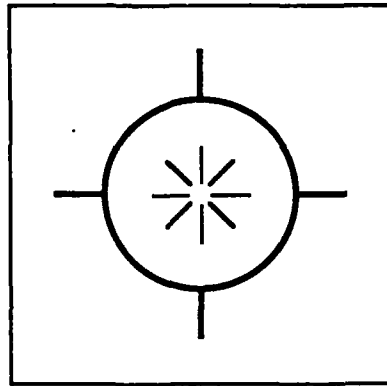
Figure 50. S0181: Side Force Coefficient

100
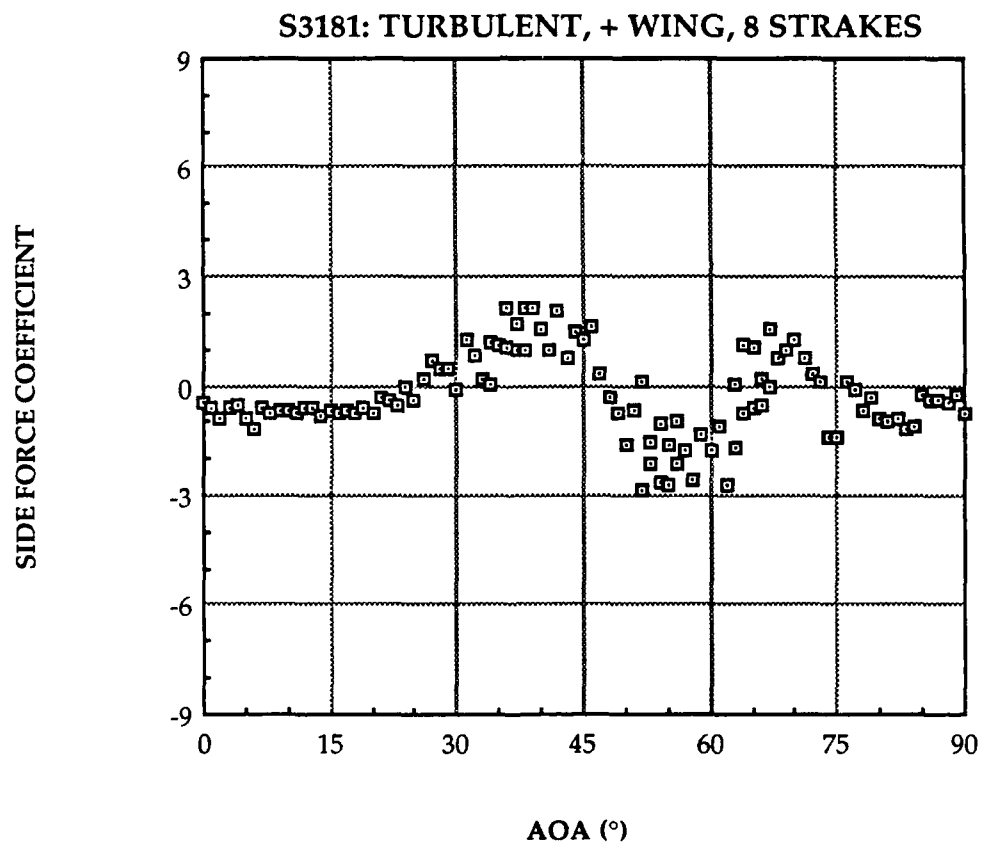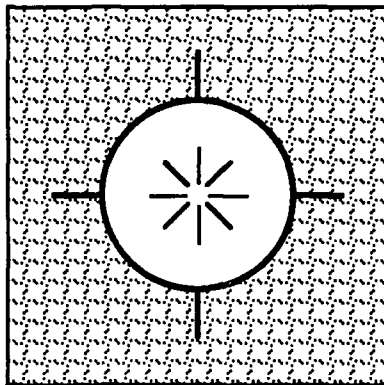
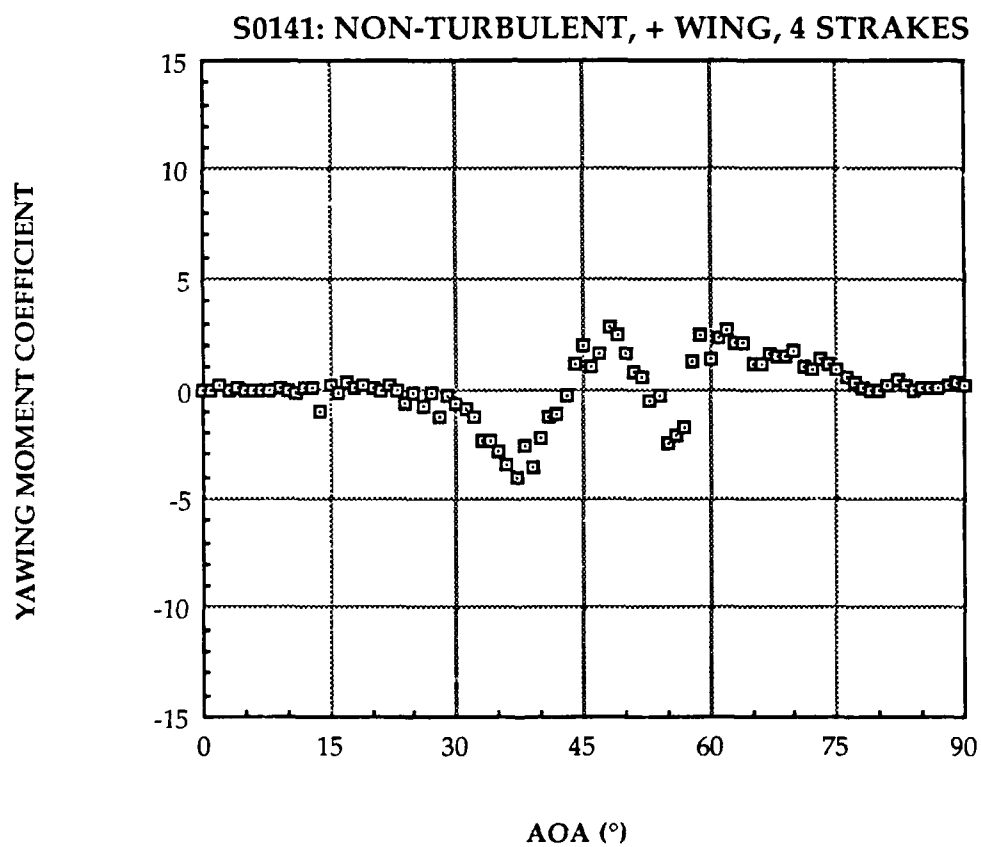Figure 51. S3181: Side Force Coefficient

101
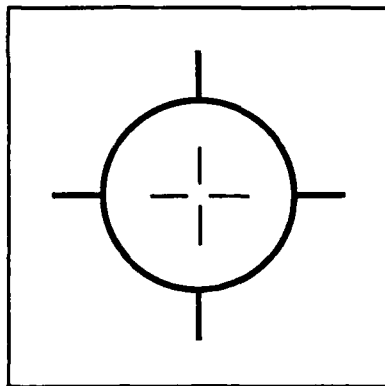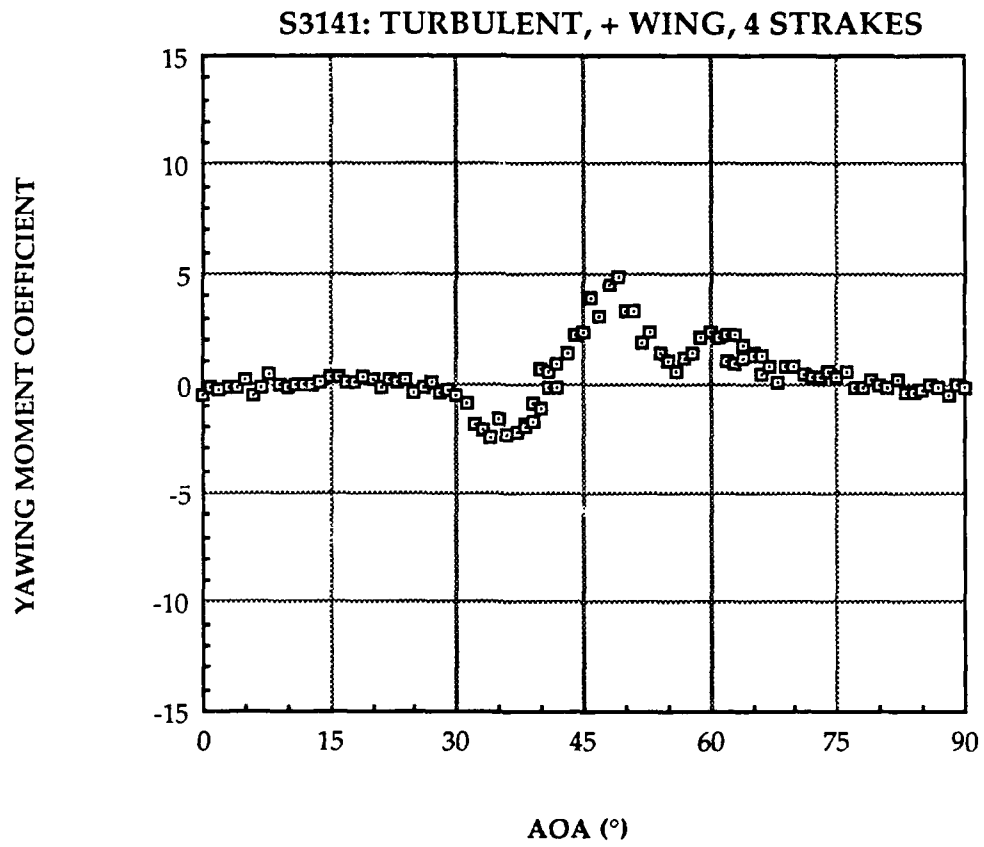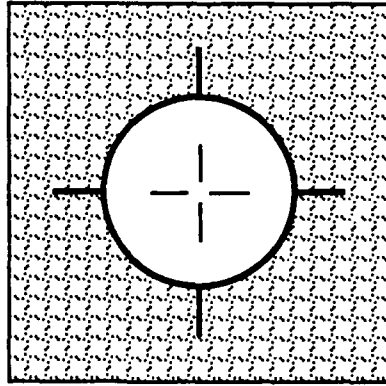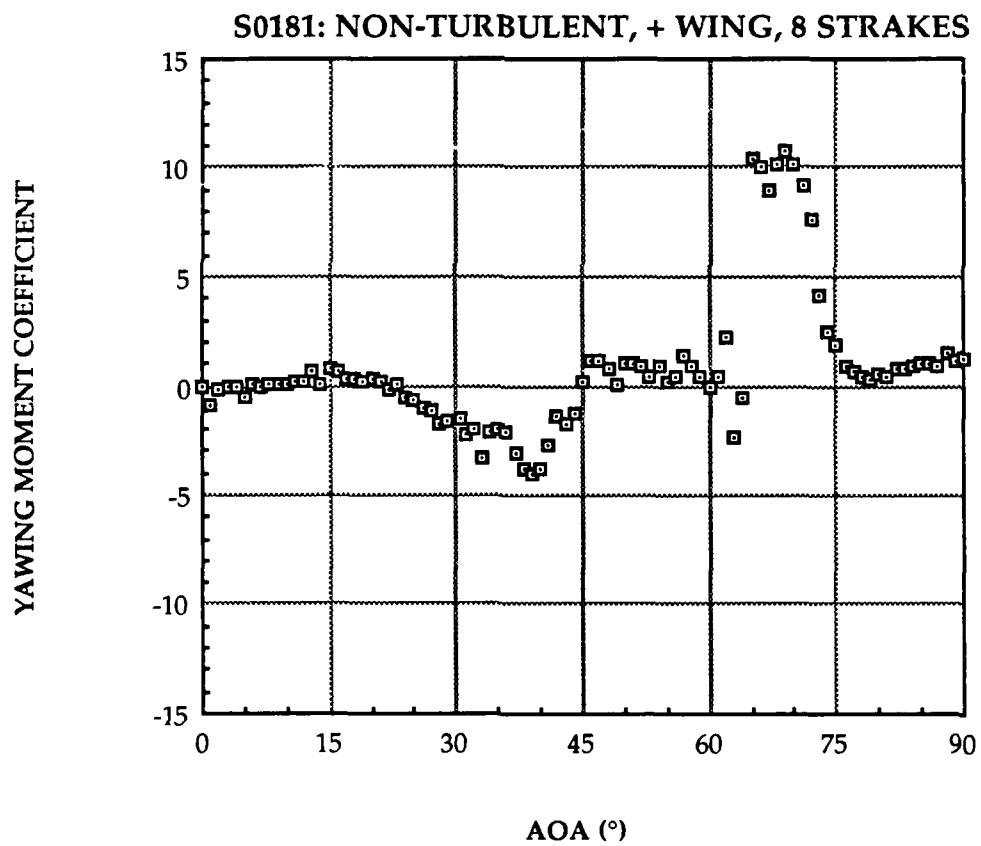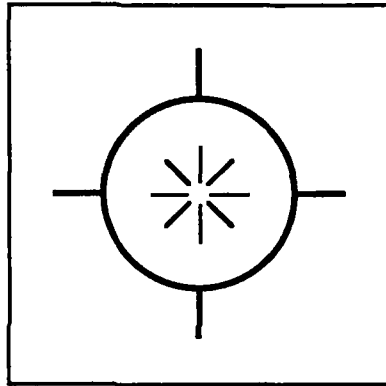
Figure 52. S0181: Yawing Moment Coefficient
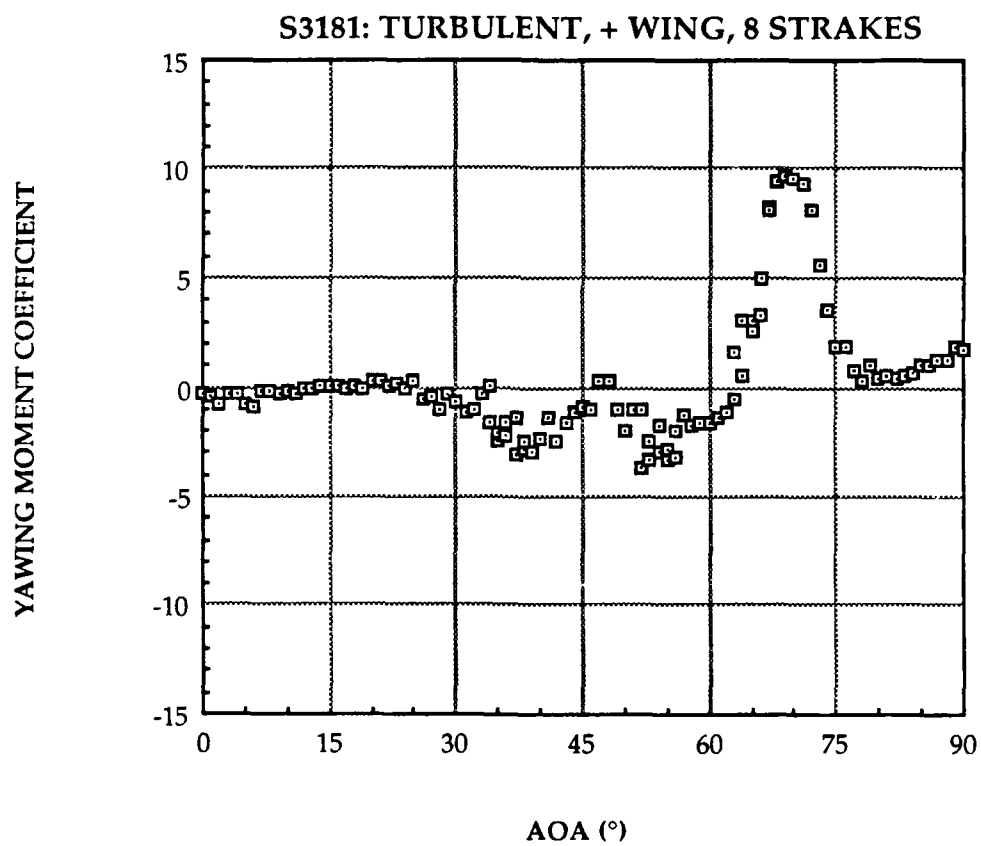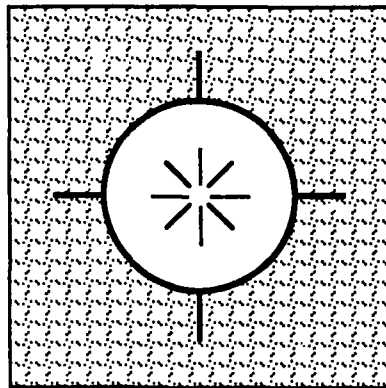
Figure 53. S3181: Yawing Moment Coefficient

2. "BODY 2" Configuration

The normal force coefficient plots in Figures 54 and 55, for the non-turbulent and turbulent conditions respectively, have the usual appearance of the other C_N plots. The C_{Nmax} is about 27.2 at AOA $\approx$ 76° for the non-turbulent condition, and for the turbulent condition is approximately 26.9 at AOA $\approx$ 83°, which is unusually high and might be due to scatter. These values are smaller than for the cases in the baseline runs, and they indicate that the C_{Nmax} of "BODY 2" are smaller and occur at a higher AOA than the ones of "BODY 1."

The side force coefficient plots for the non-turbulent and turbulent conditions, shown in Figures 56 and 57, are similar to the original ones in the baseline runs, respectively, except in the medium AOA region of 45°~60°. The side force becomes negative at AOA $\approx$ 15° for the non-turbulent condition and at AOA $\approx$ 20° for the turbulent condition; the two curves both have negative peak values at AOA $\approx$ 30°. In the intermediate AOA region from 45°~60°, the non-turbulent condition has a scatter C_Y around zero, while the turbulent condition experiences a negative C_{Ymax} $\approx$ -2.5 at AOA $\approx$ 54°. The C_{Ymax} is about 3.6 at AOA $\approx$ 63° for the non-turbulent condition, and is about 2.6 at AOA $\approx$ 67° for the turbulent condition. In comparison to the comparable cases in the baseline runs, the positive maxima are slightly smaller but in the same AOA region, and the turbulent case has an additional negative maximum in the intermediate AOA region; the onset AOAs remain about the same and the induced side force AOA ranges are smaller for both wind tunnel conditions. In general, this modification does not have an improvement in side force reduction.

104

In Figures 58 and 59, the yawing moment coefficient results also show similar appearances to the original ones in the baseline runs. For the non-turbulent condition, the yawing moment grows positively from AOA $\approx$ 15^c with a peak at about 30°, then drops to zero with a scatter trend for AOA between 35° and 60°. There is an increase to the $C_{nmax} \approx 7.9$ at AOA $\approx$ 72° followed by a drop to zero at about 77°; the maximum is smaller and at a higher AOA then for the baseline run. For the turbulent condition, the positive yawing moment also starts at AOA $\approx$ 15° with a peak around 30°; two maxima are observed, one negative $C_{nmax} \approx -5.5$ around 60° and one positive $C_n max \approx 5.9$ around 70° followed by a drop to zero about 77°. The comparison to the baseline run shows that the positive maximum is reduced but in the same AOA region, while the negative peak in the medium AOA region is increased and delayed to a higher AOA. In both conditions, the onset AOA and the induced AOA range have no significant changes. This modification does not give better performance in yawing moment alleviation.

The "8 STRAKES" modified forebody with the "BODY 2" configuration reduced side forces and yawing moments slightly at high AOAs for both wind tunnel conditions, but had a penalty of increasing negative maxima among the intermediate AOAs in both side forces and yawing moments for the turbulent condition. From another viewpoint, the onset AOA and induced AOA range have no significant changes due to the modification.

3.   Correlations Between C_Y and C_n

"BODY 1" configuration is discussed here first. For the non-turbulent condition, the induced side forces are most positive for AOA

105

between 20° and 75°; the negative yawing moments between 20° and 45° indicate the afterbody side forces are dominant. Between 45° and 60° the yawing moments are nearly equal to zero, and side forces dominate at the forebody with positive yawing moments from 60°~75°. For the turbulent condition, the positive side forces with negative yawing moments for AOA between 25° and 45° indicate the afterbody-dominant side forces; between 45° and 65° the side forces switched to negative and dominated at the forebody to give negative yawing moments. The small positive side forces with large positive yawing moments between 65° and 75° indicate that the forebody-dominant side forces move further forward but switch direction. In both wind tunnel conditions, the dominant side forces moved from the afterbody to forebody when the AOA was increased.

In the "BODY 2" configuration, the side force and yawing moment results for both wind tunnel conditions have very similar appearances with the exception in the medium AOA region between 40° and 60°. The side forces are negative and dominate at the afterbody to give positive yawing moments in the low AOA region between 15° and 40°; for high AOA between 60° and 75°, the side forces dominate at the forebody as both the side forces and yawing moments are positive. In the intermediate AOA region between 40° and 60°, the side forces and yawing moments are both nearly zero for the non-turbulent condition, while both negative side forces and yawing moments indicate forebody-dominant side forces for the turbulent condition.

Generally speaking, the side-force-dominant position moved from the afterbody to forebody with increasing AOA in this "8 STRAKES" modification case. This observation is the same pattern discovered in the

106

baseline runs and in the first set of test runs ("4 STRAKES" modified forebody).
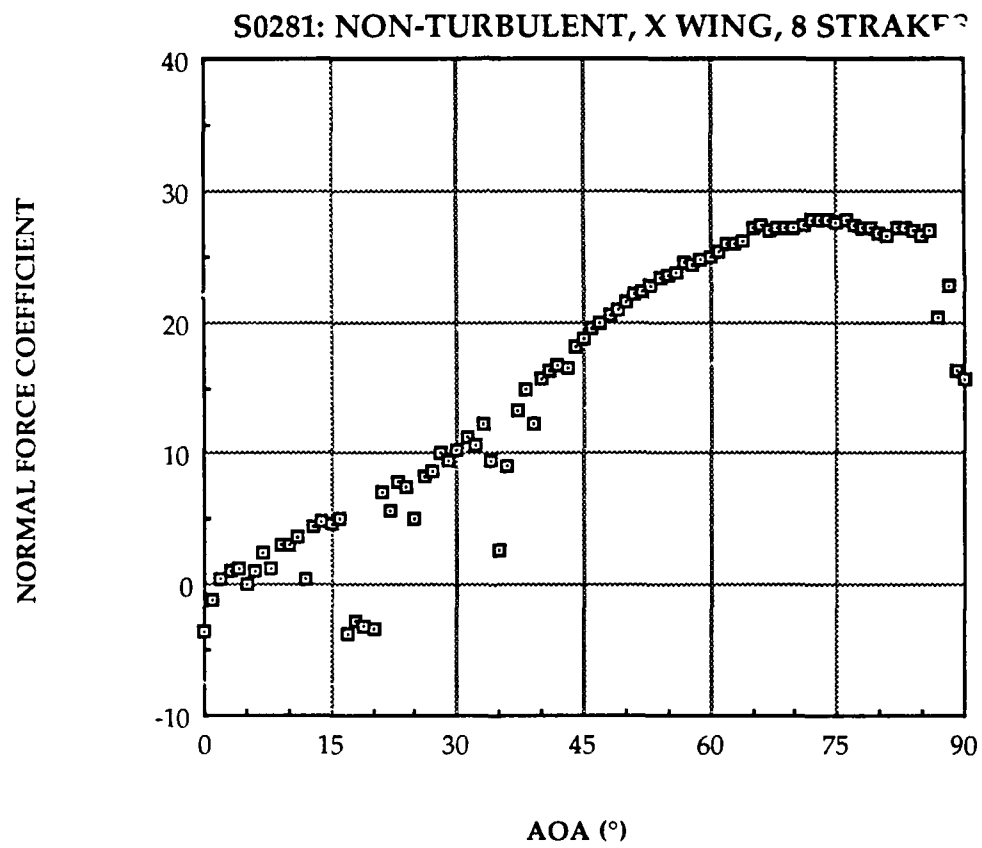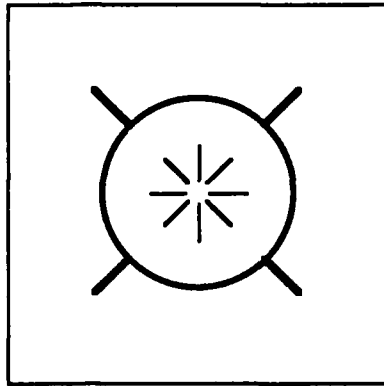
Figure 54. S0281: Normal Force Coefficient

108

## S3281: TURBULENT, X WING, 8 STRAKES
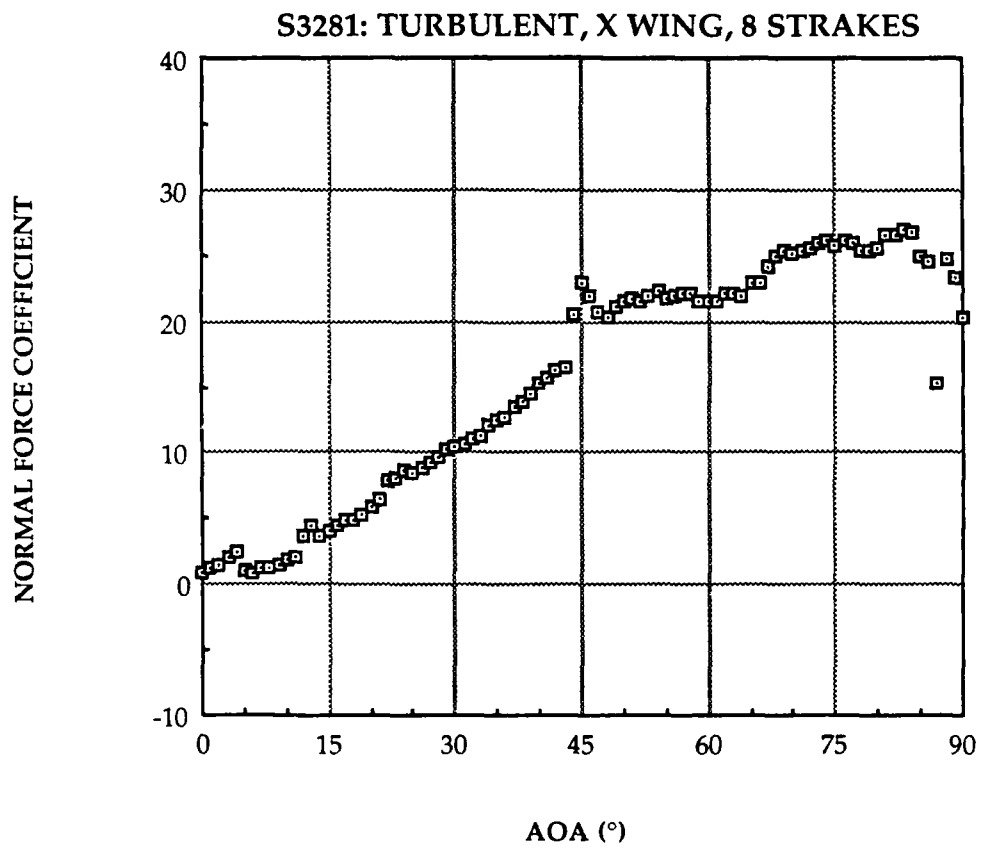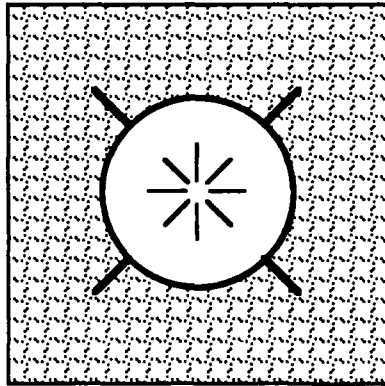
Figure 55. S3281: Normal Force Coefficient
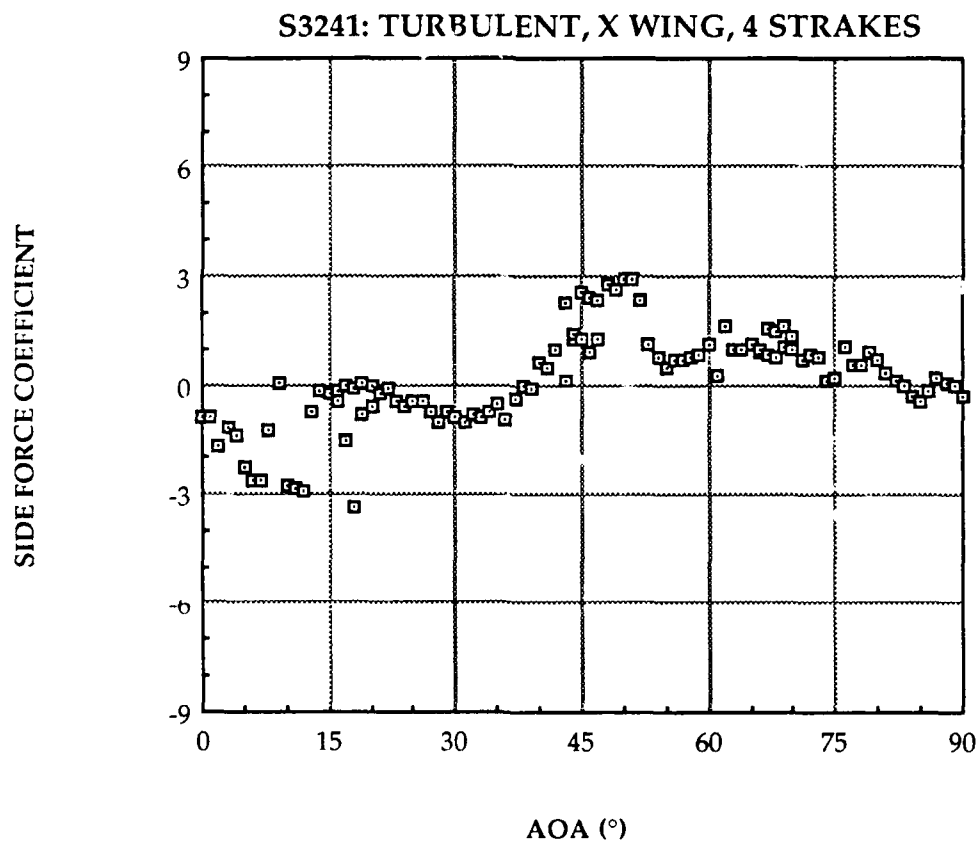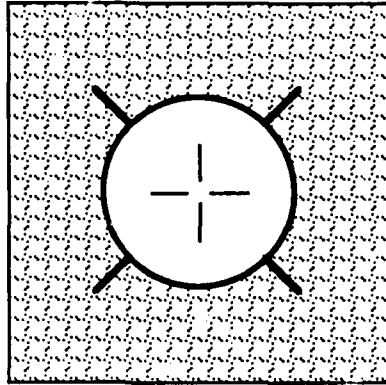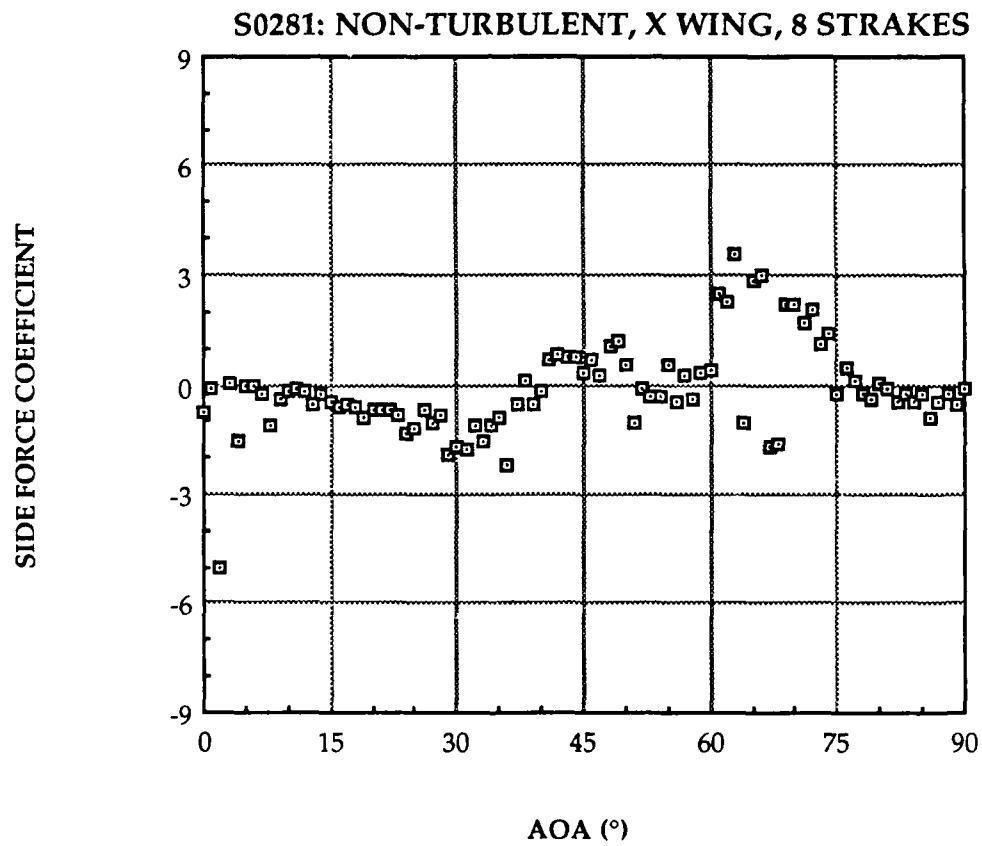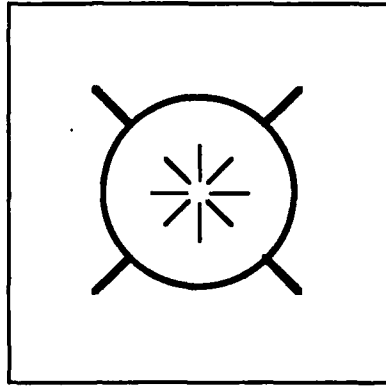
Figure 56. S0281: Side Force Coefficient

110

S3281: TURBULENT, X WING, 8 STRAKES
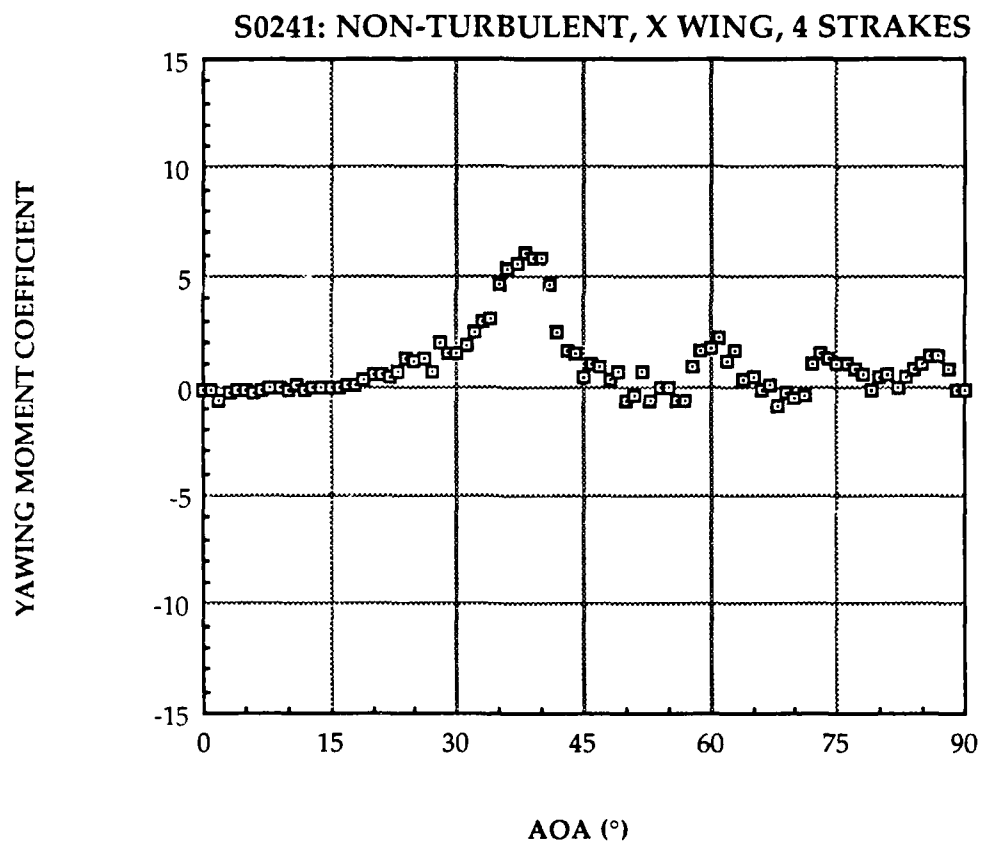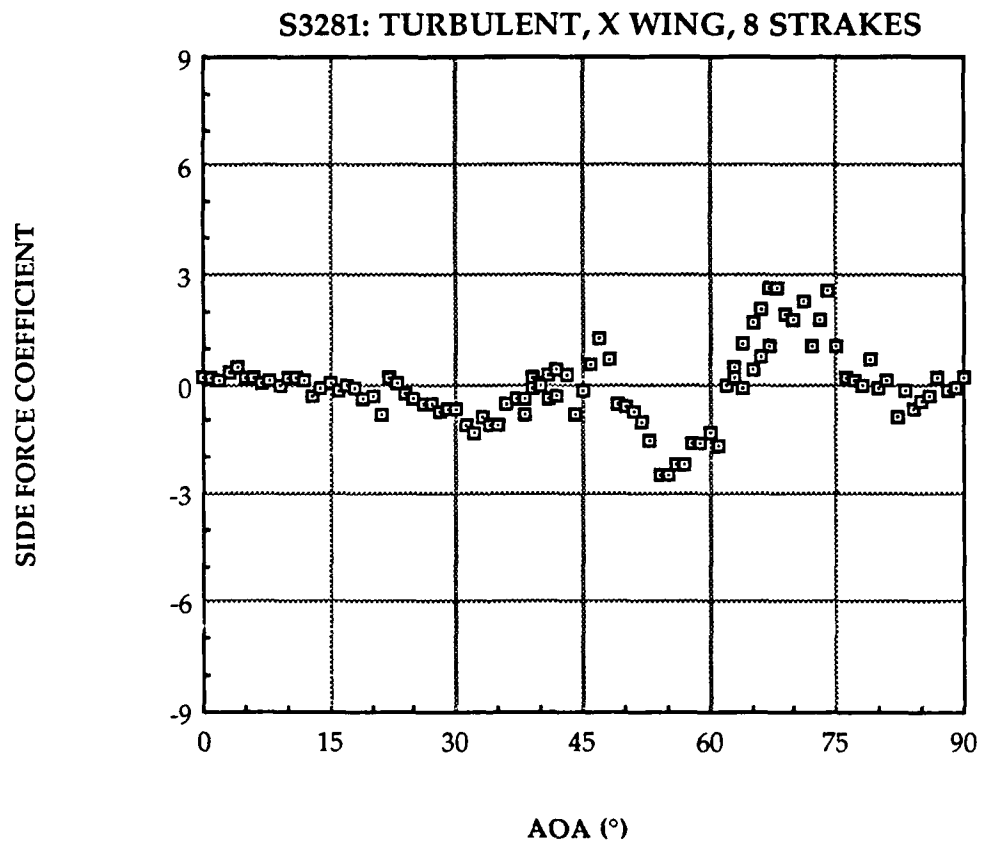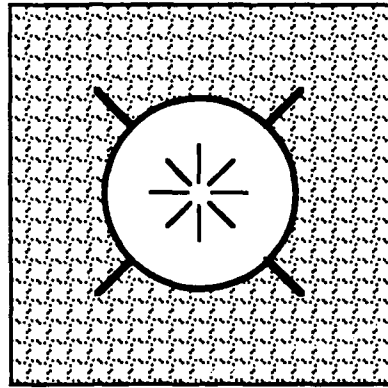

Figure 57. S3281: Side Force Coefficient

111
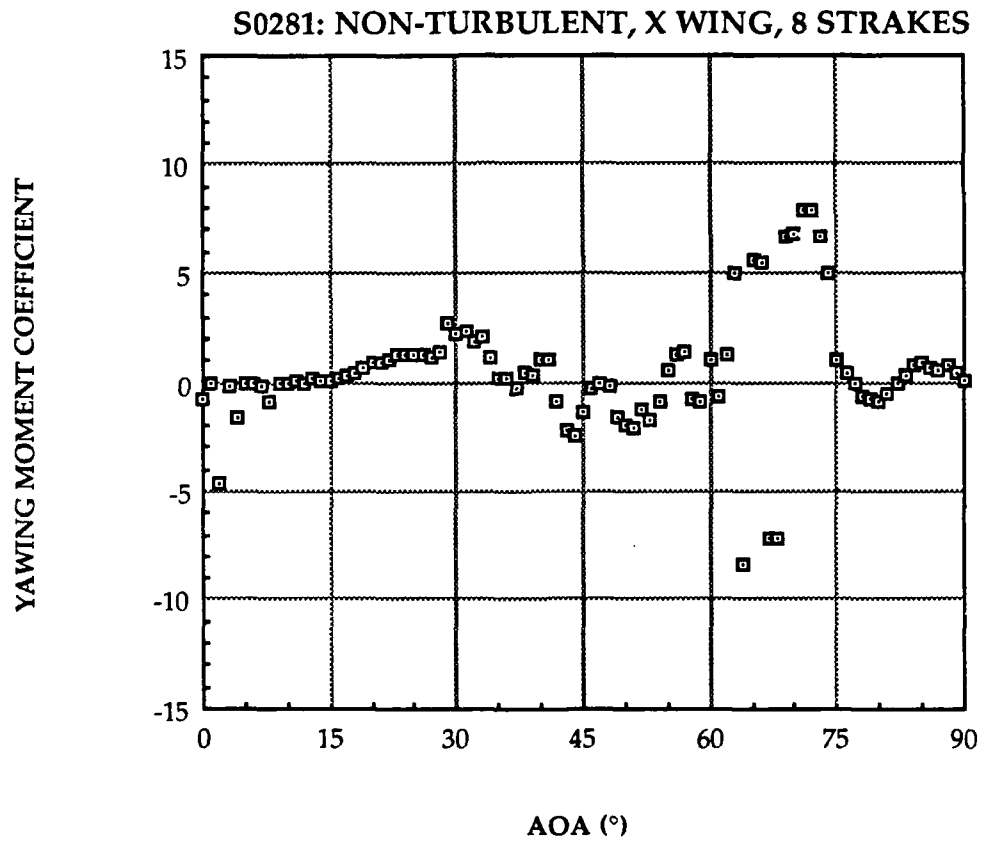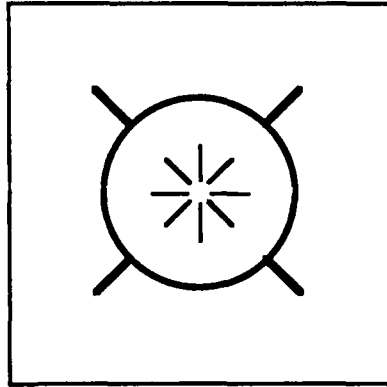
Figure 58. S0281: Yawing Moment Coefficient
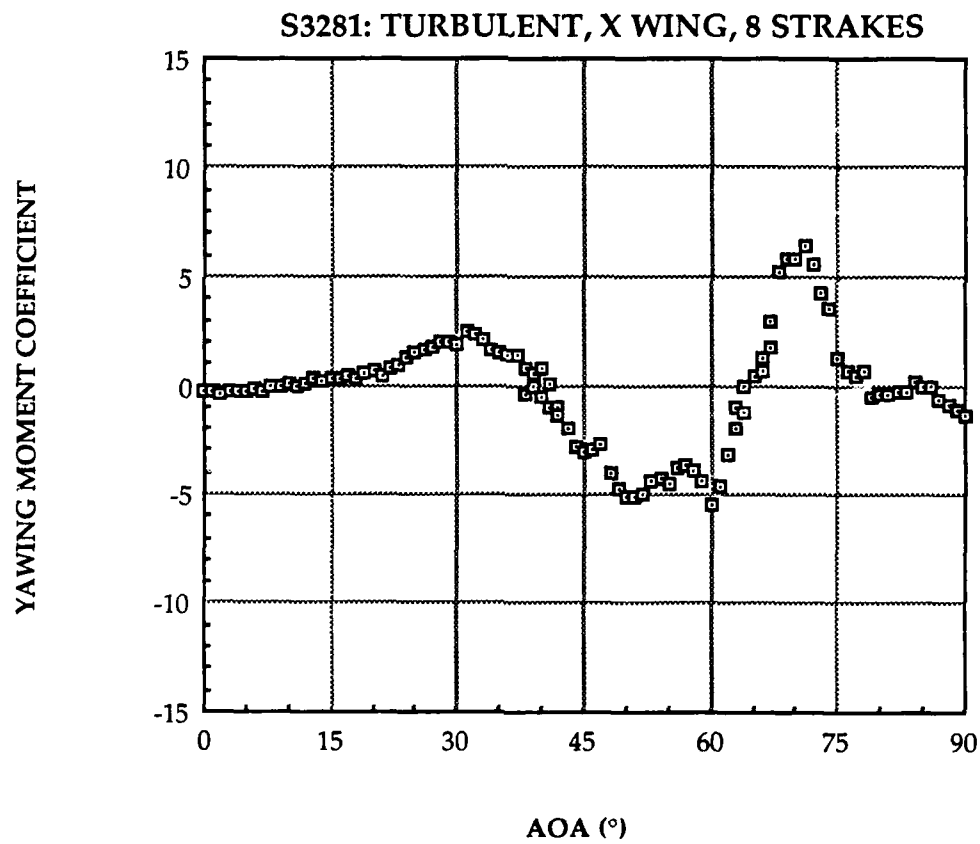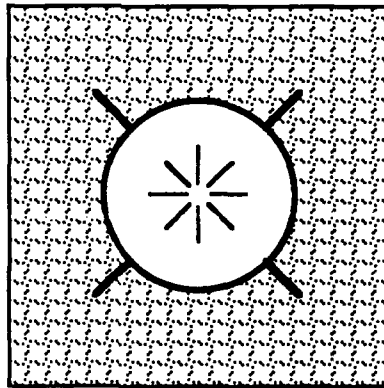
Figure 59. S3281: Yawing Moment Coefficient

113

IV. DISCUSSION AND CONCLUSIONS

A. DISCUSSION

Three test conditions treated in this experiment were the turbulence in the flowfield, the body configuration, and the strake modified forebody which was the subject of the principal investigation. The discussion is made to observe the effects of changing a single condition with the other two fixed. The main results of the experiments to be discussed include: (1) the C_{Nmax} and its pertinent AOA region; (2) the C_{Ymax} and its pertinent AOA region, and the induced side force onset AOA and the induced AOA range; and (3) the C_{nmax} and its pertinent AOA region, and the induced yawing moment onset AOA and the induced AOA range.

1. Effects of Turbulence

The turbulence was introduced in the flowfield by installing a grid in the wind tunnel as described previously. The effects of turbulence are analyzed in four categories:

a. Normal Forces

The normal force coefficient trends for both the non-turbulent and turbulent conditions had a very similar and typical pattern. The C_{Nmax} had almost the same values and occurred in about the same AOA region for both wind tunnel test conditions. In some cases, the C_{Nmax} was delayed to a slightly higher AOA with the turbulence.

A typical normal force coefficient trend is described as follows: The C_N starts at about zero at AOA = 0°, grows to a maximum at a high AOA,

and then decreases until AOA = 90°. The decrease after the maximum is due to the stall of the wings; thus the normal forces were generated almost purely by the blockage of the presented model.

b. Side Forces

The turbulence had an irregular effect on the side force coefficient trends. Normally, the C_Y graphs for the turbulent condition had a similar appearance to those for the non-turbulent condition with some exceptions. The C_{Ymax} were about the same values and occurred in about the same AOA region for both wind tunnel conditions; one exception was for the "8 STRAKES" modified forebody, which had a negative maximum for the turbulent condition and a positive maximum for the non-turbulent condition. The induced side force onset AOA and the induced side force AOA range for the turbulent condition remained approximately the same as those for the non-turbulent condition.

c. Yawing Moments

The introduced turbulence did not significantly alter the yawing moment coefficient trends. The C_{nmax} remained almost at the same values and also occurred in about the same AOA region; in some cases, the turbulence brought an extra negative maximum at a lower AOA. Both the induced yawing moment onset AOA and the induced yawing moment AOA range were not changed significantly by introducing the turbulent flow.

d. Correlations Between Side Forces and Yawing Moments

The turbulence did not influence the side force distribution patterns. For both the non-turbulent and turbulent conditions, the induced

115

side forces always dominated at the afterbody at low AOA and at the forebody at high AOA in the induced AOA range.

2. Effects of Body Configuration

The "BODY 0" configuration was used only in the preliminary runs, and will not be considered here. The results of the "BODY 1" and "BODY 2" configurations, i.e. "+" wing and "x" wing, will be discussed and compared to each other.

a. Normal Forces

The normal force coefficient plots for both the "+" wing and "x" wing had similar patterns. But the C_{Nmax} values of the "x" wing configuration were 4~5 units smaller than those of the "+" wing configuration due to less blockage by the wing span in the "x" wing configuration. The maximum C_N occurred in a higher AOA region around 70°~75° for the "x" wing configuration, and in a lower AOA region around 55°~65° for the "+" wing configuration.

b. Side Forces

The side force coefficient results for the "+" wing did not have a similarity to those for the "x" wing. It was observed in Ref. 12 that the asymmetric vortices of the "+" wing model were closer to the model body than those of the "x" wing model; this phenomenon apparently caused the differences of the side force characteristics for the two different body configurations. The "x" wing configuration usually had a smaller C_{Ymax} at a higher AOA, a lower side force onset AOA, and a broader induced side force AOA range than the "+" wing configuration.

116

c. Yawing Moments

The "+" wing and "x" wing configurations did not have similar yawing moment coefficient graphs, except for the baseline runs which had similar trends for both body configurations but slightly different amplitudes. Thus, a general tendency of the C_{nmax} was not achieved. But the the induced yawing moments were observed to start at a lower AOA for the "x" wing configuration.

In the first set of test runs ("4 STRAKES" modified forebody), the induced yawing moment AOA range for the "x" wing configuration was smaller; but in the baseline runs and the second set of test runs ("8 STRAKES" modified forebody), the "x" wing body had a broader induced yawing moment AOA range than the "+" wing body.

d. Correlations Between Side Forces and Yawing Moments

The body configuration did not affect the side force distribution patterns. The dominant side forces moved from afterbody to forebody as the AOA increased for both the "+" wing and "x" wing configurations.

3. Effects of Strake Configuration

The results of the two modified forebodies with four and eight strakes will be discussed and compared with the results of the baseline runs.

a. Normal Forces

The addition of forebody strakes did not change the general patterns of normal force coefficient trends. The C_{Nmax} was slightly reduced by the addition of strakes on the forebody, but occurred in about the same AOA region.

b. Side Forces

The "4 STRAKES" and "8 STRAKES" modified forebodies produced different effects on the side force coefficient results. But no general tendency of the effects on changing strake configuration only was observed.

With comparison to the results of the baseline runs, the "4 STRAKES" forebody with the "+" wing body caused a larger C_{Ymax} in the same AOA region; the "4 STRAKES" forebody with the "x" wing body resulted in a slightly smaller C_{Ymax} at lower AOAs. The onset AOA was kept about the same. The induced side force AOA range was reduced, especially for the "+" wing configuration.

By comparison with the results of the baseline runs, the "8 STRAKES" forebody in the non-turbulent airflow gave the same C_{Ymax}, both the magnitude and in the AOA region; in the turbulent flow, the "8 STRAKES" forebody introduced a C_{Ymax} of opposite sign in the AOA region 50°~55°. However, the side force onset AOA and the induced side force AOA range showed no significant change.

c. Yawing Moments

The "4 STRAKES" forebody gave significant results in yawing moment alleviation, and the "8 STRAKES" forebody showed about the same C_n plots as those in the baseline runs.

The "4 STRAKES" forebody eliminated the high C_{nmax} in the high AOA region observed in the results of the baseline runs, instead of producing much smaller C_{nmax} in the lower AOA region. The yawing moment onset AOA was not changed significantly. The induced yawing moment AOA range was reduced in width, especially for the "x" wing body.

118

The "8 STRAKES" forebody had similar yawing moment results to those of the baseline runs. The C_{nmax} was slightly smaller in the same AOA region; both the yawing moment onset AOA and the induced AOA range remained about the same.

d. Correlations Between Side Forces and Yawing Moments

The strake modified forebody had no any influence on the side force distribution pattern. The afterbody-dominant side forces moved to forebody-dominant side forces with increasing AOAs for all the modified and original forebodies.

4. Summary

The above discussions are summarized as follows:

a. Turbulence Effects

The introduced turbulence in the airflow did not significantly impact the induced force and moment distribution patterns.

b. Body Configuration Effects

The "x" wing configuration had a smaller C_{Nmax} in a higher AOA region.

The "x" wing configuration also had smaller C_{Ymax} at higher AOAs, a lower side force onset AOA, and a wider induced side force AOA range.

The "x" wing configuration had a lower induced yawing moment onset AOA; and no general tendencies were achieved for the changes of the C_{nmax} and the induced yawing moment AOA range.

c. Strake Configuration Effects

The forebody strakes caused a smaller C_{Nmax} in about the same AOA region.

The "4 STRAKES" forebody had a smaller induced side force AOA range, but the onset AOA was not changed; for the "x" wing body case, the C_{Ymax} was slightly reduced. The "8 STRAKES" forebody did not give good reduction in the induced side forces, and both the induced side force onset AOA and the induced AOA range remained the same as those in the baseline runs.

The "4 STRAKES" forebody reduced the high C_{nmax} in the high AOA region to much smaller C_{nmax} in the intermediate AOA region, and reduced the induced yawing moment AOA range with unchanged onset AOAs. The "8 STRAKES" forebody did not significantly reduce the C_{nmax}, and both the induced yawing moment onset AOA and the induced AOA range remained unchanged.

B. CONCLUSIONS

Because the results for each single test are the combination of all the effects brought by each individual parameter, a comprehensive conclusion of the effect on the asymmetric vortices caused by one individual parameter is difficult to reach. The results from all of the experimental runs yield the following conclusions:

1. Side force magnitude and direction change with variation in nose roll angle were verified.

2. All of the normal force coefficient results have similar patterns, no matter what the changes of the test conditions were.

120

3. The turbulence had insignificant effects on the induced side forces and yawing moments on the VLSAM.

4. The forebody modified with four strakes did not show an improvement in the side force reduction, but it gave a significant improvement in the yawing moment alleviation.

5. The "4 STRAKES" forebody significantly reduced the extent of the induced side force and yawing moment AOA range, but it had no influence on the onset AOA.

6. The forebody modified with 8 strakes did not give any improvement in the side force reduction, nor in the yawing moment alleviation.

7. The "8 STRAKES" forebody gave no significant changes in the onset AOA and induced AOA range of both the side forces and yawing moments.

8. In all the tests, the side-force-dominant tendency was to shift from the afterbody to forebody as the AOA increased in the induced side force AOA range. The AOA region for the side forces changing their dominant position was about 40°~50°.

9. From the viewpoint of one single test, the "4 STRAKES" forebody with the "x" wing body gave the best results in the side force reduction and yawing moment alleviation. This configuration also significantly reduced the induced side force and yawing moment AOA range, without influencing the onset AOA.

10. In general, the "4 STRAKES" forebody is proposed for reducing the yawing moments on a low-aspect-ratio cruciform wing missile, but not for reducing the induced side forces. The reader should note that the induced

yawing moments play a greater role in the flight control problem than the induced side forces.

Several recommendations for further study are:

1. Perform flow visualization and flowfield measurements to obtain qualified information on the asymmetric vortex system itself.

2. Examine the effects of a "4 STRAKES" modified forebody with four strakes in the "x" configuration on the asymmetric vortices.

3. The maximum capability of the balance used in this experiment was too large for the induced force and moment magnitudes. This might be the explanation of the data drift. A more suitable balance is suggested for this particular model in a low-speed wind tunnel.

APPENDIX A.   BALANCE CALIBRATION CONSTANTS

BALANCE CALIBRATION   CAL DATE: 7247   COMP DATE: 7287

INV. #: 440517   KIND: FORCE

PIN NO.: 3   SIZE: 1.00

MAKE: TASK 14B   RIG NO.: 2

GA	CAPACITY	MAX LOAD	JHMS	X GAGE	CAL SHUNT	CAL ROG
N1	400.00 lbs.	400.00 lbs.	350.	0.1667	100.K	4625
N2	400.00 lbs.	400.00 lbs.	350.	0.1667	100.K	4626
A	100.00 lbs.	100.00 lbs.	175.		50.K	4618
S1	200.00 lbs.	200.00 lbs.	350.	0.1375	100.K	4623
S2	200.00 lbs.	200.00 lbs.	350.	0.1375	100.K	4597
RM	21.00 ft-lbs.	20.83 ft-lbs.	175.		50.K	4623

	K POS (1)	K POS (2)	K NEG (1)	K NEG (2)	MAX DEV	%ACC
N1	5.0861E-02	-5.4826E-09	5.1591E-02	1.7157E-08	0.224	0.056
N2	4.7211E-02	-1.7015E-08	4.7763E-02	8.9153E-02	0.196	0.049
A	1.4309E-02	-7.1962E-10	1.4290E-02	-1.3322E-09	0.115	0.115
S1	3.1309E-02	-3.8153E-08	3.2073E-02	-8.9316E-09	-0.263	0.132
S2	3.0366E-02	-3.8607E-08	3.1167E-02	-7.2517E-09	0.315	0.153
RM	3.0885E-03	2.5672E-09	3.0908E-03	-2.4769E-09	0.042	0.204

DEG OF FIT = 2   ACCURACY = 15   INT DEG OF FIT = 2

N1/N2	+	=	-5.8036E-03	N1/N2	−	=	-1.0257E-02
N1/A	+	=	0.0000E+00	N1/A	−	=	0.0000E+00
N1/S1	+	=	-4.1655E-03	N1/S1	−	=	4.5396E-03
N1/S2	+	=	0.0000E+00	N1/S2	−	=	0.0000E+00

N1/RM	+	=	-5.8079E-02	N1/RM	–	=	4.4940E-02
N2/N1	+	=	-4.6218E-02	N2/N1	–	=	-5.1778E-02
N2/A	+	=	2.8393E-03	N2/A	–	=	4.4056E-03
N2/S1	+	=	8.1694E-03	N2/S1	–	=	9.0385E-03
N2/S2	+	=	-4.1463E-03	N2/S2	–	=	0.0000E+00
N2/RM	+	=	-7.7279E-02	N2/RM	–	=	6.1125E-02
A/N1	+	=	-8.6893E-04	A/N1	–	=	2.1217E-03
A/N2	+	=	0.0000E+00	A/N2	–	=	-9.1524E-04
A/S1	+	=	-6.0359E-04	A/S1	–	=	0.0000E+00
A/S2	+	=	-7.7722E-05	A/S2	--	=	0.0000E+00
A/RM	+	=	1.1115E-01	A/RM	–	=	9.7148E-02
S1/N1	+	=	6.3459E-04	S1/N1	–	=	7.1275E-03
S1/N2	+	=	0.0000E+00	S1/N2	–	=	0.0000E+00
S1/A	+	=	0.0000E+00	S1/A	–	=	8.9235E-03
S1/S2	+	=	0.0000E+00	S1/S2	–	=	0.0000E+00
S1/RM	+	=	1.1148E-01	S1/RM	–	=	5.2630E-02
S2/N1	+	=	2.4237E-03	S2/N1	–	=	3.7176E-03
S2/N2	+	=	0.0000E-00	S2/N2	–	=	5.2619E-03
S2/A	+	=	-2.2455E-03	S2/A	–	=	-7.2915E-03
S2/S1	+	=	-6.6785E-03	S2/S1	–	=	-6.3560E-03
S2/RM	+	=	2.6377E-01	S2/RM	–	=	6.2581E-02
RM/N1	+	=	0.0000E+00	RM/N1	–	=	-3.5945E-04
RM/N2	+	=	1.9928E-04	RM/N2	–	=	0.0000E+00
RM/A	+	=	0.0000E+00	RM/A	–	=	0.0000E+00
RM/S1	+	=	0.0000E+00	RM/S1	–	=	0.0000E+00
RM/S2	+	=	2.5893E-04	RM/S2	–	=	0.0000E+00
N1/N2*N2	+	=	7.1926E-07	N1/N2*N2	–	=	-7.9499E-07
N1/A*A	+	=	0.0000E+00	N1/A*A	–	=	0.0000E+00
N1/S1*S1	+	=	-4.0352E-06	N1/S1*S1	–	=	1.9670E-06
N1/S2*S2	+	=	0.0000E+00	N1/S2*S2	–	=	0.0000E+00
N1/RM*RM	+	=	6.7860E-04	N1/RM*RM	–	=	3.2320E-04
N2/N1*N1	+	=	6.8577E-07	N2/N1*N1	–	=	-5.2897E-06
N2/A*A	+	=	1.7755E-05	N2/A*A	–	=	-1.0467E-05
N2/S1*S1	+	=	-2.1719E-06	N2/S1*S1	–	=	4.8493E-07

124

N2/S2*S2	+	=	-1.8582E-06	N2/S2*S2	–	=	0.0000E+00
N2/RM*RM	+	=	1.9294E-03	N2/RM*RM	–	=	1.1773E-03
A/N1*N1	+	=	-4.4537E-07	A/N1*N1	–	=	4.2547E-06
A/N2*N2	+	=	0.0000E+00	A/N2*N2	–	=	-4.5946E-06
A/S1*S1	+	=	-4.7936E-06	A/S1*S1	–	=	0.0000E+00
A/S2*S2	+	=	4.1033E-06	A/S2*S2	–	=	0.0000E+00
A/RM*RM	+	=	-2.0697E-04	A/RM*RM	–	=	7.5001E-04
S1/N1*N1	+	=	-5.5350E-06	S1/N1*N1	–	=	1.2923E-05
S1/N2*N2	+	=	0.0000E+00	S1/N2*N2	–	=	0.0000E+00
S1/A*A	+	=	0.0000E+00	S1/A*A	–	=	4.0345E-05
S1/S2*S2	+	=	0.0000E+00	S1/S2*S2	–	=	0.0000E+00
S1/RM*RM	+	=	-2.4592E-03	S1/RM*RM	–	=	9.3969E-04
S2/N1*N1	+	=	-1.7099E-06	S2/N1*N1	–	=	5.2110E-07
S2/N2*N2	+	=	0.0000E+00	S2/N2*N2	–	=	8.6265E-06
S2/A*A	+	=	-1.2072E-05	S2/A*A	–	=	-3.7054E-05
S2/S1*S1	+	=	2.7825E-06	S2/S1*S1	–	=	-9.9830E-06
S2/RM*RM	+	=	-6.2217E-03	S2/RM*RM	–	=	-8.0007E-04
RM/N1*N1	+	=	0.0000E+00	RM/N1*N1	–	=	-1.5497E-07
RM/N2*N2	+	=	-1.1512E-07	RM/N2*N2	–	=	0.0000E+00
RM/A*A	+	=	0.0000E+00	RM/A*A	–	=	0.0000E+00
RM/S1*S1	+	=	0.0000E+00	RM/S1*S1	–	=	0.0000E+00
RM/S2*S2	+	=	5.1560E-08	RM/S2*S2	–	=	0.0000E+00

APPENDIX B.   DATA ACQUISITION PROGRAM

This data acquisition program was written in BASIC by the original author Sestak [Ref. 34] and was modified by Rabang [Ref. 17]. It was also modified by the author for use with this experiment, and was renamed as READ.BAS. Any reader intending to adapt this program for his own interest should be cautioned that this program has not been applied to a variety of cases. The reader should read and exercise this program before applying it for his own purpose.

The SHELL program which controls the Hewlett-Packard data acquisition hardware was implemented in the READ.BAS program as a subprogram. This subprogram initiated the hardware and detected error messages from the instruments during the test run processing.

The data output file was named by the operator right after this program was executed. The temperature of the settling chamber and the angle of attack were manually input by the operator. For each balance reading routine, the sampling time of the relay multiplexer was set to 0.8 second between each channel; thus, the sampling time interval for one specific channel was 4.8 seconds. The program took ten readings per channel, and calculated the mean and standard deviation. Any readings out of one standard deviation range from the mean values were discarded, and the number of discarded readings was viewed on the computer screen; the operator could then decide whether to recycle the balance reading routine. The mean values then were taken as the direct balance output.

The direct balance outputs were calculated with the balance calibration constants and conversion factors listed in Appendix A to yield the force and moment readings per channel. The readings were computed to the normal, side and axial force measurements in pounds, and the pitching, rolling and yawing moments in foot-pounds. These measurements were stored in the force/moment data file after each balance reading routine for each AOA; thus, the data file could be resumed if the test runs had been interrupted.

Before this program was terminated, the experimental conditions including the title of this run, date, wind tunnel test condition, body-wing configuration, strake number, average temperature, static pressure difference setting (Δp), and the ambient pressure were also recorded in the data file. The details of the program procedure can be read in the program listing as follows.

```
1000  DEF SEG: CLEAR, &HFE00: GOTO" 1030      'Begin PCIB Program
      Shell
1010  GOTO 2900          'User program
1020  GOTO 2670          'Error handling
1030  I=&HFE00           'Copyright Hewlett-Packard 1984,1985
1040  PCIB.DIR$=ENVIRON$("PCIB")
1050  I$=PCIB.DIR$+"\PCIBILC.BLD"
1060  BLOAD I$,I
1070  CALL I(PCIB.DIR$,I%,J%): PCIB.SEG=I%
1080  IF J%=0  THEN GOTO 1120
1090  PRINT "Unable to load.";
1100  PRINT "   (Error #";J%;")"
1110  END
1120  '
1130  DEF SEG=PCIB.SEG: O.S=5: C.S=10: I.V=15
1140  I.C=20: L.P=25: LD.FILE=30
1150  GET.MEM=35: L.S=40: PANELS=45: DEF.ERR=50
1160  PCIB.ERR$=STRING$(64,32): PCIB.NAME$=STRING$(16,32)
1170  CALL  DEF.ERR(PCIB.ERR,PCIB.ERR$,PCIB.NAME$,PCIB.GLBERR):
      PCIB.BASERR=255
1180  ON ERROR GOTO 1020
1190  J=-1
1200  I$=PCIB.DIR$+"\PCIB.SYN"
1210  CALL O.S(I$)
1220  IF PCIB.ERR<>0  THEN ERROR PCIB.BASERR
1230  I=0
1240  CALL  I.V(I,  READ.REGISTER,  READ.SELFID,  DEFINE,
      INITIALIZE.SYSTEM)
1250  IF PCIB.ERR<>0  THEN ERROR PCIB.BASERR
1260  CALL  I.V(I,  ENABLE.SYSTEM,  DISABLE.SYSTEM,  INITIALIZE,
      POWER.ON)
1270  IF PCIB.ERR<>0  THEN ERROR PCIB.BASERR
1280  CALL I.V(I, MEASURE, OUTPUT, START, HALT)
1290  IF PCIB.ERR<>0  THEN ERROR PCIB.BASERR
1300  CALL  I.V(I,  ENABLE.INT.TRIGGER,  DISABLE.INT.TRIGGER,
      ENABLE.OUTPUT, DISABLE.OUTPUT)
1310  IF PCIB.ERR<>0  THEN ERROR PCIB.BASERR
1320  CALL  I.V(I,  CHECK.DONE,  GET.STATUS,  SET.FUNCTION,
      SET.RANGE)
1330  IF PCIB.ERR<>0  THEN ERROR PCIB.BASERR
1340  CALL I.V(I, SET.MODE, WRITE.CAL, READ.CAL, STORE.CAL)
1350  IF PCIB.ERR<>0  THEN ERROR PCIB.BASERR
1360  CALL I.V(I, DELAY, SAVE.SYSTEM, J, J)
```

```
1370  IF PCIB.ERR<>0  THEN ERROR PCIB.BASERR
1380  I=1
1390  CALL   I.V(I,  SET.GATETIME,  SET.SAMPLES,  SET.SLOPE,
      SET.SOURCE)
1400  IF PCIB.ERR<>0  THEN ERROR PCIB.BASERR
1410  CALL I.C(I, FREQUENCY, AUTO.FREQ, PERIOD, AUTO.PER)
1420  IF PCIB.ERR<>0  THEN ERROR PCIB.BASERR
1430  CALL I.C(I, INTERVAL, RATIO, TOTALIZE, R100MILLI)
1440  IF PCIB.ERR<>0  THEN ERROR PCIB.BASERR
1450  CALL I.C(I, R1, R10, R100, R1KILO)
1460  IF PCIB.ERR<>0  THEN ERROR PCIB.BASERR
1470  CALL I.C(I, R10MEGA, R100MEGA, CHAN.A, CHAN.B)
1480  IF PCIB.ERR<>0  THEN ERROR PCIB.BASERR
1490  CALL I.C(I, POSITIVE, NEGATIVE, COMN, SEPARATE)
1500  IF PCIB.ERR<>0  THEN ERROR PCIB.BASERR
1510  I=2
1520  I=3
1530  CALL I.V(I, ZERO.OHMS, SET.SPEED, J, J)
1540  IF PCIB.ERR<>0  THEN ERROR PCIB.BASERR
1550  CALL I.C(I, DCVOLTS, ACVOLTS, OHMS, R200MILLI)
1560  IF PCIB.ERR<>0  THEN ERROR PCIB.BASERR
1570  CALL I.C(I, R2, R20, R200, R2KILO)
1580  IF PCIB.ERR<>0  THEN ERROR PCIB.BASERR
1590  CALL I.C(I, R20KILO, R200KILO, R2MEGA, R20MEGA)
1600  IF PCIB.ERR<>0  THEN ERROR PCIB.BASERR
1610  CALL I.C(I, AUTOM, R2.5, R12.5, J)
1620  IF PCIB.ERR<>0  THEN ERROR PCIB.BASERR
1630  I=4
1640  CALL I.V(I,  SET.COMPLEMENT,  SET.DRIVER,  OUTPUT.NO.WAIT,
      ENABLE.HANDSHAKE)
1650  IF PCIB.ERR<>0  THEN ERROR PCIB.BASERR
1660  CALL   I.V(I,   DISABLE.HANDSHAKE,   SET.THRESHOLD,
      SET.START.BIT, SET.NUM.BITS)
1670  IF PCIB.ERR<>0  THEN ERROR PCIB.BASERR
1680  CALL I.V(I, SET.LOGIC.SENSE, J, J, J)
1690  IF PCIB.ERR<>0  THEN ERROR PCIB.BASERR
1700  CALL I.C(I, POSITIVE, NEGATIVE, TWOS, UNSIGNED)
1710  IF PCIB.ERR<>0  THEN ERROR PCIB.BASERR
1720  CALL I.C(I, OC, TTL, R0, R1)
1730  IF PCIB.ERR<>0  THEN ERROR PCIB.BASERR
1740  CALL I.C(I, R2, R3, R4, R5)
1750  IF PCIB.ERR<>0  THEN ERROR PCIB.BASERR
1760  CALL I.C(I, R6, R7, R8, R9)
```

```
1770   IF PCIB.ERR<>0  THEN ERROR PCIB.BASERR
1780   CALL I.C(I, R10, R11, R12, R13)
1790   IF PCIB.ERR<>0  THEN ERROR PCIB.BASERR
1800   CALL I.C(I, R14, R15, R16, J)
1810   IF PCIB.ERR<>0  THEN ERROR PCIB.BASERR
1820   I=6
1830   CALL I.V(I, SET.FREQUENCY, SET.AMPLITUDE, SET.OFFSET,
       SET.SYMMETRY)
1840   IF PCIB.ERR<>0  THEN ERROR PCIB.BASERR
1850   CALL I.V(I, SET.BURST.COUNT, J, J, J)
1860   IF PCIB.ERR<>0  THEN ERROR PCIB.BASERR
1870   CALL I.C(I, SINE, SQUARE, TRIANGLE, CONTINUOUS)
1880   IF PCIB.ERR<>0  THEN ERROR PCIB.BASERR
1890   CALL I.C(I, GATED, BURST, J, J)
1900   IF PCIB.ERR<>0  THEN ERROR PCIB.BASERR
1910   I=7
1920   CALL I.V(I, AUTOSCALE, CALIBRATE, SET.SENSITIVITY,
       SET.VERT.OFFSET)
1930   IF PCIB.ERR<>0  THEN ERROR PCIB.BASERR
1940   CALL I.V(I, SET.COUPLING, SET.POLARITY, SET.SWEEPSPEED,
       SET.DELAY)
1950   IF PCIB.ERR<>0  THEN ERROR PCIB.BASERR
1960   CALL I.V(I, SET.TRIG.SOURCE, SET.TRIG.SLOPE, SET.TRIG.LEVEL,
       SET.TRIG.MODE)
1970   IF PCIB.ERR<>0  THEN ERROR PCIB.BASERR
1980   CALL I.V(I, GET.SINGLE.WF, GET.TWO.WF, GET.VERT.INFO,
       GET.TIMEBASE.INFO)
1990   IF PCIB.ERR<>0  THEN ERROR PCIB.BASERR
2000   CALL I.V(I, GET.TRIG.INFO, CALC.WFVOLT, CALC.WFTIME,
       CALC.WF.STATS)
2010   IF PCIB.ERR<>0  THEN ERROR PCIB.BASERR
2020   CALL I.V(I, CALC.RISETIME, CALC.FALLTIME, CALC.PERIOD,
       CALC.FREQUENCY)
2030   IF PCIB.ERR<>0  THEN ERROR PCIB.BASERR
2040   CALL I.V(I, CALC.PLUSWIDTH, CALC.MINUSWIDTH,
       CALC.OVERSHOOT, CALC.PRESHOOT)
2050   IF PCIB.ERR<>0  THEN ERROR PCIB.BASERR
2060   CALL I.V(I, CALC.PK.TO.PK, SET.TIMEOUT, SCOPE.START,
       MEASURE.SINGLE.WF)
2070   IF PCIB.ERR<>0  THEN ERROR PCIB.BASERR
2080   CALL I.V(I, MEASURE.TWO.WF, J, J, J)
2090   IF PCIB.ERR<>0  THEN ERROR PCIB.BASERR
2100   CALL I.C(I, R10NANO, R100NANO, R1MICRO, R10MICRO)
```

```
2110   IF PCIB.ERR<>0  THEN ERROR PCIB.BASERR
2120   CALL I.C(I, R100MICRO, R1MILLI, R10MILLI, R100MILLI)
2130   IF PCIB.ERR<>0  THEN ERROR PCIB.BASERR
2140   CALL I.C(I, R1, R10, R20NANO, R200NANO)
2150   IF PCIB.ERR<>0  THEN ERROR PCIB.BASERR
2160   CALL I.C(I, R2MICRO, R20MICRO, R200MICRO, R2MILLI)
2170   IF PCIB.ERR<>0  THEN ERROR PCIB.BASERR
2180   CALL I.C(I, R20MILLI, R200MILLI, R2, R20)
2190   IF PCIB.ERR<>0  THEN ERROR PCIB.BASERR
2200   CALL I.C(I, R50NANO, R500NANO, R5MICRO, R50MICRO)
2210   IF PCIB.ERR<>0  THEN ERROR PCIB.BASERR
2220   CALL I.C(I, R500MICRO, R5MILLI, R50MILLI, R500MILLI)
2230   IF PCIB.ERR<>0  THEN ERROR PCIB.BASERR
2240   CALL I.C(I, R5, R50, CHAN.A, CHAN.B)
2250   IF PCIB.ERR<>0  THEN ERROR PCIB.BASERR
2260   CALL I.C(I, EXTERNAL, POSITIVE, NEGATIVE, AC)
2270   IF PCIB.ERR<>0  THEN ERROR PCIB.BASERR
2280   CALL I.C(I, DC, TRIGGERED, AUTO.TRIG, AUTO.LEVEL)
2290   IF PCIB.ERR<>0  THEN ERROR PCIB.BASERR
2300   CALL I.C(I, X1, X10, STANDARD, AVERAGE)
2310   IF PCIB.ERR<>0  THEN ERROR PCIB.BASERR
2320   I=8
2330   CALL I.V(I, OPEN.CHANNEL, CLOSE.CHANNEL, J, J)
2340   IF PCIB.ERR<>0  THEN ERROR PCIB.BASERR
2350   CALL C.S
2360   IF PCIB.ERR<>0  THEN ERROR PCIB.BASERR
2370   I$=PCIB.DIR$+"\PCIB.PLD"
2380   CALL L.P(I$)
2390   IF PCIB.ERR<>0  THEN ERROR PCIB.BASERR
2400   I$="DMM.01": I=3: J=0: K=0: L=1
2410   CALL DEFINE(DMM.01, I$,I, J, K, L)
2420   IF PCIB.ERR<>0  THEN ERROR PCIB.BASERR
2430   I$="Func.Gen.01": I=6: J=0: K=1: L=1
2440   CALL DEFINE(FUNC.GEN.01, I$,I, J, K, L)
2450   IF PCIB.ERR<>0  THEN ERROR PCIB.BASERR
2460   I$="Scope.01": I=7: J=0: K=2: L=1
2470   CALL DEFINE(SCOPE.01, I$,I, J, K, L)
2480   IF PCIB.ERR<>0  THEN ERROR PCIB.BASERR
2490   I$="Counter.01": I=1: J=0: K=3: L=1
2500   CALL DEFINE(COUNTER.01, I$,I, J, K, L)
2510   IF PCIB.ERR<>0  THEN ERROR PCIB.BASERR
2520   I$="Dig.In.01": I=4: J=0: K=4: L=1
2530   CALL DEFINE(DIG.IN.01, I$,I, J, K, L)
```

```
2540  IF PCIB.ERR<>0  THEN ERROR PCIB.BASERR
2550  I$="Dig.Out.01": I=4: J=1: K=4: L=1
2560  CALL DEFINE(DIG.OUT.01, I$,I, J, K, L)
2570  IF PCIB.ERR<>0  THEN ERROR PCIB.BASERR
2580  I$="Relay.Act.01": I=8: J=0: K=5: L=1
2590  CALL DEFINE(RELAY.ACT.01, I$,I, J, K, L)
2600  IF PCIB.ERR<>0  THEN ERROR PCIB.BASERR
2610  I$="Relay.Mux.01": I=2: J=0: K=6: L=1
2620  CALL DEFINE(RELAY.MUX.01, I$,I, J, K, L)
2630  IF PCIB.ERR<>0  THEN ERROR PCIB.BASERR
2640  I$=ENVIRON$("PANELS")+"\PANELS.EXE"
2650  CALL L.S(I$)
2660  GOTO 1010
2670  IF ERR=PCIB.BASERR THEN GOTO 2700
2680  PRINT "BASIC error #";ERR;" occurred in line ";ERL
2690  STOP
2700  TMPERR=PCIB.ERR: IF TMPERR=0  THEN TMPERR=PCIB.GLBERR
2710  PRINT "PC Instrument error #";TMPERR;" detected at line ";ERL
2720  PRINT "Error: ";PCIB.ERR$
2730  IF  LEFT$(PCIB.NAME$,1)<>CHR$(32) THEN  PRINT  "Instrument:
      ";PCIB.NAME$
2740  STOP
2750  COMMON PCIB.DIR$,PCIB.SEG
2760  COMMON LD.FILE, GET.MEM, PANELS, DEF.ERR
2770  C O M M O N        P C I B . B A S E R R ,        P C I B . E R R ,
      PCIB.ERR$,PCIB.NAME$,PCIB.GLBERR
2780  COMMON   READ.REGISTER,   READ.SELFID,   DEFINE,
      INITIALIZE.SYSTEM,  ENABLE.SYSTEM,  DISABLE.SYSTEM,
      INITIALIZE, POWER.ON, MEASURE, OUTPUT, START, HALT,
      ENABLE.INT.TRIGGER, DISABLE.INT.TRIGGER, ENABLE.OUTPUT,
      DISABLE.OUTPUT, CHECK.DONE, GET.STATUS
2790  COMMON SET.FUNCTION, SET.RANGE, SET.MODE, WRITE.CAL,
      READ.CAL, STORE.CAL, DELAY, SAVE.SYSTEM, SET.GATETIME,
      SET.SAMPLES, SET.SLOPE, SET.SOURCE, ZERO.OHMS, SET.SPEED,
      SET.COMPLEMENT,   SET.DRIVER,   OUTPUT.NO.WAIT,
      ENABLE.HANDSHAKE, DISABLE.HANDSHAKE
2800  COMMON SET.THRESHOLD, SET.START.BIT, SET.NUM.BITS,
      SET.LOGIC.SENSE, SET.FREQUENCY, SET.AMPLITUDE, SET.OFFSET,
      SET.SYMMETRY, SET.BURST.COUNT, AUTOSCALE, CALIBRATE,
      SET.SENSITIVITY,   SET.VERT.OFFSET,   SET.COUPLING,
      SET.POLARITY, SET.SWEEPSPEED
2810  COMMON SET.DELAY, SET.TRIG.SOURCE, SET.TRIG.SLOPE,
      SET.TRIG.LEVEL, SET.TRIG.MODE, GET.SINGLE.WF, GET.TWO.WF,
```

GET.VERT.INFO, GET.TIMEBASE.INFO, GET.TRIG.INFO, CALC.WFVOLT, CALC.WFTIME, CALC.WF.STATS, CALC.RISETIME, CALC.FALLTIME, CALC.PERIOD
2820 COMMON CALC.FREQUENCY, CALC.PLUSWIDTH, CALC.MINUSWIDTH, CALC.OVERSHOOT, CALC.PRESHOOT, CALC.PK.TO.PK, SET.TIMEOUT, SCOPE.START, MEASURE.SINGLE.WF, MEASURE.TWO.WF, OPEN.CHANNEL, CLOSE.CHANNEL
2830 COMMON FREQUENCY, AUTO.FREQ, PERIOD, AUTO.PER, INTERVAL, RATIO, TOTALIZE, R100MILLI, R1, R10, R100, R1KILO, R10MEGA, R100MEGA, CHAN.A, CHAN.B, POSITIVE, NEGATIVE, COMN, SEPARATE, DCVOLTS, ACVOLTS, OHMS, R200MILLI, R2, R20, R200, R2KILO, R20KILO, R200KILO
2840 COMMON R2MEGA, R20MEGA, AUTOM, R2.5, R12.5, POSITIVE, NEGATIVE, TWOS, UNSIGNED, OC, TTL, R0, R1, R2, R3, R4, R5, R6, R7, R8, R9, R10, R11, R12, R13, R14, R15, R16, SINE, SQUARE, TRIANGLE, CONTINUOUS, GATED, BURST, R10NANO, R100NANO, R1MICRO, R10MICRO, R100MICRO
2850 COMMON R1MILLI, R10MILLI, R100MILLI, R1, R10, R20NANO, R200NANO, R2MICRO, R20MICRO, R200MICRO, R2MILLI, R20MILLI, R200MILLI, R2, R20, R50NANO, R500NANO, R5MICRO, R50MICRO, R500MICRO, R5MILLI, R50MILLI, R500MILLI, R5, R50, CHAN.A, CHAN.B, EXTERNAL, POSITIVE
2860 COMMON NEGATIVE, AC, DC, TRIGGERED, AUTO.TRIG, AUTO.LEVEL, X1, X10, STANDARD, AVERAGE
2870 COMMON DMM.01, FUNC.GEN.01, SCOPE.01, COUNTER.01, DIG.IN.01, DIG.OUT.01, RELAY.ACT.01, RELAY.MUX.01
2880 'End PCIB Program Shell
2890 '
2900 'Program to scan with the DMM and RELAY.MUX.01
2910 'This program was writen by T.SESTAK and modified by P. ROANE,
2920 'P. RABANG, J. SOMMERS, and C.C. YUAN for use with the TASK 6
2930 'component balance. The TASK balance used with this program is the
2940 '1.00", MK. XIV intrenal balance with NASA inventory #440517.
2950 '
2960 'This section after the SHELL program directs reading the voltages
2970 'from the balance, computes forces measured by the strain guages,
2980 'then stores the values in two arrays, one for the TARE one for FORCE.
2990 'This data file can then be used for graphs or other displays. Each test
3000 'run will generate a windtun.dat file which should be copied under
3010 'another name before the next test run so that it will not be
3020 'overwritten.
3025 '

```
3030    'dimension arrays
3040    DIM READING[7],FORCE[140,°],TARE[8],TREAD[7,10],LAB[7],DROP[7]
3050    COLOR 14,1,1
3060    CLS
3070    KEY OFF
3080    AOA=0
3085    TEMP=0
3090    VALUE=5
3092    CLS:LOCATE 11,10:PRINT "IN THIS PROGRAM,"
3094    LOCATE 12,10:PRINT "YOU HAVF TO ANSWER ALL THE
        QUESTION BY CAPITAL LETTERS."
3096    LOCATE 13,10:PRINT "SO, PLEASE TURN ON THE 'CAPS LOCK',
        THANKS!"
3098    LOCATE 15,10:INPUT "ENTER <CR> TO CONTINUE";INPT$
3100    CLS:LOCATE 11,28
3110    PRINT"SETTING UP DATA FILES"
3115    LOCATE 13,20:INPUT "ENTER THE OUTPUT DATA FILE NAME";D$
3120    D$=D$+".DAT"
3130    'The program will write the data to several files.
3140    STATEFILE$ = "C:\PCIB\WIND.HPC"     'stored in PCIB subdirectory
3150    DATAFILE$ = "C:\LAWRENCE\"+D$     'stored on drive C
3160    DISKFILE$ = "A:"+D$                         'stored on drive A
3170    BALANFILE$ = "C:\LAWRENCE\BALANCE.DAT" 'stored on drive C
3180    '
3190    RELAY.SETTLING.TIME = .8          '800 ms
3200    LOCATE 16,35:PRINT"D O N E"
3210    CALL DELAY(VALUE)
3220    '
3230    CLS:LOCATE 12,28:PRINT"INITIALIZING INSTRUMENTS"
3240    CALL INITIALIZE.SYSTEM(STATEFILE$)
3250    IF PCIB.ERR <> 0  THEN ERROR PCIB.BASERR
3260    CALL ENABLE.SYSTEM
3270    IF PCIB.ERR <> 0  THEN ERROR PCIB.BASERR
3280    LOCATE 16,35:PRINT"D O N E"
3290    CALL DELAY(VALUE)
3300    '
3310    'This part of the program i   o preserve the data if
3320    'if the program is aborted i.. mid run.  Parity errors
3330    'in the Hewlett Packard PC Instruments setup caused by
3340    'electrical noise and undervoltage at NPS requires
3350    'this.  A voltage regulated, uninteruptible power source
3360    'would ameliorate this problem. Just in case- this little
3370    'sequence allows reentry into the program and the data
```

```
3380   'arrays with minimal inconvenience.
3390   '
3400   CLS:LOCATE 12,20:INPUT"WERE YOU INTERRUPTED (Y OR N)";A$
3410   IF A$="Y" THEN GOTO 3500
3420   '
3430   'The next two variables are counters in the arrays
3440   'FORCE and TARE
3450   '
3460   TRIAL = 0
3470   TRY = 0
3480   GOTO 3690
3490   '
3500   LOCATE  14,15:INPUT  "WHAT'S  THE  INTERRUPTED  FILE
       NAME";ITDF$
3510   ITDF$="C:\LAWRENCE\"+ITDF$+".DAT"
3520   OPEN ITDF$ FOR INPUT AS #1
3530   INPUT  #1,TARE(1),TARE(2),TARE(3),TARE(4),TARE(5),TARE(6),
       TARE(7),TARE(8)
3540   FOR X = 1 TO 140
3550        INPUT  #1,  FORCE(X,1),FORCE(X,2),FORCE(X,3),FORCE(X,4),
       FORCE(X,5),FORCE(X,6),FORCE(X,7),FORCE(X,8),FORCE(X,9)
3560   IF FORCE(X,1)=0 THEN ABCD=X:GOTO 3590
3570   AOA=FORCE(X,2)
3575   TEMP=FORCE(X,9)
3580   NEXT X
3590   TRY=ABCD-1
3600   TRIAL=ABCD-1
3610   CLOSE #1
3620        GOTO 3700
3640   '
3650   'A$ is used as a marker for interrupted run sequences
3660   'in the program, it is set to "N" so the
3670   'uninterrupted sequences are used unless otherwise directed
3680   '
3690   A$="N"
3700   OFV=0.2
3710   '
3720   'prompt to begin each scan or quit program if desired
3730   '
3740   CLS:LOCATE 12,10
3750   INPUT "TO  START  SCAN  ENTER  ANY  KEY  EXCEPT  Q,  Q  TO
       QUIT";ANSWER$
3760   IF ANSWER$ = "Q" THEN GOTO 6655
```

```
3770  '
3780  'this enters the AOA for each trial and displays is in the printout
3790  '
3800  CLS:LOCATE 12,10
3810  PRINT "THE LAST ANGLE OF ATTACK IS ";AOA
3820  LOCATE 13,10:PRINT "THE LAST TEMPERATURE (F) IS ";TEMP
3830  '
3840  LOCATE 15,10:INPUT "ENTER THE ANGLE OF ATTACK (AOA) FOR
       THIS TRIAL";AOA
3850  LOCATE 16,10:INPUT "ENTER THE TEMPERATURE FOR THIS
       TRIAL";TEMP
3860  '
3870  '
3880  READING(1)=AOA
3890  '
3900  'This variable is a marker in the iteration loop
3910  'interaction equations for convergence.
3920  '
3930  CYCLE = 0
3940  '
3950  'This loop scans the pitch angle and 6 balance channels
3960  'and stores the values in the array READING
3970  'Each channel is read ten times and averaged.
3980  'The user may reject the current readings and input a new set.
3990  '
4000  CLS
4010  PRINT"*******************  DIRECT   BALANCE   READINGS
       *********************
4020  PRINT"             CHECK OF SYSTEM OPERATION
4030  PRINT                              " IN VOLTS   N1    N2
       S1    S2    A     R "
4040  PRINT                                      " ********   ******
       ******   ******   ******   ******   ******"
4050  '
4060  'This file is for storing the direct voltage readings and averages.
4070  'The data file is continually appended.
4080  'The data is for further analysis of the direct voltage readings.
4090  OPEN BALANFILE$ FOR APPEND AS #3
4100  '
4110  FOR CNT = 1 TO 10
4120  FOR CHANNEL = 2 TO 7
4130   CALL OUTPUT(RELAY.MUX.01, CHANNEL)
4140       IF PCIB.ERR <> 0  THEN ERROR PCIB.BASERR
```

136

```
4150   CALL DELAY(RELAY.SETTLING.TIME)
4160       IF PCIB.ERR <> 0  THEN ERROR PCIB.BASERR
4170   CALL MEASURE(DMM.01, READING[CHANNEL])
4180       IF PCIB.ERR <> 0  THEN ERROR PCIB.BASERR
4185   READING(CHANNEL)=READING(CHANNEL)-OFV
4190   TREAD(CHANNEL,CNT) = READING(CHANNEL)
4200   NEXT CHANNEL
4210   PRINT USING                              "      +.######
       +.######    +.######    +.######    +.######    +.######";
       READING(2),READING(3),READING(4),READING(5),READING(6),RE
       ADING(7)
4220   PRINT #3, USING                               "   +.###.#
       +.######   +.######   +.######   +.######   +.######   +.######";
       READING(1),READING(2),READING(3),READING(4),READING(5),RE
       ADING(6),READING(7)
4230   NEXT CNT
4240   '
4250   ' CALL SUBROUTINE TO AVERAGE READINGS
4260   GOSUB 6690
4270   '
4280   PRINT"- - - - - - - - - - - - - - - - - - - - - - - - - - - - - - - -"
4290   PRINT USING                               "MEAN VALUE
       +.######   +.######   +.######   +.######   +.######   +.######";
       READING(2),READING(3),READING(4),READING(5),READING(6),RE
       ADING(7)
4300   PRINT #3, USING                               "   +.###.#
       +.######   +.######   +.######   +.######   +.######   +.######";
       READING(1),READING(2),READING(3),READING(4),READING(5),RE
       ADING(6),READING(7)
4310   CLOSE #3
4320   PRINT" ":BEEP
4330   PRINT"<CR> TO CONTINUE, "1" TO GET NEW READINGS"
4340   INPUT XYZ
4350   IF XYZ=1 GOTO 3940
4360   '
4370   'These equations take voltage readings from the balance,
4380   'converts them to counts, then applys the primary force
4390   'equations to the results.  These values are applied to
4400   'the balance interaction equations. Each channel has
4410   'separate equations for positive and negative readings and
4420   'may have a "+" or "-" reading on any test run so the
4430   'rather involved logic path below is my solution to the
4440   'problem.  For more information consult Calibration laboratory
```

```
4450   'guidelines at NASA Ames Research Facility for TASK balances
4460   '
4470   '************** CONVERT SIGNAL TO FORCES ***************
4480   '********************************************************
4490   '
4500   'Direct balance readings are multiplied by a scale factor
4510   '5000000 then divided by the balance exitation voltage to
4520   'get a readiing in COUNTS. The program will send each reading
4530   'to the appropriate equation and convert to force or moment
4540   'then return to send the next reading for calculation
4550   'The data acquisition system for using this program used an
4560   'amplifier with 1000 gain. The scale factor is divided by 1000.
4570   '(5000000 => VEX=5000 mV, AND GAIN=1000)
4580   VEX=5                  'Excitation Voltage
4590   N1=READING(2)*5000!/VEX
4600   N2=READING(3)*5000!/VEX
4610   S1=READING(4)*5000!/VEX
4620   S2=READING(5)*5000!/VEX
4630   A=READING(6)*5000!/VEX
4640   R=READING(7)*416.67#/VEX
4650   '
4660   'send each reading to the appropriate equation
4670   '
4680   IF READING(2)>0  THEN GOTO 4770 ELSE GOTO 4920
4690   IF READING(3)>0  THEN GOTO 4790 ELSE GOTO 4940
4700   IF READING(4)>0  THEN GOTO 4830 ELSE GOTO 4980
4710   IF READING(5)>0  THEN GOTO 4850 ELSE GOTO 5000
4720   IF READING(6)>0  THEN GOTO 4810 ELSE GOTO 4960
4730   IF READING(7)>0  THEN GOTO 4870 ELSE GOTO 5020
4740   '
4750   '************** POSITIVE  FORMULAS *************
4760   '
4770   EN1 = .050861*N1 - 5.4826E-09*(N1*N1)
4780   GOTO 4690
4790   EN2 = .047211*N2 - 1.7015E-08*(N2*N2)
4800   GOTO 4700
4810   EA = .014309*A - 7.1962E-10*(A*A)
4820   GOTO 4730
4830   ES1 = .031309*S1 - 3.8153E-08*(S1*S1)
4840   GOTO 4710
4850   ES2 = .030366*S2 - 3.8607E-08*(S2*S2)
4860   GOTO 4720
4870   ER = .0030885*R + 2.5672E-09*(R*R)
```

```
4880    GOTO 5030
4890    '
4900    '************** NEGATIVE  FORMULAS *************
4910    '
4920    EN1 = .051591*N1 + 1.7157E-08*(N1*N1)
4930    GOTO 4690
4940    EN2=.047763*N2+8.915299E-09*(N2*N2)
4950    GOTO 4700
4960    EA = .01429*A - 1.3322E-09*(A*A)
4970    GOTO 4730
4980    ES1 = .032073*S1 - 8.931601E-09*(S1*S1)
4990    GOTO 4710
5000    ES2 = .031167*S2 - 7.2517E-09*(S2*S2)
5010    GOTO 4720
5020    ER = .0030908*R - 2.4769E-09*(R*R)
5030    '
5040    '
5050    'a heading for the iteration values
5060    '
5070    PRINT"                              "
5080    PRINT"******************** FORCE  INTERACTION  ITERATIONS
        ******************
5090    PRINT"            CHECK FOR CONVERGENCE
5100    PRINT                              " CYCLE  AOA   N1
        N2    S1    S2    A     R "
5110    PRINT                              "  #    DEG  POUNDS
        POUNDS  POUNDS  POUNDS  POUNDS  FT-LBS"
5120    PRINT                              "  *****  ***  ******
        ******  ******  ******  ******  ******"
5130    '
5140    'The loop that controls the balance interaction
5150    'equations and allows a visual convergence check
5160    '
5170    FOR I = 1 TO 10
5180    IF READING(2)>0  THEN GOTO 5270 ELSE GOTO 5470
5190    IF READING(3)>0  THEN GOTO 5300 ELSE GOTO 5500
5200    IF READING(4)>0  THEN GOTO 5360 ELSE GOTO 5560
5210    IF READING(5)>0  THEN GOTO 5390 ELSE GOTO 5590
5220    IF READING(6)>0  THEN GOTO 5330 ELSE GOTO 5530
5230    IF READING(7)>0  THEN GOTO 5420 ELSE GOTO 5620
5240    '
5250    '*************POSITIVE  FORMULAS*************
5260    '
```

```
5270  XN1=    EN1+.0058036*N2+.0041655*S1+.058079*R-7.1926E-
      07*(N2*N2)+4.0352E-06*(S1*S1)-.0006786*(R*R)
5280  GOTO 5190
5290  '
5300  XN2= EN2+.046218*N1-.0028393*A-.0081694*S1+.0041463*S2+.077279*R
      -6.8577E-07*(N1*N1)-1.7755E-05*(A*A)+2.1719E-06*(S1*S1)+1.8582E-
      06*(S2*S2)-.0019294*(R*R)
5310  GOTO 5200
5320  '
5330  XA=    EA+8.6893E-04*N1+6.0359E-04*S1+7.7722E-05*S2-.11115*R+
      4.4537E-07*(N1*N1)+4.7936E-06*(S1*S1)-4.1033E-06*(S2*S2)+2.0597E-
      04*(R*R)
5340  GOTO 5230
5350  '
5360  XS1 = ES1-6.3459E-04*N1-.11148*R+5.535E-06*(N1*N1)+.0024592*(R*R)
5370  GOTO 5210
5380  '
5390  XS2=   ES2-.0024237*N1+.0022455*A+.0066785*S1-.26377*R+1.7099E-
      06*(N1*N1)+1.2072E-05*(A*A)-2.7825E-06*(S1*S1)+.0062217*(R*R)
5400  GOTO 5220
5410  '
5420  XR=    ER-1.9928E-04*N2-2.5893E-04*S2+1.1512E-07*(N2*N2)-5.156E-
      08*(S2*S2)
5430  GOTO 5630
5440  '
5450  '************** NEGATIVE  FORMULAS  ************
5460  '
5470  XN1=   EN1+.010257*N2-.0045396*S1-.04494*R+7.9499E-07*(N2*N2)-
      1.967E-06*(S1*S1)-.0003232*(R*R)
5480  GOTO 5190
5490  '
5500  XN2= EN2+.051778*N1-.0044056*A-9.038499E-03*S1-.061125*R+5.2897E-
      06*(N1*N1)+1.0467E-05*(A*A)-4.8493E-07*(S1*S1)-.0011773*(R*R)
5510  GOTO 5200
5520  '
5530  XA=    EA-.0021217*N1+9.1524E-04*N2-.097148*R-4.2547E-
      06*(N1*N1)+4.5846E-06*(N2*N2)-7.5001E-04*(R*R)
5540  GOTO 5230
5550  '
5560  XS1=  ES1-.0071275*N1-.0089235*A-.05268*R-1.2923E-05*(N1*N1)-
      4.0345E-05*(A*A)-9.3969E-04*(R*R)
5570  GOTO 5210
5580  '
```

```
5590  XS2= ES2-.0037176*N1-.0052619*N2+.0072915*A+.006856*S1-.062581*R-
      5.211E-07*(N1*N1)-8.6265E-06*(N2*N2)+3.7054E-05*(A*A)+9.983001E-
      06*(S1*S1)+8.0007E-04*(R*R)
5600  GOTO 5220
5610  '
5620  XR= ER+3.5945E-04*N1+1.5497E-07*(N1*N1)
5630  '
5640  'Shift all the new variables back to the old name
5650  'for the next iteration
5660  N1=XN1
5670  N2=XN2
5680  A=XA
5690  S1=XS1
5700  S2=XS2
5710  R=XR
5720  '
5730  'A marker for the interations
5740  CYCLE = CYCLE + 1
5750  'print the iterations to watch for convergence
5760  '
5770  PRINT USING                                   "  ##  +##.#
      +###.##   +###.##   +###.##   +###.##   +###.##   +###.##";
      CYCLE,AOA,N1,N2,S1,S2,A,R
5780  NEXT I
5790  '
5800  INPUT "IF CONVERGENCE IS ADEQUATE ENTER Y; OTHEREISE,
      ENTER N FOR ANOTHER RUN:";ANSWR$
5810  IF ANSWR$ = "N" THEN GOTO 5060
5820  '
5830  NORMAL = N1 + N2
5840  SIDE = S1 + S2
5850  AXIAL = A
5860  PITCH = (N1-N2) * .1667
5870  YAW = (S1-S2) * .1375
5880  ROLL = R/12.0
5890  '
5900  TRIAL = TRIAL + 1
5910  INPUT "IS THIS A TARE READING, Y OR N";AN$
5920  IF AN$ <> "Y" GOTO 6190
5930  COLOR 0,10,10:CLS
5935  IF A$="Y" THEN TRIAL=TRIAL-1:GOTO 5950
5940  TRIAL = 0
5950  TRY = TRY + 1
```

```
6000   TARE(1) = TRY
6010   TARE(2) = AOA
6020   TARE(3) = NORMAL
6030   TARE(4) = SIDE
6040   TARE(5) = AXIAL
6050   TARE(6) = PITCH
6060   TARE(7) = ROLL
6070   TARE(8) = YAW
6080   '
6090   ' PRINT THE TARING DATA
6100   PRINT"                              "
6110   PRINT"* * * * * * * * * * * TARE CALCULATIONS * * * * * * * * * * *
       * *
6120   PRINT                                      " TRIAL   A0A
       NORMAL  SIDE  AXIAL  PITCH  ROLL   YAW"
6130   PRINT                                  " #   DEG  POUNDS
       POUNDS  POUNDS  FT-LBS  FT-LBS  FT-LBS"
6140   PRINT                              " *****  *****  ******
       ******  ******  ******  ******  *****"
6150   '
6160   PRINT USING"   ##   +##.##   ###.##   ###.##   ###.##   ###.##
       ###.##    ###.##"; TARE(1),TARE(2),TARE(3),TARE(4),TARE(5),
       TARE(6),TARE(7),TARE(8)
6170   BEEP:INPUT "ENTER <CR> TO CONTINUE";INPT$:IF A$="Y" THEN
       GOTO 6350
6180   GOTO 6460
6190   '
6240   FORCE(TRIAL,1) = TRIAL
6250   FORCE(TRIAL,2) = AOA
6260   FORCE(TRIAL,3) = NORMAL - TARE(3)
6270   FORCE(TRIAL,4) = SIDE - TARE(4)
6280   FORCE(TRIAL,5) = AXIAL - TARE(5)
6290   FORCE(TRIAL,6) = PITCH - TARE(6)
6300   FORCE(TRIAL,7) = ROLL - TARE(7)
6310   FORCE(TRIAL,8) = YAW - TARE(8)
6320   FORCE(TRIAL,9) = TEMP
6330   'print the values and store in file
6340   '
6350   PRINT"                              "
6360   PRINT"* * * * * * * * * * * FORCE CALCULATIONS * * * * * * * * * * *
       * *
6370   PRINT                                        " TRIAL   A0A
       NORMAL  SIDE  AXIAL  PITCH  ROLL   YAW"
```

```
6380   PRINT                                   "  #   DEG  POUNDS
       POUNDS  POUNDS  FT-LBS  FT-LBS  FT-LBS"
6390   PRINT                                   "  *****  *****  ******
       ******   ******   ******   ******   ******"
6400   'a loop to list all values so far
6410   '
6420   FOR J = 1 TO TRIAL
6430   PRINT USING"  ##   +###.#  +###.##  +###.##  +###.##  +###.##
       +###.##   +###.##";FORCE(J,1),FORCE(J,2),FORCE(J,3),FORCE(J,4),
       FORCE(J,5),FORCE(J,6),FORCE(J,7),FORCE(J,8)
6440   NEXT J
6450   BEEP:INPUT "ENTER <CR> TO CONTINUE";INPT$
6460   '
6470   'Write the data to the output data files
6480   COLOR 14,1,1:CLS
6490   OPEN DATAFILE$ FOR OUTPUT AS #1
6500   OPEN DISKFILE$ FOR OUTPUT AS #2
6510   WRITE #1, TARE(1),TARE(2),TARE(3),TARE(4),TARE(5),TARE(6),
       TARE(7),TARE(8)
6520   WRITE #2, TARE(1),TARE(2),TARE(3),TARE(4),TARE(5),TARE(6),
       TARE(7),TARE(8)
6530   FOR X = 1 TO 140
6550        WRITE #1, FORCE(X,1),FORCE(X,2),FORCE(X,3),FORCE(X,4),
       FORCE(X,5),FORCE(X,6),FORCE(X,7),FORCE(X,8),FORCE(X,9)
6560        WRITE #2, FORCE(X,1),FORCE(X,2),FORCE(X,3),FORCE(X,4),
       FORCE(X,5),FORCE(X,6),FORCE(X,7),FORCE(X,8),FORCE(X,9)
6570   NEXT X
6580   CLOSE #1
6590   CLOSE #2
6600   '
6610   '
6620    'Prompt for next scan
6630   '
6640   INPUT "DO YOU WANT ANOTHER SCAN (Y OR N)";ANSW$
6645   A$="N"
6650   IF ANSW$ <>"N" THEN GOTO 3700
6655   CLS:LOCATE 12,15:INPUT "DO YOU REALLY WANT TO QUIT";AW$
6660   IF AW$<>"Y" THEN GOTO 3700
6665   GOSUB 7060
6670   END
6680   '
6690    'This subroutine averages the balance voltage readings
6700    'by computing the mean and standard deviation.
```

143

```
6710   'Any readings less or greater than one standard deviation
6720   'are thrown out and a new mean is computed
6730   '
6740   FOR CHANNEL = 2 TO 7
6750   N=10:FLAG=0
6760   SSDEV=0
6770   'Mean of balance voltage readings
6780   SREAD = 0
6790   FOR CNT = 1 TO 10
6800   SREAD = SREAD + TREAD(CHANNEL,CNT)
6810   NEXT CNT
6820   MEAN = SREAD/N
6830   READING(CHANNEL) = MEAN
6840   IF (FLAG=1) THEN GOTO 7010
6850   'Standard deviation routine
6860   FOR CNT = 1 TO 10
6870   DIF = TREAD(CHANNEL,CNT) - MEAN
6880   SDEV = DIF * DIF
6890   SSDEV = SSDEV + SDEV
6900   NEXT CNT
6910   DEV = SQR(SSDEV/N)
6920   HI = MEAN + DEV
6930   LO = MEAN - DEV
6940   FOR CNT = 1 TO 10
6950   ARG = TREAD(CHANNEL,CNT)
6960   IF (ARG < HI) AND (ARG > LO) THEN GOTO 6990
6970   TREAD(CHANNEL,CNT) = 0
6980   N = N - 1:FLAG=1
6990   NEXT CNT
7000   DROP(CHANNEL)=10-N:GOTO 6780
7010   NEXT CHANNEL
7020   PRINT "READINGS DROP        ";DROP(2);"        ";DROP(3);"
       ";DROP(4);"    ";DROP(5);"    ";DROP(6);"    ";DROP(7)
7030   RETURN
7040   END
7050   '
7060   'This subroutine enters the experiment conditions.
7070   CLS:COLOR 14,1,1
7080   INPUT "ENTER EXPERIMENT DATE (YYMMDD)";YMD:LAB(1)=YMD
7090   INPUT "ENTER EXPERIMENT GRID NO.";G:LAB(2)=G
7100   INPUT "ENTER EXPERIMENT BODY NO. (0='O', 1='+',
       2='X')";B:LAB(3)=B
7110   INPUT "ENTER EXPERIMENT STRAKE NO. (0, 4, OR 8)";S:LAB(4)=S
```

```
7115  TEMPSUM=0
7120  FOR X=1 TO TRIAL
7125    TEMPSUM=TEMPSUM+FORCE(X,9)
7130  NEXT X
7135  TAV=TEMPSUM/TRIAL:LAB(5)=TAV
7140  INPUT "ENTER EXPERIMENT WIND TUNNEL DYNAMIC
      PRESSURE (cmH2O)";DP:LAB(6)=DP
7150  INPUT "ENTER EXPERIMENT PRESSURE (in.
      Hg)";PRE:LAB(7)=PRE*70.739
7160  '
7170  OPEN DATAFILE$ FOR OUTPUT AS #1
7180  OPEN DISKFILE$ FOR OUTPUT AS #2
7190  WRITE #1, TARE(1),TARE(2),TARE(3),TARE(4),TARE(5),TARE(6),
      TARE(7),TARE(8)
7200  WRITE #2, TARE(1),TARE(2),TARE(3),TARE(4),TARE(5),TARE(6),
      TARE(7),TARE(8)
7210  FOR X = 1 TO 140
7220      WRITE #1,FORCE(X,1),FORCE(X,2),FORCE(X,3),FORCE(X,4),
      FORCE(X,5),FORCE(X,6),FORCE(X,7),FORCE(X,8),FORCE(X,9)
7230      WRITE #2, FORCE(X,1),FORCE(X,2),FORCE(X,3),FORCE(X,4),
      FORCE(X,5),FORCE(X,6),FORCE(X,7),FORCE(X,8),FORCE(X,9)
7240  NEXT X
7250  WRITE #1, LAB(1),LAB(2),LAB(3),LAB(4),LAB(5),LAB(6),LAB(7)
7260  WRITE #2, LAB(1),LAB(2),LAB(3),LAB(4),LAB(5),LAB(6),LAB(7)
7270  CLOSE #1
7280  CLOSE #2
7290  '
7300  '
7310  CLS:LOCATE 12,10
7320  PRINT "THIS PROGRAM IS TERMINATED BY USER."
7330  RETURN
7340  END
```

APPENDIX C.   DATA REDUCTION PROGRAM

This data reduction program was written in BASIC by Rabang [Ref. 17], and was modified and renamed as COEFF.BAS by the author for this experiment.   The reader is encouraged to examine this program before intending to operate it in other applications.

The COEFF.BAS program read the force and moment measurements, and the experimental conditions from the force/moment data file generated by the data acquisition program (READ.BAS) introduced in Appendix B.

Based on the experimental conditions, the COEFF.BAS program converted the force and moment measurements into the non-dimensional coefficients, with the blockage correction.   The mathematical expressions for producing coefficients were introduced in the Chapter II on page 49.   The program also calculated the average velocity and Reynolds number.   The results were recorded in a coefficient data file named by the operator.

This program also provided a hardcopy of the data output including the experimental conditions, force/moment measurements and force/moment coefficients.   The complete program is listed below.

```
1000   'PROGRAM BY M.P. RABANG TO READ FORCE AND
1005   'MOMENT VALUES FROM A DATA FILE CREATED BY THE
1010   'DATA ACQUISITION PROGRAM.  THIS PROGRAM HAS
1020   'BEEN MODIFIED BY LT. YUAN, C.C.
1030   DIM TARE[8], FORCE[140,9], COEF[140,9], LAB[11]
1040   COLOR 14,1,1
1050   CLS
1060   KEY OFF
1070   '
1080   LOCATE 11,7
1090   INPUT"ENTER THE NAME OF THE INPUT FILE";D$
1100   F$=D$+".DAT"
1110   INFILE$="C:\LAWRENCE\"+F$
1120   CF$="CF"+F$
1130   OUTFILE$="C:\LAWRENCE\"+CF$
1140   DISKFILE$="A:"+CF$
1150   ' READ THE FORCE VALUES FROM THE INPUT DATA FILE
1160   OPEN INFILE$ FOR INPUT AS #1
1170   INPUT   #1,   TARE(1),TARE(2),TARE(3),TARE(4),TARE(5),
       TARE(6),TARE(7),TARE(8)
1180   FOR X = 1 TO 140
1190   INPUT   #1,   FORCE(X,1),FORCE(X,2),FORCE(X,3),FORCE(X,4),
       FORCE(X,5),FORCE(X,6),FORCE(X,7),FORCE(X,8),FORCE(X,9)
1200   NEXT X
1210   INPUT #1, LAB(1),LAB(2),LAB(3),LAB(4),LAB(5),LAB(6),LAB(7)
1220   CLOSE #1
1225   '
1230   YMD=LAB(1)
1240   SCR=LAB(2)
1250   BODY=LAB(3)
1260   STR=LAB(4)
1270   TAV=LAB(5)
1280   DP=LAB(6)
1290   PRE=LAB(7)
1300   '
1330   ' OPEN THE DATA FILE SO EACH SCAN IS RECORDED
1340   TRANSFILE$="C:\LAWRENCE\TRANS.DAT"
1370   '
1400   CLS:LOCATE 12,5
1410   INPUT"INPUT  FILE  HAS  BEEN  LOADED,  ENTER  <CR>  TO
       CONTINUE";INPT$
1420   '
1430   ' BEGIN COEFFICIENTS CALCULATION
```

```
1440    A=.0167
1450    MU=3.719E-07
1460    RHO=PRE/(1545*(459.7+TAV))
1470    IF SCR=0 THEN Q=-0.026749+1.1149*DP:GOTO 1490
1480    IF SCR=3 THEN Q=0.018985+0.6957*DP
1490    Q=Q*2.046
1500    VEL=SQR(2*Q/RHO)
1510    RED=(RHO*VEL*(1.75/12))/MU
1520    '
1530    FLAG=0
1540    FOR X   1 TO 140
1550    IF FORCE(X,1)=0 THEN GOTO 1730
1560    FLAG=FLAG+1
1570    'ROUTINE TO CALCULATE THE COEFFICIENTS AND TO
1580    'CORRECT THE DYNAMIC PRESSURE FOR BLOCKAGE
1590    COEF(X,1)=FORCE(X,1)
1600    COEF(X,2)=FORCE(X,2)
1610    ALPHA = FORCE(X,2)
1620    IF FORCE(X,2) < 0 THEN ALPHA = ABS(FORCE(X,2))
1630    IF FORCE(X,2) > 90 THEN ALPHA = 180-FORCE(X,2)
1640    IF BODY=0 THEN EPS=.0000908*ALPHA+.007759
1650    IF BODY=1 THEN EPS=.0000126*ALPHA+.007759
1660    IF BODY=2 THEN EPS=.0000101*ALPHA+.007759
1670    D1=A*Q*(1+(2*EPS)):D2=A*Q*(1+(2*EPS))*1.75/12
1680    FOR Y = 3 TO 5:COEF(X,Y) = FORCE(X,Y)/D1:NEXT Y
1700    FOR Y = 6 TO 8:COEF(X,Y) = FORCE(X,Y)/D2:NEXT Y
1710    COEF(X,9)=COEF(X,4)/COEF(X,3)
1720    NEXT X
1730    LAB(8)=RHO
1740    LAB(9)=Q
1750    LAB(10)=VEL
1760    LAB(11)=RED
1770    '
1780    ' WRITE THE COEFFICIENTS TO THE OUTPUT FILE
1790    OPEN OUTFILE$ FOR OUTPUT AS #1
1800    OPEN DISKFILE$ FOR OUTPUT AS #2
1810    OPEN TRANSFILE$ FOR APPEND AS #3
1820        WRITE #1, LAB(1),LAB(2),LAB(3),LAB(4),LAB(5),LAB(6),LAB(7),
        LAB(8),LAB(9),LAB(10),LAB(11)
1830        WRITE #2, LAB(1),LAB(2),LAB(3),LAB(4),LAB(5),LAB(6),LAB(7),
        LAB(8),LAB(9),LAB(10),LAB(11)
1840        WRITE #3, LAB(1),LAB(2),LAB(3),LAB(4),LAB(5),LAB(6),LAB(7),
        LAB(8),LAB(9),LAB(10),LAB(11)
```

```
1850   FOR X=1 TO FLAG
1860   WRITE  #1,  COEF(X,1),COEF(X,2),COEF(X,3),COEF(X,4),COEF(X,9),
       COEF(X,5),COEF(X,6),COEF(X,7),COEF(X,8)
1870   WRITE  #2,  COEF(X,1),COEF(X,2),COEF(X,3),COEF(X,4),COEF(X,9),
       COEF(X,5),COEF(X,6),COEF(X,7),COEF(X,8)
1880   WRITE  #3,  COEF(X,1),COEF(X,2),COEF(X,3),COEF(X,4),COEF(X,9),
       COEF(X,5),COEF(X,6),COEF(X,7),COEF(X,8)
1890   NEXT X
1900   CLOSE #1
2000   CLOSE #2
2010   CLOSE #3
2020   '
2060   ' DISPLAY ROUTINE
2070   CLS:BEEP:LOCATE 10,5:INPUT "DO YOU WANT TO VIEW THE
       OUTPUT";PANS$
2080   IF PANS$<>"Y" THEN GOTO 2290
2090   COLOR 0,10,10
2100   CLS
2110   PRINT"FILE NAME: ";CF$:PRINT" "
2120   PRINT"DATE (YYMMDD)                    ";YMD
2125   PRINT"SCREEN NO.                   ";SCR
2130   PRINT"BODY CONFIGURATION NO.            ";BODY
2135   PRINT"STRAKE NO.                   ";STR
2140   PRINT"STATIC PRESSURE (LB/FT^2)         ";PRE
2145   PRINT"AVERAGE TEMPERATURE (F)           ";TAV
2150   PRINT"WIND TUNNNEL VELOCITY (FT/SEC)        ";VEL
2155   PRINT"WIND TUNNNEL DYNAMIC PRESSURE (cmH2O)";DP
2160   PRINT"AIR DENSITY (LBm/FT^3)          ";RHO
2170   PRINT"REYNOLDS NUMBER             ";RED
2180   PRINT"ACTUAL DYNAMIC PRESSURE (LB/FT^2)    ";Q
2185   BEEP:INPUT "ENTER <CR> TO CONTINUE";INPT$
2190   PRINT" "
2200   PRINT"* * * * * * * * * * * * * FORCE COEFFICIENTS * * * * * * * * * *
       * * * * *
2210   PRINT" "
2220   PRINT                                    " TRIAL   A0A
       NORMAL   SIDE    AXIAL    PITCH   ROLL    YAW"
2230   PRINT                                    " ***** ***** ********
       ********    ********    ********    ********    ********"
2240   FOR X = 1 TO FLAG
2250   PRINT USING" ###   +###.#   +##.####    +##.####    +##.####
       +##.####          +##.####          +##.####";
```

149

```
     COEF(X,1),COEF(X,2),COEF(X,3),COEF(X,4),COEF(X,5),COEF(X,6),COEF(
     X,7),COEF(X,8)
2260 IF X=20 OR X=40 OR X=60 OR X=80 OR X=100 OR X=120 THEN INPUT
     "ENTER <CR> TO CONTINUE";INPT$
2270 NEXT X
2280 BEEP:INPUT "ENTER <CR> TO CONTINUE";INPT$
2290 CLS:LOCATE   10,5:BEEP:INPUT   "DO   YOU   WANT   A
     HARDCOPY";ANS$
2300 IF ANS$<>"Y" THEN GOTO 2640
2310 ' HARDCOPY ROUTINE
2320 LPRINT"FORCE DATA FILENAME:";F$
2330 LPRINT"COEFFICIENT DATA FILENAME:";CF$:LPRINT" "
2340 LPRINT"DATE (YYMMDD)              ";YMD
2345 LPRINT"SCREEN NO.                ";SCR
2350 LPRINT"BODY CONFIGURATION NO.        ";BODY
2355 LPRINT"STRAKE NO.                ";STR
2360 LPRINT"STATIC PRESSURE (LB/FT^2)       ";PRE
2370 LPRINT"AVERAGE TEMPERATURE (F)         ";TAV
2380 LPRINT"WIND TUNNEL VELOCITY (FT/SEC)       ";VEL
2390 LPRINT"WIND TUNNEL DYNAMIC PRESSURE (cmH2O)";DP
2400 LPRINT"AIR DENSITY (LBm/FT^3)          ";RHO
2410 LPRINT"REYNOLDS NUMBER             ";RED
2420 LPRINT"ACTUAL DYNAMIC PRESSURE (LB/FT^2)   ";Q
2430 LPRINT" "
2440 LPRINT" "
2450 LPRINT"* * * * * * * * * * * * * FORCE READINGS * * * * * * * * * * * *
     * * * * *
2460 LPRINT" "
2470 LPRINT                              " TRIAL  A0A
     NORMAL    SIDE    AXIAL    PITCH    ROLL    YAW"
2480 LPRINT                               " #   DEG   POUNDS
     POUNDS   POUNDS   FT-LBS   FT-LBS   FT-LBS"
2490 LPRINT                               " ***** ***** *******
     *******  *******  ***:***  *******  *******"
2500 FOR J = 1 TO FLAG
2520 LPRINT USING" ###   +###.#   +##.####   +##.####   +##.####
     +##.####        +##.####           +##.####";
     FORCE(J,1),FORCE(J,2),FORCE(J,3),FORCE(J,4),FORCE(J,5),FORCE(J,6),F
     ORCE(J,7),FORCE(J,8)
2530 NEXT J
2540 LPRINT" "
2550 LPRINT" "
```

```
2560   LPRINT"* * * * * * * * * * * * * FORCE COEFFICIENTS * * * * * * * * *
       * * * * * *
2570   LPRINT" "
2580   LPRINT                                          " TRIAL   A0A
       NORMAL    SIDE    AXIAL    PITCH    ROLL    YAW"
2590   LPRINT                                          " ***** **** ********
       ********   ********   ********   ********   ********"
2600   FOR X = 1 TO FLAG
2610   LPRINT USING" ###  +###.#   +##.####   +##.####   +##.####
       +##.####          +##.####          +##.####";
       COEF(X,1),COEF(X,2),COEF(X,3),COEF(X,4),COEF(X,5),COEF(X,6),COEF(
       X,7),COEF(X,8)
2630   NEXT X
2640   COLOR 14,1,1:CLS:LOCATE 12,7:BEEP
2650   INPUT"DO YOU WANT ANOTHER RUN";AANS$
2660   IF AANS$<>"N" THEN GOTO 1050
2670   CLS:LOCATE 12,10:PRINT "THE PROGRAM IS TERMINATED!"
2680   END
```

APPENDIX D. RUN MATRIX

This run matrix lists all the tests conducted for this thesis research. All tests were conducted by the author in the Naval Postgraduate School wind tunnel test facility. The run names were listed by a sequence code. The first letter indicates what type the run is; "T" is for the preliminary runs, and "S" is for the baseline runs and test runs.

"Txx" was named for the preliminary runs. The first digit after the initial letter is the nose number; nose#1 was at 0° roll angle, and the subsequent nose number each represents a 45° roll angle increment clockwise. The second digit is the sequence run number for this particular nose roll angle.

"Sxxxx" was named for the baseline runs and test runs. The first digit after the initial letter is the wind tunnel test condition; "0" represents a non-turbulent (no grid) wind tunnel test condition, and "3" represents a turbulent (grid) condition. The second digit indicates the body-wing configuration; "0" is for "body 0," "1" is for "body 1," and "2" is for "body 2." The third digit simply represents the strake number. The last digit is the subsequent number for this particular run.

Run	Grid	Body	Strake	T_{av} (°F)	Pressure (in. Hg)	Re_d (x10^5)	Dynamic Pressure (lb/ft^2)	Velocity (fps)	Mach No.
T11	0	0	0	61.67	29.90	1.15	16.30	111.43	0.10
T21	0	0	0	62.71	29.95	1.16	16.55	112.30	0.11
T31	0	0	0	63.39	30.09	1.16	16.55	112.11	0.11
T41	0	0	0	65.38	30.09	1.16	16.55	112.32	0.11
T51	0	0	0	66.41	30.09	1.15	16.55	112.43	0.11
T61	0	0	0	65.41	29.24	1.15	16.55	112.61	0.11
T71	0	0	0	67.14	29.26	1.15	16.55	112.76	0.11
T81	0	0	0	65.74	30.05	1.15	16.55	112.44	0.11
S0101	0	1	0	70.27	30.11	1.15	16.55	112.81	0.11
S3101	3	1	0	73.97	29.81	1.14	16.55	113.77	0.11
S0201	0	2	0	69.49	30.19	1.15	16.55	112.58	0.11
S3201	3	2	0	77.81	29.84	1.14	16.55	114.12	0.11
S0141	0	1	4	70.80	30.04	1.15	16.55	113.00	0.11
S3141	3	1	4	75.80	30.14	1.15	16.55	113.33	0.11
S0241	0	2	4	70.14	31.02	1.15	16.55	112.78	0.11
S3241	3	2	4	76.02	30.08	1.14	16.55	113.47	0.11
S0181	0	1	8	71.22	29.96	1.15	16.55	113.19	0.11
S3181	3	1	8	76.77	29.81	1.14	16.55	114.06	0.11
S0281	0	2	8	72.90	30.01	1.15	16.55	113.28	0.11
S3281	3	2	8	76.15	29.86	1.14	16.55	113.90	0.11

LIST OF REFERENCES

1. Friedman, N., "Naval Vertical Launch Missile System," *Military Technology,* page 24-31, May 1985.

2. Roane, D. P., *The Effect of a Turbulent Airstream on a Vertically-launched Missile at High Angles of Attack,* Master's Thesis, Naval Postgraduate School, Monterey, CA, December 1987.

3. Keener, E. R. and Chapman, G. T., *Onset of Aerodynamic Side Forces At Zero Sideslip on Symmetric Forebodies at High Angle of Attack,* AIAA paper 74-770, August 1974.

4. Deane, J. R., *Experimental Investigations into the Interaction between Body Vortices and Wing Panels on a Missile Configuration at Low Speed,* AIAA paper 80-0032, January 1980.

5. Modi, V. J., Ries, T., Kwan, A. and Leung, E., "Aerodynamics of Pointed Forebodies at High Angles of Attack," *Journal of Aircraft,* Vol. 10, No. 6, page 428-432, June 1984.

6. Almosnino, D. and Rom, J., "Lateral forces on a Slender body and Their Alleviation at High Incidence," *Journal of Spacecraft,* Vol. 18, No. 5, page 393-400, September-October 1984.

7. Moskovitz, C. A., Hall, R. M. and DeJarnette, F. R., *Effects of Surface Perturbations on the Asymmetric Vortex Flow Over a Slender Body,* AIAA paper 88-0483, January 1988.

8. Howard, R. M. and others, *Aerodynamic Effects of a Turbulent Flowfield on a Vertically-launched Missile,* AIAA paper 89-0329, January 1989.

9. Moskovitz, C. A., Hall, R. M. and DeJarnette, F. R., *Effects of Nose Bluntness, Roughness and Surface Perturbations on the Asymmetric Flow Past Slender Bodies at Large Angle of Attack,* AIAA paper 89-2236, July 1989.

10. Moskovitz, C. A., Hall, R. M. and DeJarnette, F. R., *Experimental Investigation of a New Device to Control the Asymmetric Flowfield on Forebodies at Large Angle of Attack,* AIAA paper 90-0069, January 1990.

11. Zilliac, G. G., Degani, D. and Tobak, M., *Asymmetric Vortices on a Slender Body of Revolution*, AIAA paper 90-0388, January 1990.

12. Howard, R. M. and others, *Wing Effects on Asymmetric Vortex Formation for a Ship-launched Missile*, AIAA paper 90-2851, August 1990.

13. Ericsson, L. E. and Reding, J. P., "Asymmetric Vortex Shedding from Bodies of Revolution," *Tactical Missile Aerodynamics*, AIAA, NY, 1986.

14. Dahlem, Valentine, and others, High Angle of Attack Missile *Aerodynamics at Mach Numbers 0.3 to 1.5*, AFWAL-TR-80-3070, November 1980.

15. Keener, E. R., *Flow-Separation Patterns on Symmetric Forebodies*, NASA TM-86016, January 1986.

16. Ericsson, L. E. and Reding, J. P., "Re-examination of the Maximum Normalized Vortex-Induced Side Force," *Journal of Spacecraft*, Vol. 21, No. 5, September-October 1984.

17. Rabang, M. P., *Turbulence Effects on the High Angles of Attack Aerodynamics of a Vertically Launched Missile*, Master's Thesis, Naval Postgraduate School, Monterey, CA, June 1988.

18. Lamar, J. E. and Frink, N. T., "Aerodynamic Features of Designed Strake-Wing configurations," *Journal of Aircraft*, Vol. 19, No. 8, August 1982.

19. Neilson, J. N., "Missile Aerodynamics - Past, Present, Future," *Journal of Spacecraft*, Vol. 17, No. 3, page 165-176, May-June 1980.

20. Hinze, J. O., *Turbulence, An Introduction to Its Mechanism and Theory*, McGRAW-HILL Book Company, 1959

21. Bradshaw, P., and Hancock, P. E., "The Effect of Free-Stream Turbulence on Turbulent Boundary Layers," *Journal of Fluids Engineering*, Vol. 105, page 284-289, September 1983.

22. Malcolm, G. N., Terry Ng, T., Lewis, L. C. and Murri, D. G., *Development of Non-Conventional Control Methods for High Angle of Attack Flight Using Vortex Manipulation*, AIAA paper 89-2192, July 1989.

23. Dunne, A. L., Black, S., Schmidt, G. S. and Lewis, T. L., "VLA Missile Development and High Angle of Attack Behavior," *Proceedings of NEAR Conference on Missile Aerodynamics*, page 13-1 to 13-68, Monterey, California, 31 Oct.-2 Nov. 1988.

24. Tieleman, H. W., *A Survey of the Turbulence in the Marine Surface Layer for the Operation of Low-Reynolds Number Aircraft*, Virginia Polytechnic Institute Report, VPI-E-85-10, Blacksburg, VA., March 1985.

25. Healey, J. V., *Simulating the Helicopter-Ship Interface as an Alternative to Current Methods of Determining the Safe Operating Envelopes*, Naval Postgraduate School Report, NPS-67-86-003, Monterey, CA., September 1986.

26. Gregoriou, G. and Knoche, H. G., *High Incidence Aerodynamics of Missiles During Launch Phase*, MBB GMBH Report UA-523/80, Munich, West Germany, January 1980.

27. Bertin, J. J., and others, *The Launch-Tube Flow-Field for a Vertical Launching System*, AIAA paper 88-0332, January 1988.

28. *NPS LABORATORY MANUAL FOR LOW SPEED WIND TUNNEL TESTING*, Department of Aeronautics, Naval Postgraduate School, Monterey, CA, January 1989

29. *Calibration for TASK Mark 14-C Balance*, Balance Calibration Laboratory, NASA-Ames Research Facility, July 1987.

30. Hewlett-Packard, Inc., *PC Instruments System Owner's Guide Using HP 610618 System Interface*, February 1986.

31. *Model 8256 Transducer Amplifier Operation and Maintenance Manual*, Pacific Instruments, March 1986.

32. Portfors, E. A., and Keffer, J. F., "Isotropy in Initial Period Grid Turbulence," *Topics of Fluids*, Vol. 12, No. 7, page 1519-1521, July 1969.

33. Summer, J.D., *An Experimental Investigation of Support Strut Interference on a Three-Percent Fighter Model at High Angles of Attack*, Master's Thesis, Naval Postgraduate School, Monterey, CA, September 1989.

34. Sestak, T. A., *Measurement of the Aerodynamic Forces Generated by Flight Crew Helmets in Supercritical Subsonic Flow*, Master's Thesis, Naval Postgraduate School, Monterey, CA, March 1987.

INITIAL DISTRIBUTION LIST

		No. Copies
1.	Defense Technical Information Center Cameron Station Alexandria, Virginia 22304-6145	2
2.	Library, Code 52 Naval Postgraduate School Monterey, California 93943-5100	2
3.	Chairman, Code AA Department of Aeronautics and Astronautics Naval Postgraduate School Monterey, CA 93943	1
4.	Commander Naval 'Veapons Center, Code 406 China Lake, CA 93555	1
5.	Standard Missile Program Office PMS 422, G205 ATTN: Thomas McCants Dr. Jesse East Naval Surface Warfare Center Dahlgren, VA 22448-5000	2
6.	Commander Naval Surface Warfare Center Dahlgren, VA 22448-5000	1
7.	Commander Naval Surface Weapons Center Silver Spring, MD 20903-5000	1
8.	Commander Pacific Missile Test Center Point Mugu, CA 93041	1

9. NASA Ames Research Center 1
   Technical Library
   Moffett Field, CA 93041

10. Prof. R. M. Howard, Code AA/HO 10
    Department of Aeronautics and Astronautics
    Naval Postgraduate School
    Monterey, CA 93943-5000

11. Prof. J. V. Healey, Code AA/HE 1
    Department of Aeronautics and Astronautics
    Naval Postgraduate School
    Monterey, CA 93943-5000

12. Prof. S. K. Hebbar, Code AA/HB 1
    Department of Aeronautics and Astronautics
    Naval Postgraduate School
    Monterey, CA 93943-5000

13. Library of Chinese Naval Academy 2
    P.O. Box 8494 Tso-Ying,
    Kaohsiung, Taiwan
    Republic of China

14. Library of Chung-Cheng Institute of Technology 2
    Tashih, Tao-Yuan, Taiwan
    Republic of China

15. LT. Yuan, Chih-Chung 2
    4th. Fl., No. 8, 8th. Alley, 61st. Lane,
    4th. Sec., Cherng-Gong Road, Nei Hu,
    Taipei, Taiwan
    Republic of China